Title: Biokinetics and Biodynamics of Nanomaterial Interactions

USAFOSR Contract Number: FA9550-08-1-0182

Final Report Period: March 1, 2008 – June 30, 2009

Program Manager: Walter Kozumbo, Ph.D.

Principal Investigators: Nancy A. Monteiro-Riviere, Ph.D.

Co-Investigators Jim E. Riviere, D.V.M, Ph.D.DSc(hon)
Xin-Rui Xia, Ph.D.

Principal Investigator: Nancy A. Monteiro-Riviere, Ph.D., FATS, ACT
Professor of Investigative Dermatology and Toxicology
Center for Chemical Toxicology Research and Pharmacokinetics
North Carolina State University
4700 Hillsborough Street
Raleigh, NC 27606
Telephone: (919) 513-6426
Fax: (919) 513-6358
E-mail: Nancy_Monteiro@ncsu.edu

Report Documentation Page

Form Approved
OMB No. 0704-0188

1. REPORT DATE	2. REPORT TYPE	3. DATES COVERED
30 SEP 2009		**01-03-2008 to 30-06-2009**

4. TITLE AND SUBTITLE	5a. CONTRACT NUMBER
Biokinetics And Biodynamics Of Nanomaterial Interactions	5b. GRANT NUMBER
	5c. PROGRAM ELEMENT NUMBER
6. AUTHOR(S)	5d. PROJECT NUMBER
	5e. TASK NUMBER
	5f. WORK UNIT NUMBER
7. PERFORMING ORGANIZATION NAME(S) AND ADDRESS(ES) **North Carolina State University,Center for Chemical Toxicology and Pharmacokinetics,4700 Hillsborough Street,Raleigh,NC,27606**	8. PERFORMING ORGANIZATION REPORT NUMBER **; AFRL-OSR-VA-TR-11-045**
9. SPONSORING/MONITORING AGENCY NAME(S) AND ADDRESS(ES)	10. SPONSOR/MONITOR'S ACRONYM(S)
	11. SPONSOR/MONITOR'S REPORT NUMBER(S) **AFRL-OSR-VA-TR-11-045**

12. DISTRIBUTION/AVAILABILITY STATEMENT
Approved for public release; distribution unlimited

13. SUPPLEMENTARY NOTES

14. ABSTRACT

15. SUBJECT TERMS

16. SECURITY CLASSIFICATION OF:			17. LIMITATION OF ABSTRACT	18. NUMBER OF PAGES	19a. NAME OF RESPONSIBLE PERSON
a. REPORT	b. ABSTRACT	c. THIS PAGE			
unclassified	**unclassified**	**unclassified**	**Same as Report (SAR)**	**63**	

Table of Contents

A. Executive Summary

A requirement to assess toxicity of nanomaterials is to assess their interactions with available viability assays. Single-walled carbon nanotubes (SWCNT), fullerenes (C_{60}), carbon black (CB), nC_{60}, and quantum dots (QD) were studied in vitro to determine their toxicity in a number of cell types. The classical dye-based assays such as MTT and neutral red (NR) that determine cell viability produced invalid results with some NM (nanomaterials) due to NM/dye interactions and/or NM adsorption of the dye/dye products. In this study, human epidermal keratinocytes (HEK) were exposed in vitro to CB, SWCNT, C_{60}, nC_{60}, and QD to assess viability with calcein AM (CAM), Live/Dead (LD), NR, MTT, Celltiter 96® AQueous One (96 AQ), alamar Blue (aB), Celltiter-Blue® (CTB), CytoTox One™ (CTO), and flow cytometry. In addition, trypan blue (TB) was quantitated by light microscopy. Assay linearity (R^2 value) was determined with HEK plated at concentrations from 0 to 25,000 cells per well in 96-well plates. HEK were treated with serial dilutions of each NM for 24 h and assessed with each of the viability assays. TB, CAM and LD assays, which depend on direct staining of living and/or dead cells, were difficult to interpret due to physical interference of the NM with cells. Results of the dye-based assays varied a great deal, depending on the interactions of the dye/dye product with the carbon nanomaterials (CNM). The optimal assay for use with carbon and noncarbon NM was 96 AQ. Unlike small molecules, CNM interact with assay markers to cause variable results with classical toxicology assays and may not be suitable for assessing nanoparticle cytotoxicity. Therefore, more than one assay may be required when determining nanoparticle toxicity for risk assessment.

Quantum dots were used to determine endocytic pathways of nanoparticles (NP). Due to the superior photoemission and photostability characteristics, quantum dots (QD) are novel tools in biological and medical applications. However, the toxicity and mechanism of QD uptake are poorly understood. QD NP with an emission wavelength of 655 nm are ellipsoid in shape and consist of a cadmium/selenide core with a zinc sulfide shell. It was shown that QD with a carboxylic acid surface coating were recognized by lipid rafts but not by clathrin or caveolae in human epidermal keratinocytes (HEK). QD were internalized into early endosomes and then transferred to late endosomes or lysosomes. In addition, 24 endocytic interfering agents were used to investigate the mechanism by which QD enter cells. Our results showed that QD endocytic pathways are primarily regulated by the G-protein–coupled receptor associated pathway and low density lipoprotein receptor/scavenger receptor, whereas other endocytic interfering agents may play a role but with less of an inhibitory effect. Lastly, low toxicity of QD was shown with the 20nM dose in HEK at 48 h but not at 24 h by the live/dead cell assay. QD induced more actin filaments formation in the cytoplasm, which is different from the actin depolymerization by cadmium. These findings provide insight into the specific mechanism of QD nanoparticle uptake in cells. The surface coating, size, and charge of QD NP are important parameters in determining how nanoparticle uptake occurs in mammalian cells for cancer diagnosis and treatment, and drug delivery.

The toxicity of silver nanoparticles (Ag NP) was evaluated. Products utilizing the antimicrobial properties of silver may be found in health and consumer products. To assess the potential cytotoxicity, inflammatory potential, and interactions of Ag NP in neonatal HEK, their interference with common toxicity assays, and their penetration into porcine skin in vivo was studied. Eight different types of Ag NP were defined as: *unwashed* and uncoated (20, 50 and 80nm), *washed* and uncoated (20, 50 and 80nm), and carbon-coated (25 and 35nm). Cell

viability was assessed by MTT, alamarBlue (aB), and CellTiter 96Aqueous One (96AQ), and inflammation was assessed with cytokines IL-1β, IL-6, IL-8, IL-10, and TNF-α. The effect of the *unwashed* and uncoated Ag NP on HEK viability after 24 h exposure indicated a significant dose dependent decrease ($p<0.05$) at 0.34μg/ml with aB and 96AQ and at 1.7μg/ml with MTT. However, the *washed* and uncoated Ag NP and the carbon-coated Ag NP showed no significant decrease ($p<0.05$) in viability for any of the concentrations assessed by MTT, aB or 96AQ. For each of the *unwashed* and uncoated Ag NP a significant increase ($p<0.05$) in concentration of the cytokines IL-1β, IL-6, IL-8, and TNF-α was noted. TEM depicted localization of all Ag NP in cytoplasmic vacuoles of HEK. Solutions of 34, 3.4, and 0.34μg/ml of 20nm and 50nm *washed* and *unwashed* Ag NP were topically applied daily to *in vivo* porcine skin for 14 days. Macroscopic observations showed no gross irritation, while microscopic and ultrastructural observations of the Ag NP showed focal inflammation and localization of Ag NP in the stratum corneum layers of the skin. This study provides a better understanding of the toxicity of Ag NP *in vitro* as well as provides a basis for occupational and risk assessment.

The toxicity of aluminum nanoparticles (Al NP) were also evaluated. Al NP have been used in applications as diverse as drug delivery, material surface coatings, and as an ingredient for solid rocket fuel in military explosives and artillery. Although Al NP are used in many civilian and military applications, the health and safety implications of these nanosize particles are not known. HEK were exposed to 50nm and 80nm Al NP ranging from 4.0mg/ml to 0.0004mg/ml to assess the cytotoxicity and inflammatory potential. Viability did not decrease in HEK exposed to both the 50nm and the 80nm Al NP at all treatment concentrations with MTT, CellTiter 96® AQueous One, and alamar Blue® viability assays. TEM depicted Al NP localized within the cytoplasmic vacuoles of the cells. Cytokine data was variable, indicating possible nanoparticle interactions with the cytokine assays. These studies illustrate the difficulties involved in assessing the biological safety of nanomaterials such as Al NP due to media- and temperature-dependent particle agglomeration and nanoparticle interactions with biomarkers of cytotoxicity.

Fullerenes were also assessed for toxicity. Carbon fullerenes (C_{60}) possess unique properties, and thus have widespread applications in a number of disciplines. Although industrial production continues to increase, toxicity of colloidal C_{60} (nC_{60}) on living cells has not been completely established. Fullerenes were suspended in water to yield nC_{60} at a concentration of 107μg/ml. HEK were exposed to nC_{60} at concentrations ranging from 8.5 μg/ml to 0.000544μg/ml (n=24 wells/treatment) for 24h. MTT and 96 AQ viability assays showed no cell death at the highest nC_{60} concentrations, while alamar Blue (aB) data was variable. Nanoparticle controls (with cells and without cells) revealed nonspecific interactions of the nC_{60} with the viability assays. The UV-Vis spectra was determined for MTT, 96 AQ, and aB, media in the presence of nC_{60}. The spectra for MTT and aB were consistent with the nanoparticle controls, while the 96 AQ spectrum showed no nC_{60} effect. The inflammatory mediator IL-6 showed a significant ($p<0.05$) concentration response, while IL-8, IL-1β, and TNF-α showed no response; IL-10 concentrations were below detectable limits. TEM revealed that the nC_{60} were readily internalized by HEK, bioconcentrated in cytoplasmic vacuoles.

The biologically active surface area (BASA) index was developed for Ag, Al, and nC_{60} NP. The framework of the BASA index was established with a set of 32 diverse probe compounds, which backed our hypothesis that the adsorption of a set of diverse probe compounds can be used to characterize the surface properties of NM in a biologically-relevant context. These surface physicochemical properties can be indexed with a set of five solvation

parameters and depicted in a radar graph, which can be used to predict the biological activity of the nanomaterials. The adsorption coefficients of fullerenes can be predicted from the solvation index following the established model, Log k_{nano} = –1.32 + 0.64R – 0.64 P + 0.43A – 1.29 B + 2.28V, with correlation coefficient (R^2) of 0.90. Ag NP showed weak adsorption toward the probe compounds, indicating weak biological interactions of the Ag NP in biological systems. Al NP may be safe to the environment because the adsorption property of Al NP is altered completely in aqueous solutions. The Al NP showed moderate adsorption toward the probe compounds, with no adsorption when oxidized in aqueous solutions. Fullerenes showed strong adsorption toward the probe compounds and the adsorption strength coefficients can be predicted using the established membrane-coated fiber (MCF) indexes with a correlation coefficient (R^2) of 0.93.

Most of these studies have been published in peer-reviewed journals or have been submitted to peer-reviewed journals.

B. Studies with Silver Nanoparticles

Introduction

Historically, silver (Ag) compounds have been used in numerous fields to prevent microbial growth. Like many non-essential heavy metals Ag is a natural biocide, but compared to titanium, zinc, and copper, Ag nanoparticles (Ag NP) show the highest antimicrobial efficacy against bacteria, viruses and other eukaryotic microorganisms (Gong et al., 2007). The Phoenicians coated milk bottles with Ag to inhibit bacterial growth, doctors have administered drops of Ag nitrate solutions to newborn babies to prevent neonatal conjunctivitis (Crede, 1881), and Ag sulfadiazine creams have long been considered the standard of care for the prevention of widespread bacterial growth on burn patient's denuded skin (Moyer et al., 1967). Both dietary supplements and homemade varieties of Ag colloids have been sold for decades as a "cure-all" for diseases such as tuberculosis, syphilis, scarlet fever, shingles, herpes, pneumonia, and arthritis (NCCAM, 2006). Furthermore, advances in nanotechnology have facilitated the increase of Ag-containing merchandise available to the public, making Ag the most used nanomaterial of all manufacturer-identified products in the world (www.nanotechproject.org). Products such as room deodorizing sprays, acne creams, clothing that prevents body odor, baby wipes, and pacifiers all exploit the natural antimicrobial activity of Ag (www.nanotechproject.org).

The increasing number of consumer products utilizing nanomaterials requires toxicity tests to ensure their safety. Such tests have reported on the ability for quantum dots of diverse physiochemical properties and fullerenes to penetrate into the intercellular lipid layers of the stratum corneum of porcine skin (Zhang et al., 2007; Ryman-Rasmussen et al., 2006; Rouse et al., 2007), and multifocal pulmonary granulomas to develop in rats after exposure to carbon nanotubes (Lam et al., 2004). Additionally, topical application of zinc oxide localized NP in the upper stratum corneum with minimal penetration (Cross et al., 2007; Gamer et al., 2006).

Although rare, studies indicating Ag toxicity do exist; as early as 1983, Rungby and Danscher showed that intraperitoneal administered Ag salts can accumulate in neurons and in protoplasmic glial cells of the brain and spinal cord. Additionally, internalized Ag may lead to neurological defects such as vertigo and seizures (Westhofen et al., 1986; Ohbo et al., 1996; Mirsattari et al., 2004). Studies on *in vitro* cell lines illustrate that 25µg/ml with 25nm Ag NP produce reactive oxygen species and oxidative stress that could potentially contribute to neurodegenerative diseases (Schrand et al., 2008), toxicity has been shown in hepatic cells from 5-50µg/ml of 15nm and 100nm Ag NP (Hussain et al., 2005), and to germ-line stem cells at 10µg/ml for 15nm Ag NP (Braydich-Stolle et al., 2005). HEK and fibroblasts treated with Ag NP dissolved out from commercially bought Ag-based wound dressings showed cytotoxicity at 15µg/ml (Burd et al., 2007), and interactions between Ag NP ranging in size from 7-20nm and human skin carcinoma cells showed the onset of apoptosis at 0.78µg/ml and 1.56µg/ml respectively (Arora et al., 2008), and polyvinylpyrrolidone-stabilized Ag NP with a mean size of 25nm have shown to penetrate into the upper layers of the epidermis in excised human skin in static diffusion cells (Larese et al., 2007).

It has long been known that Ag is responsible for causing argyria, the benign condition characterized by the bluish-graying of the skin that occurs through its preferential deposition in the basal lamina of soft tissues such as the skin, liver and spleen (Fung and Bowen, 1996), choroid plexus (Van Breemen and Clemente, 1955), and blood vessels, gastrointestinal tract, liver, and kidney (Danscher, 1980). Although argyria is most commonly reported clinically after excessive Ag ingestion, silver deposition has been seen after Ag sulfadiazine treatment of burned

skin (Lee and Lee, 1994; Marshall, 1979; Temple and Farooqi, 1985). In response to argyria, not to Ag toxicity, the National Institute for Occupational Safety and Health set a daily exposure limit for all forms of Ag at 0.01 mg/m^3, and the Environmental Protection Agency established the oral reference dose at 0.005mg/kg/day (NIOSH, 2003; EPA, 1996). Furthermore, over-the-counter Ag colloid products were banned by the Federal Drug Administration in 1999 to reduce the number of cases of argyria (FDA, 1999).

The ability for Ag NP to reduce the bacterial loads that people encounter without toxic side effects has not been supported by adequate research. Coupled with an increase in exposure to Ag NP, the ability for Ag NP to enter cells and cause toxicity calls for further research. The present study utilized HEK to evaluate the cytotoxic potential of Ag NP of varying size and surface conditions. Porcine skin was topically dosed daily for 14 days to evaluate the inflammatory and penetrating potential of Ag NP. Additionally, since it has been shown that NP are capable of interfering with viability assay dye and dye products (Monteiro-Riviere et al., 2009; Zhang et al., 2007; Monteiro-Riviere and Inman 2006), the interactions of Ag NP with common, dye-based *in vitro* toxicity tests were evaluated.

Materials and Methods

Silver nanoparticles

Eight types of Ag NP were used in this study, the properties of which are summarized in Table 1.

Table 1: Silver nanoparticle properties

Manufacturer-Designated Diameter (nm)	Actual Diameter (nm)	State of Ag NP	Ag Stock Concentration (mg/ml)	Particle Concentration (particles/ml)	ZetaPotential in deionized water (mV)
20, uncoated, unwashed	22.4±2.6	Colloid in deionized water	0.20	2.41E+12	-29.7
50, uncoated, unwashed	49.4±6.2	Colloid in deionized water	0.20	4.44E+11	-27.8
80, uncoated, unwashed	79.2±8	Colloid in deionized water	0.20	7.09E+10	-33.2
20, uncoated, washed	21.41±3.11	Colloid in deionized water	2.86	1.89E+14	-46.0
50, uncoated, washed	50.00±5.88	Colloid in deionized water	3.45	5.01E+12	-44.3
80, uncoated, washed	77.03±6.02	Colloid in deionized water	2.79	1.07E+12	-43.7
25, carbon-coated, unwashed	27.2±10.3	Powder	N/A	N/A	-24
35, carbon-coated, unwashed	37.0±11.6	Powder	N/A	N/A	-29

The Ag NP used in this study consisted of the following: *unwashed* and uncoated Ag NP suspended in deionized water with manufacturer-designated diameters of 20nm, 50nm and 80nm

(0.2mg/ml, 0.2mg/ml, 0.2mg/ml), *washed* and uncoated Ag NP suspended in deionized water with manufacturer-designated diameters of 20nm, 50nm and 80nm (2.86mg/ml, 3.45mg/ml, 2.79mg/ml), carbon-coated Ag NP with manufacturer-designated diameters of 25nm and 35nm. The sizes of each type of Ag NP was determined by the manufacturer and also confirmed by the authors by dynamic light scattering (DLS) and transmission electron microscopy (TEM) prior to any experimentation. TEM of each type of Ag NP are shown in Figure 1.

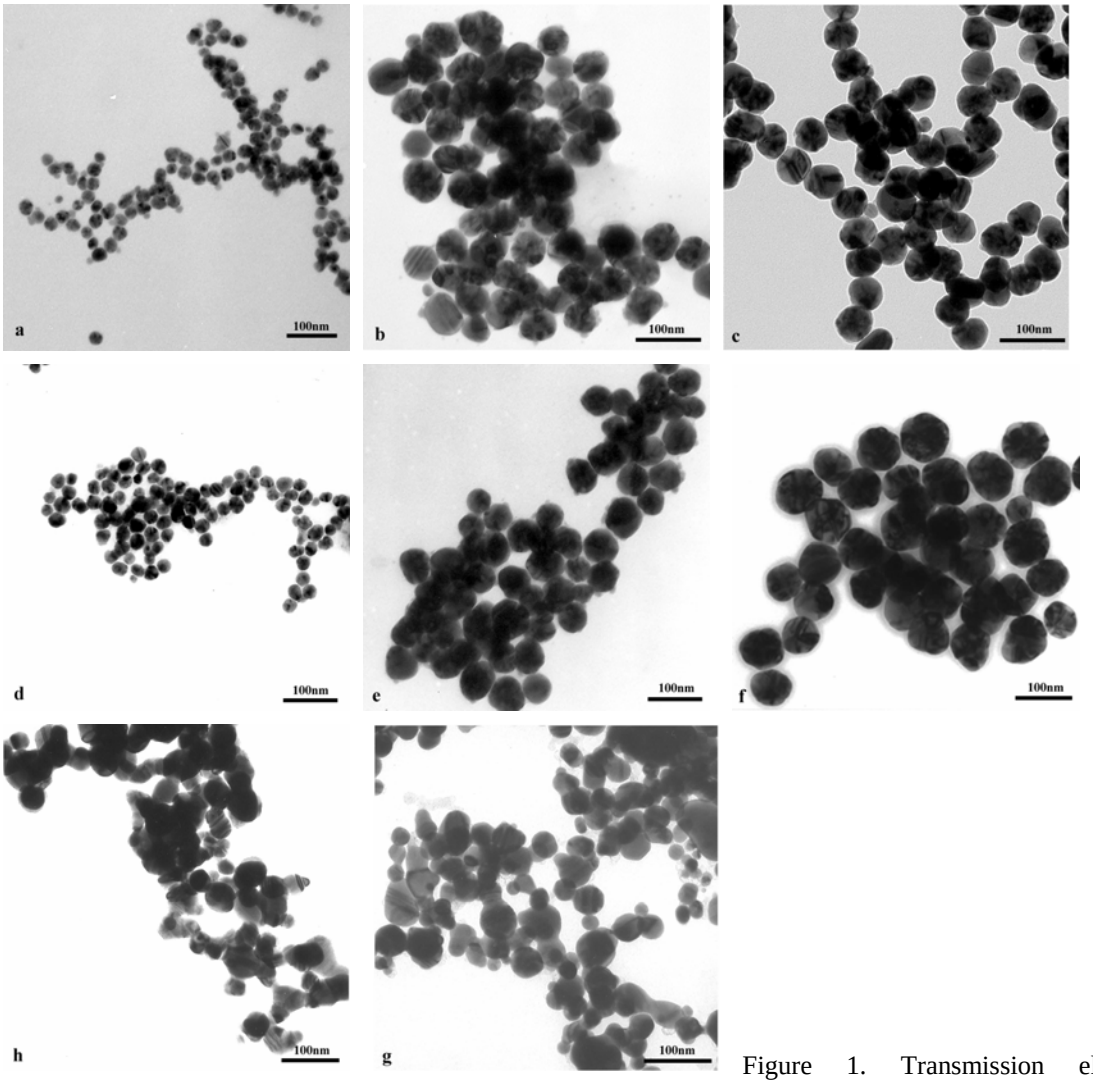

Figure 1. Transmission electron micrographs of Ag NP. (a) 20nm *unwashed* and uncoated; (b) 50nm *unwashed* and uncoated; (c) 80nm *unwashed* and uncoated; (d) 20nm *washed* and uncoated; (e) 50nm *washed* and uncoated; (f) 80nm *washed* and uncoated; (g) 25nm carbon-coated; (h) 35nm carbon-coated.

The Ag NP were provided by nanoComposix (San Diego, CA). Both the unwashed and washed Ag NP were synthesized by ammonium hydroxide catalyzed growth of Ag onto 5nm gold (Au) seed particles. Concentration of the particles was achieved via tangential flow filtration (TFF). The *unwashed* samples included minute amounts of the unreacted solvent formaldehyde and the byproduct methanol from the formation of the particles. The *washed* Ag NP were identical to the *unwashed* Ag NP, but were washed 20 times with 2mM phosphate

buffer to remove contaminants. The supernatant from the synthesized particles ("as synthesized") as well as from the washing process was collected from the 5th, 10th, 15th and 20th washes. The samples were ultracentrifuged (Beckman Coulter, Inc.; Fullerton, CA) for 30 min at 40,000rpm to obtain the supernatant samples. The Ag NP were stored at 4ºC in the dark. The carbon-coated Ag NP were synthesized by a pulsed plasma reactor. The particles were dried and stored at room temperature.

Cell culture and silver nanoparticle treatment

Cryopreserved primary neonatal HEK (Lonza, Walkersville, MD) were grown in keratinocyte growth medium-2 (KGM-2; Lonza, Walkersville, MD) in cell culture flasks (75cm^2; 1,000,000 cells) and grown to approximately 80% confluency in a 37ºC humidified 5% CO_2 incubator. The cells were passed into clear or black 96-well microplates (12,500cell/well; 200µl) where the peripheral wells contained only KGM-2 to prevent the evaporation of treatment medium. Between 18-24h later, after reaching approximately 80% confluency, the HEK were exposed to either KGM-2 (control) or serial dilutions of each Ag NP (n=6).

An initial dose response study was conducted to assess the concentrations of Ag NP that could affect HEK after 24h exposure. The majority of the colloidal Ag NP tested were supplied in both low volume and concentration which limited the highest HEK dosing concentration to 1.7µg/ml. The dosing concentrations of all subsequent samples were matched to that of the original samples. Combined with KGM-2 medium, a 1.7µg/ml stock solution of the Ag NP was serially diluted (1:5) to provide concentrations ranging from 1.7 to 0.000544µg/ml. The effect of the Ag NP on the HEK viability was assessed by 3-(4,5-dimethylthiazol-2-yl)-2,5-diphenyltetrazolium bromide (MTT), alamarBlue (aB), and CellTiter 96 AQueous (96 AQ) assays.

MTT viability assay

Cell culture medium containing Ag NP was removed from each treatment well and 200µl of 0.5mg/ml MTT (Sigma-Aldrich, St. Louis, MO) in KGM-2 warmed to 37ºC was added to Ag NP and vehicle-treated wells. The plates were incubated for 3 h, the MTT medium was removed, and HEKs rinsed with 200µl of Hank's balanced salt solution (HBSS) for 2 min. The HBSS was removed, 100µl of 70% isopropanol was added to each well, and the plates were agitated for 25 min. Microplates were read at 550nm in a Multiskan RC microplate reader (LabSystems, Helsinki, Finland) equipped with Ascent software (version 2.6). Data was plotted as a percentage of the vehicle-treated control. Data are expressed as the means ± SEM of the two experiments.

aB viability assay

One hundred microliters of cell culture medium containing Ag NP was removed and 10µl of aB (Molecular Probes, Invitrogen, Eugene, OR) solution was added to Ag NP and vehicle-treated wells. The plates were incubated for 3h and the microplates were read on a Molecular Dynamics Gemini EM (Molecular Devices Corp.; Sunnyvale, CA) spectrophotometer at the excitation wavelength of 560nm and emission wavelength of 590nm. Data was plotted as a percentage of the vehicle-treated control. Data are expressed as the means ± SEM of the two experiments.

96 AQ viability assay

One hundred microliters of cell culture medium containing Ag NP was removed and 20µl of 96 AQ (Promega, Madison, WI) was added to Ag NP and vehicle-treated wells. The plates were incubated for 3h, and the microplates were read at 450nm in a Multiskan RC microplate reader (LabSystems, Helsinki, Finland) equipped with Ascent software (version 2.6). Data was plotted as a percentage of the vehicle-treated control. Data are expressed as the means ± SEM of the two experiments.

When Ag NP did not show toxicity at 1.7µg/ml, and if higher concentrations and volumes were available, their dosing concentrations were scaled upward. Additionally, to differentiate the potential cytotoxicity between the particles and the contaminants present in the colloidal solution, the "as synthesized" supernatant and the 5^{th}, 10^{th}, 15^{th} and 20^{th} washing supernatant was evaluated against HEK after 24h at concentrations ranging from 1.7µg/ml to 0.068µg/ml.

Two different controls were run in parallel with each viability assay as described by Monteiro-Riviere et al. (2009). One control was to assess nonspecific interactions between the Ag NP and the assay dye without the use of cells (nanoparticle control). In this case, Ag NP dosing solutions equal to those used for viability tests were placed into collagen-coated 96-well plates devoid of cells, incubated for 24h, replaced the media with the assay solution, and read according to normal assay protocol as described above. Any change in absorbance values was reported and compared to control. The second control was to assess the specific interactions between the Ag NP and the metabolized dye (nanoparticle/cell control). In this case, two plates were involved: in one 96-well plate, Ag NP dosing solutions equal to those used for viability tests were placed into collagen-coated wells devoid of cells; in the other 96-well plate, cells were plated and grown. After incubating each plate for 24h, the cell-containing plate was assayed according to normal protocol and read as described above. Immediately after reading, the particle-containing plate was spun down, the medium removed, and the assay solution from each well of the cell-containing plate was transferred into the corresponding well of the particle-containing plate. After incubation for 3h, the plate was read and the difference in absorbance (before and after Ag NP) was recorded.

Cytokine release

To determine the inflammatory potential of the Ag NP cytokine analysis was conducted by assessing the release of interleukin (IL)-8, IL-6, tumor necrosis factor (TNF)-α, IL-10, and IL-1β. Analysis was performed for Ag NP that showed toxicity, at the concentrations that decreased HEK viability. The medium from each treatment set of the dosed cells was removed, pooled into a microfuge tube, and quickly frozen to -80ºC until assayed. On the day of the assay, samples were thawed and 50µl of each sample added (in triplicate) to a filler plate with beads coupled to the cytokine antibodies (Bio-Plex Cytokine Assay, Bio-Rad Laboratories, Hercules, CA) and the assay performed following the manufacturer's instructions. Samples were assayed on a Bio-Plex System (Luminex x MAP Technology) equipped with Bio-Plex software (version 4.0). Unknowns were quantified by linear regression to logarithmic standard curves. Cytokine levels were normalized relative to MTT absorbance. Data was expressed as the means ± SEM of the two experiments.

In vivo macroscopic porcine skin exposure

The effects of the *unwashed* and uncoated colloidal Ag NP were compared to the *washed* and uncoated colloidal Ag NP *in vivo*. Due to site number limitations the comparison was limited to the 20 and 50nm washed and unwashed samples. Combined with deionized water, a 34µg/ml stock solution of each sample was made to provide serial dilutions (1:10) from 34.0 to 0.34µg/ml. The final dilution was chosen in order to compare to the *in vitro* studies. Two female weanling pigs (Sus scrofa) weighing 20-30kg were housed in an AALAC accredited facility on elevated floors and were provided water and 15% protein pig and sow pellets ad libitum. Approximately 24h before the topical application of the Ag NP, the pigs were sedated with an injection of telazol-ketamine-xylazine (TKX) and the excess hair on the dorsum carefully clipped. On the first day of the experiment each pig was sedated with TKX, and placed in a sling. Fourteen sites, 7 on each side of the midline, were randomly assigned on the back of each pig and photographed with a digital camera. All sites were immediately topically dosed with 500µl of the appropriate Ag NP solution, allowed to air dry and then occluded with a Hilltop® chamber inset with a cotton pad (19mm inside diameter, 283.53mm^2 surface area). The chambers were secured with non-irritating Medipore® (3M, St. Paul, MN) tape, followed by tape to secure the chamber. Lastly, a body stocking was placed over the entire dorsum of each pig to further secure the chambers. After 24h, the pigs were sedated with TKX, the chambers were removed and erythema and edema evaluated using the Draize scoring system (erythema: 0, no change; 1, very slight change; 2, pale red in defined area; 3, definite red in well-defined area; 4, crimson red; edema: 0, no change; 1, very slight change; 2, slight change with edges barely defined; 3, moderate change, with area raised 1 mm; 4, severe change, with area raised more than 1mm and extending beyond the exposure area) (Draize et al., 1944). Any change in the skin was recorded and photographed. After this, the pigs were redosed, chambers replaced, and secured as described above and the dosing regiment was repeated for 14 days. At the conclusion of the 14 day study, a final Draize score was assessed, all sites photographed, and pigs were euthanized with 100mg/kg Euthasol® (Delmarva Laboratories, Inc., Midlothian, VA). The dosing sites were biopsied and placed in 10% neutral buffered formalin for light microscopy (LM) and in Trump's fixative for TEM. In addition, samples were also frozen in liquid nitrogen and stored at -80ºC.

Microscopic observations

To assess morphological alterations during the *in vivo* study, tissue samples were quickly harvested after the pigs were euthanized, cut into approximately 2mm x 3mm sections, and immersed into NBF fixative for several days. The fixed tissue was rinsed in 70% ethanol, processed through graded ethanol, cleared in Clear-Rite 3 and infiltrated and embedded in Paraplast® Plus tissue embedding medium (Fisher Scientific; Houston, TX). Approximately 5µm thick sections were mounted on positive-charged slides and stained with hematoxylin and eosin (H&E) for evaluation on an Olympus BH-2 light microscope. The sections were evaluated for intercellular and intracellular epidermal edema and dermal edema and inflammation using the following scoring system: 0, no change; +1, inflammation on less than half the sample; +2, inflammation on half the sample; +3, inflammation on greater than half the sample.

Ultrastructural observations

Particle size analysis was conducted to confirm the manufacturer-identified diameters and surface characterization. Information was collected on a Zetasizer (Malvern Instruments Ltd.) at 25ºC. Samples were prepared by either diluting the uncoated Ag NP with deionized water, or

suspending the carbon-coated Ag NP in deionized water and sonicating for 10 min. Additionally, TEM was used to visualize particle morphology uniformity. Images were observed with an FEI/Philips EM 208S transmission electron microscope operating at an accelerating voltage of 80 kV. The samples were prepared by placing a drop of homogenous suspension of each Ag NP (colloid; dry Ag NP suspended in deionized water) onto a formvar-coated copper mesh grid and allowed to air dry. Images of the 20, 50 and 80nm uncoated, 25 and 35nm carbon-coated Ag NP were taken (Figure 1).

To localize Ag NP uptake in vitro, HEK were grown to approximately 70% confluency in cell culture flasks ($25cm^2$) and treated for 24h with each Ag particle at 1.7µg/ml in KGM-2. The cells were harvested with trypsin, rinsed in HBSS, and fixed for at least 24h in Trump's fixative at 4ºC. The cells were rinsed in 0.1M phosphate buffer (pH 7.2), pelleted in a microfuge tube, resuspended, and quickly pelleted in 3% molten agar. Agar embedded samples were post fixed in 1% osmium tetroxide (Polysciences, Inc., Warrington, PA) in 0.1M phosphate buffer for one hour at 4ºC, washed with deionized water, dehydrated through an ascending ethanol series, cleared in acetone, infiltrated with Spurr resin, and polymerized at 70ºC overnight. Ultrathin sections, 800-1000Å thick, were mounted on copper grids, and examined on a FEI/Philips EM 208S TEM operating at an accelerating voltage of 80 kV. Cells were not stained to allow for better visualization of the Ag NP and to ensure the absence of stain artifacts resulting from lead citrate and uranyl acetate. Additionally, unstained samples were analyzed by X-ray microanalysis (EDS) with a Hitachi HF2000 FE TEM equipped with an Oxford Instruments INCA EDS.

To assess the penetration of the Ag NP in vivo, skin samples were quickly harvested, cut into approximately 1mm thin sections and immersed in Trump's fixative at 4ºC. The sections were then dehydrated and embedded in Spurr resin as described above. The samples were sectioned on a diamond knife and placed onto formvar-coated copper mesh grids for added stability and to help prevent both rolling of the edges and separation of the stratum corneum from the epidermis. The sections were observed on an FEI/Philips EM 208S TEM operating at an accelerating voltage of 80 kV. Additionally, unstained samples were analyzed by X-ray microanalysis (EDS) with a Hitachi HF2000 FE TEM equipped with an Oxford Instruments INCA EDS.

Statistical analysis

The mean values for HEK percent viability and cytokine concentration (normalized by viability) for each treatment were calculated and the significant differences ($p < 0.05$) determined using the PROC GLM Procedure (SAS 9.1 for Windows; SAS Institute, Cary, NC). When significant differences were found, multiple comparisons were performed using Tukey's Studentized Range HSD test at $p<0.05$ level of significance. For cell cultures, the Dunnett's t-test was performed to determine the significance at $p<0.5$ of differences between control and treatment groups.

Results

Treatment of HEK with silver nanoparticles

Exposure of HEK to 20, 50 and 80nm *unwashed* and uncoated Ag NP ranging in concentration from 0.000544 to 1.7µg/ml for 24h resulted in a dose-dependent viability decrease with all three assays. Figure 2a shows that 20nm *unwashed* Ag NP caused a significant decrease

in viability at 0.034µg/ml for both aB and 96AQ and at 1.7µg/ml for MTT. In this case, aB showed the greatest decrease in viability at both 0.034µg/ml and 1.7µg/ml, while MTT was the least sensitive of the three assays. The toxicity of the 50nm *unwashed* Ag NP is similar to the 20nm *unwashed* Ag NP, showing a significant decrease in viability at 0.034µg/ml for aB and 96AQ while at 1.7µg/ml for MTT (Figure 2b). For these Ag NP, aB was again the most sensitive assay at both the 0.034µg/ml and 1.7µg/ml concentrations, and MTT was the least sensitive assay at the 0.034µg/ml concentration while 96AQ was the least sensitive at the 1.7µg/ml concentration. Conversely, Figure 2c shows that 80nm *unwashed* Ag NP caused a significant decrease in viability at 0.034µg/ml for all three assays. At the 0.034µg/ml concentration aB is the most sensitive assay while at the 1.7µg/ml concentration MTT is the most sensitive while at both levels 96AQ is the least sensitive assay. The "as synthesized" supernatant obtained from the *unwashed* Ag NP showed a significant decrease in viability at 0.034µg/ml for MTT and aB assays and at 1.7µg/ml for 96AQ (Figure 2d). 96AQ was the most sensitive assay at both the 0.034µg/ml and 1.7µg/ml concentrations. Toxicity was not present for any of the supernatant obtained from the 5th, 10th, 15th or 20th washing steps.

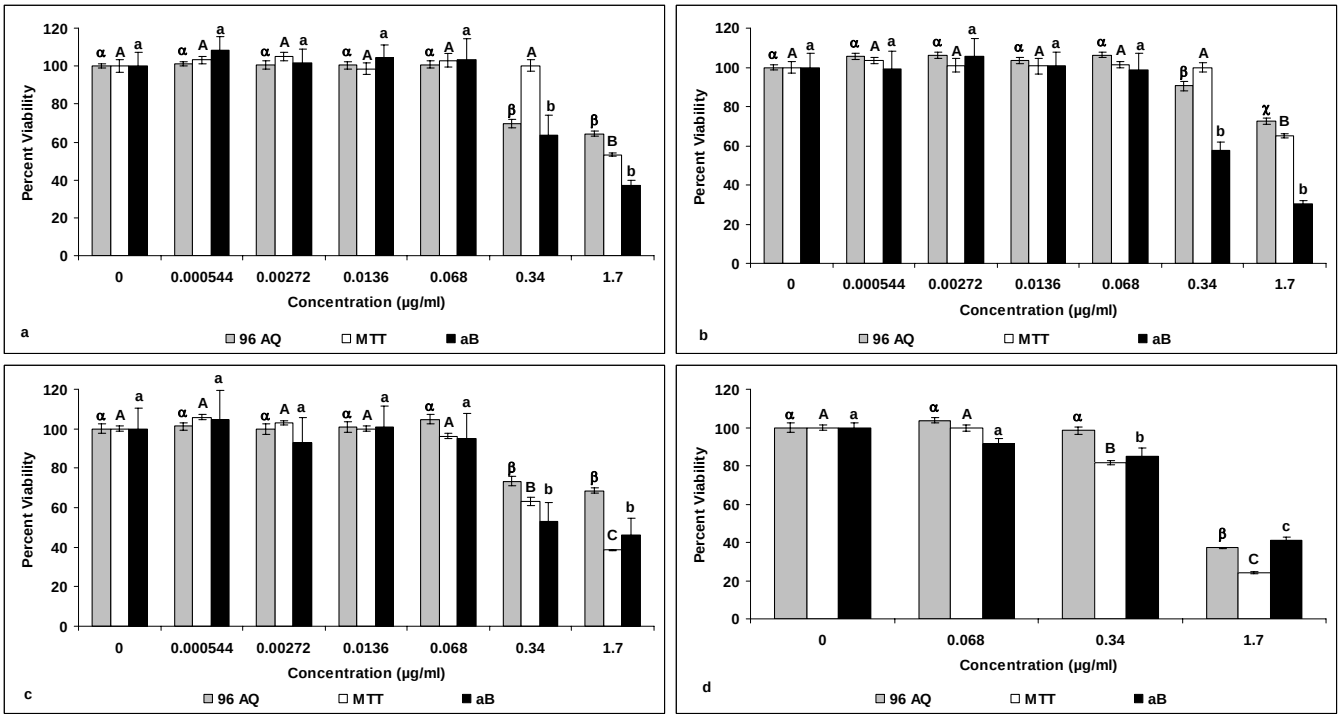

Figure 2. Comparison between the three viability assays for HEK treated with different Ag NP (a) 20nm *unwashed* and uncoated; (b) 50nm *unwashed* and uncoated; (c) 80nm *unwashed* and uncoated; (d) As synthesized *unwashed* Ag NP supernatant. Capital letters, lower case letters, or Greek letters denote significant differences ($p<0.05$) between each Ag NP at different concentrations.

Exposure of HEK to washed 20nm (Figure 3a), 50nm (Figure 3b), and 80nm (Figure 3c) Ag NP ranging in concentration from 0.000544 to 1.7µg/ml for 24h showed no significant decrease in viability with any assay. HEK treated with 25nm (Figure 4a) and 35nm (Figure 4b) carbon-coated Ag NP at concentrations ranging from 0.000544 to 1.7µg/ml for 24h did not cause a decrease in viability.

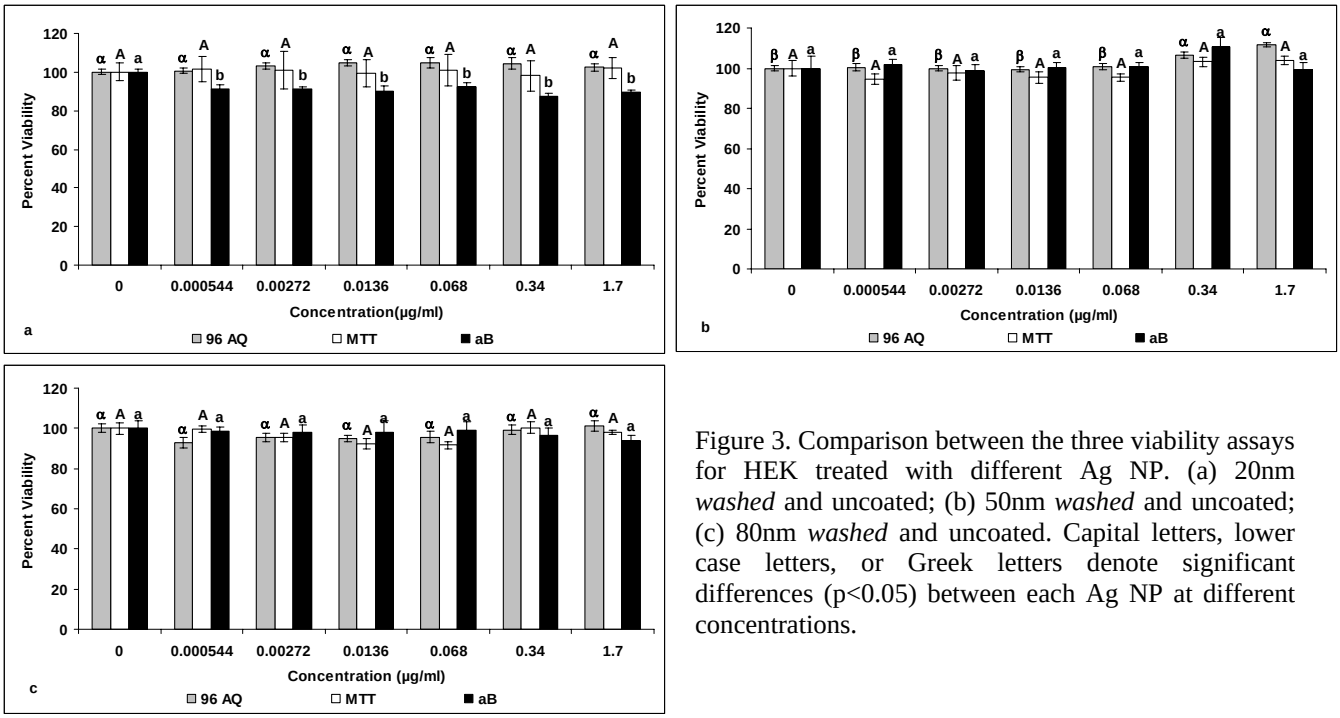

Figure 3. Comparison between the three viability assays for HEK treated with different Ag NP. (a) 20nm *washed* and uncoated; (b) 50nm *washed* and uncoated; (c) 80nm *washed* and uncoated. Capital letters, lower case letters, or Greek letters denote significant differences ($p<0.05$) between each Ag NP at different concentrations.

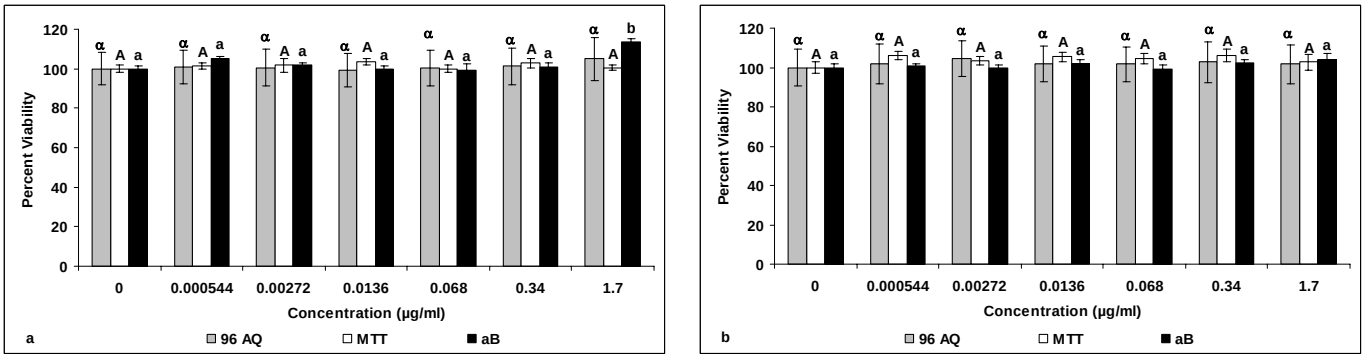

Figure 4. Comparison between the three viability assays for HEK treated with different Ag NP. (a) 25nm carbon-coated; (b) 35nm carbon-coated. Capital letters, lower case letters, or Greek letters denote significant differences ($p<0.05$) between each Ag NP at different concentrations.

The nanoparticle controls that assessed the nonspecific interactions between the Ag NP and unreacted dye showed a statistically significant increase in absorbance at the highest dosing concentration of 1.7µg/ml for the majority of Ag NP. The *unwashed* 20nm (Figure 5a), 50nm (Figure 5b), and 80nm (Figure 5c) Ag NP caused a significant increase in absorbance values at 1.7µg/ml concentration for both 96AQ and MTT assays but not for aB assays. The 20nm *washed* Ag NP caused a significant *decrease* in absorbance value at the 1.7µg/ml concentration for 96AQ and a significant increase in the aB fluorescence value at the 0.034µg/ml concentration (Figure 5d). The 50nm *washed* Ag NP caused a significant increase in absorbance values for 96AQ at the 1.7µg/ml concentration and for aB at the 0.034µg/ml concentration (Figure 5e). The 80nm *washed* Ag NP caused a significant increase in absorbance and fluorescence values at the 1.7µg/ml concentration for all three assays (Figure 5f). The 25nm carbon-coated Ag NP caused a

significant increase in absorbance values for both 96AQ and MTT assays at the 1.7µg/ml concentrations (Figure 5g). The 35nm carbon-coated Ag NP caused a significant increase in absorbance for 96AQ at the 0.034µg/ml concentration and at 1.7µg/ml for MTT (Figure 5h).

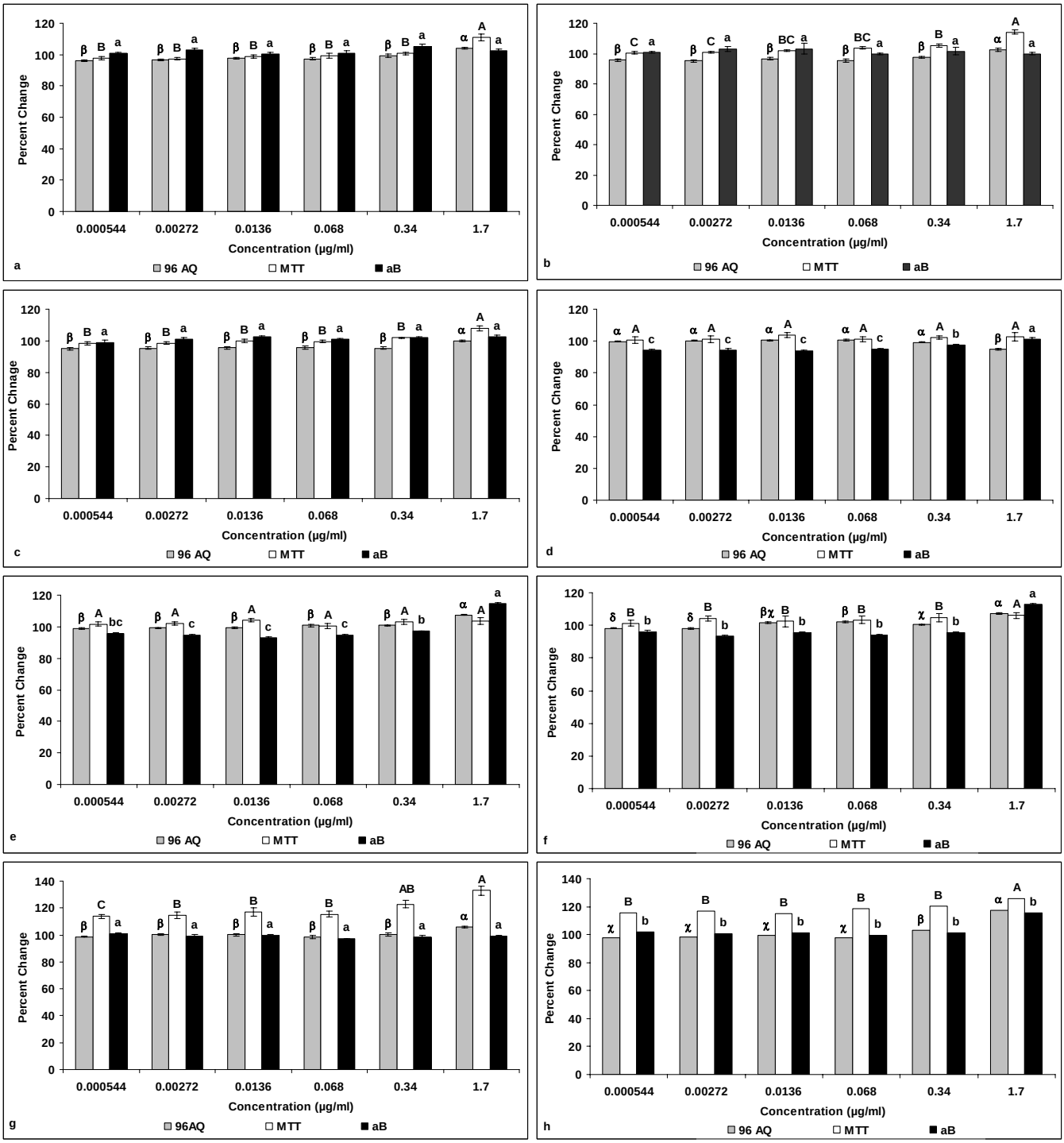

Figure 5. The nanoparticle controls indicating nonspecific interaction between each assay and Ag NP. (a) 20nm *unwashed* and uncoated; (b) 50nm *unwashed* and uncoated; (c) 80nm *unwashed* and uncoated; (d) 20nm *washed* and uncoated; (e) 50nm *washed* and uncoated; (f) 80nm *washed* and uncoated (g) 25nm carbon-coated; (h) 35nm carbon-coated. Capital letters, lower case letters, or Greek letters denote significant differences ($p<0.05$) between each Ag NP at different concentrations.

The nanoparticle/cell controls depict a statistically significant increase in Ag NP absorbance greater than for cells alone for both the 25nm (Figure 6a) and 35nm (Figure 6b) carbon-coated Ag NP at the concentration of 1.7g/ml for the MTT assay only.

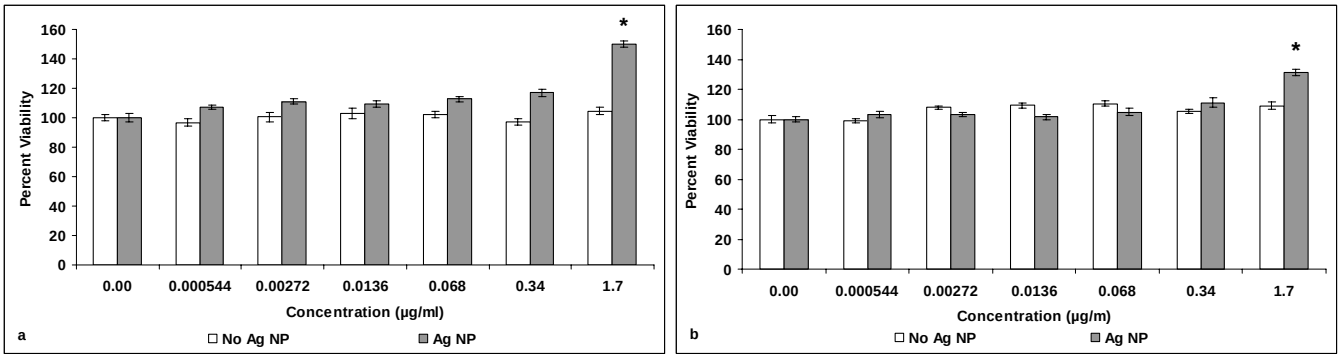

Figure 6. Nanoparticle/cell controls indicating interaction between viability assays and different Ag NP. (a) 25nm carbon-coated; (b) 35nm carbon-coated. Asterisk denotes significant differences ($p<0.05$) with paired treatment.

Cytokine release

There was a significant increase in IL-1β (Figure 7a), IL-6 (Figure 7b), IL-8 (Figure 7c) and TNF-α (Figure 7d) release from the HEK normalized to viability after exposure to 0.34µg/ml *unwashed* and uncoated 20, 50 and 80nm Ag NP for 24h. The limit of detection for each cytokine is denoted by a horizontal solid red line on each graph (IL-1β, 0.8pg/ml; IL-6, 1.1pg/ml; IL-8, 0.5pg/ml; IL-10, 0.9pg/ml; TNF-α, 3.0pg/ml). The values for IL-10 were below the detectable limit of the assay (data not shown).

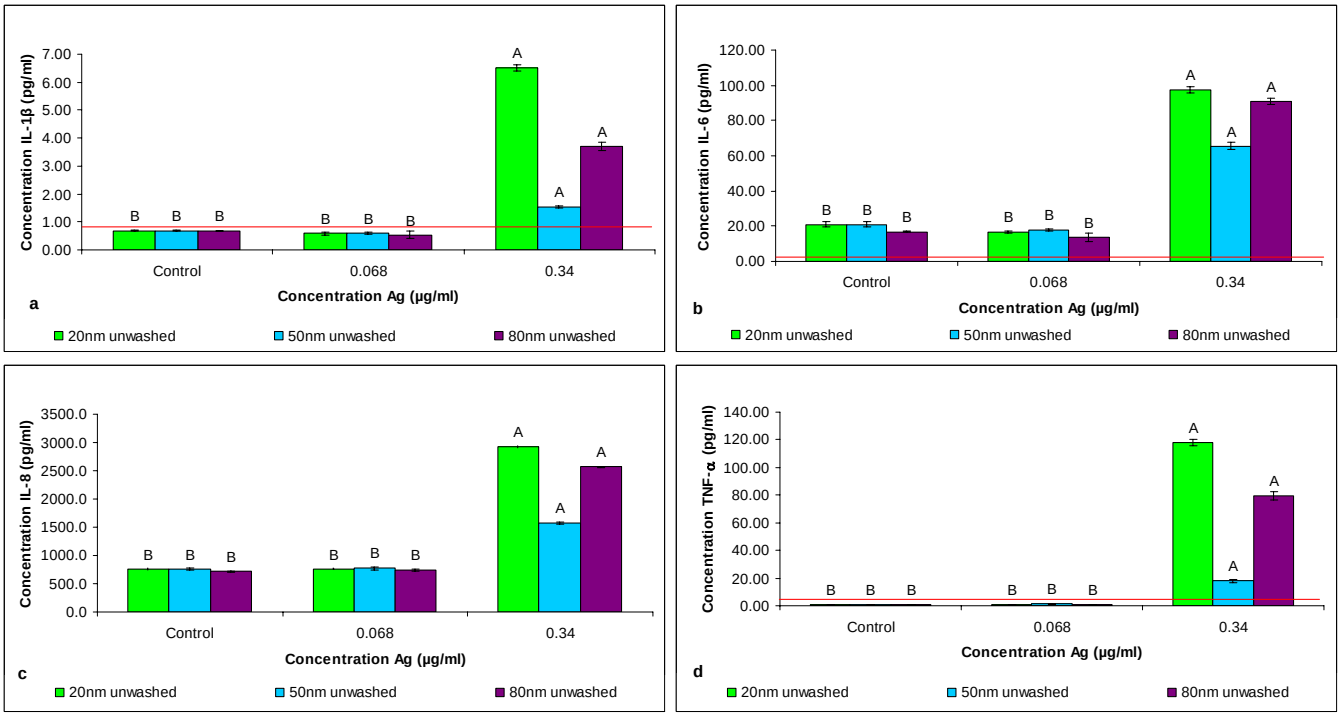

Figure 7. Cytokine release by HEK normalized to cell viability. (a) IL-1β; (b) IL-6; (c) IL-8; (d) TNF-α.. Capital letters denote significant differences ($p < 0.05$) between each nanoparticle at different concentrations. Red line denotes detectable limit for each cytokine; IL-8 detectable limit 0.5pg/ml.

Macroscopic observations of silver nanoparticles on porcine skin in vivo

No erythrema or edema was noted in any of the treated sites during the entire 14 day study. At the completion of the 14 day study, the dosed skin appeared gray but no irritation, edema, or lesions was present.

Microscopic observations

Porcine skin treated with deionized water appeared normal with a compact stratum corneum (Figure 8a). Porcine skin dosed daily with Ag NP for 14 days exhibited a concentration-dependent response, regardless of particle size or purity (washed or unwashed). Porcine skin treated with the lowest dosing concentration of 0.34µg/ml of 20nm *washed* Ag NP showed +1 intercellular epidermal edema (Figure 8b), treatment with 3.4µg/ml of the 20nm *washed* Ag NP showed +2 intracellular and intercellular epidermal edema (Figure 8c) and treatment with the highest concentration of 34µg/ml of the 20nm *washed* Ag NP showed +3 intracellular and intercellular epidermal edema with focal dermal inflammation and parakeratosis (Figure 8d).

At the lowest concentration of 0.34µg/ml, the 20nm *unwashed* Ag NP showed +1 intercellular epidermal edema (Figure 8e). Treatment with 3.4µg/ml of the 20nm *unwashed* Ag NP showed +2 intracellular and intercellular epidermal edema (Figure 8f). The highest concentration of 34µg/ml of the 20nm *unwashed* Ag NP showed +3 intracellular and intercellular epidermal edema with focal areas of intraepidermal infiltrates, superficial dermal edema and papillary inflammation (Figure 8g).

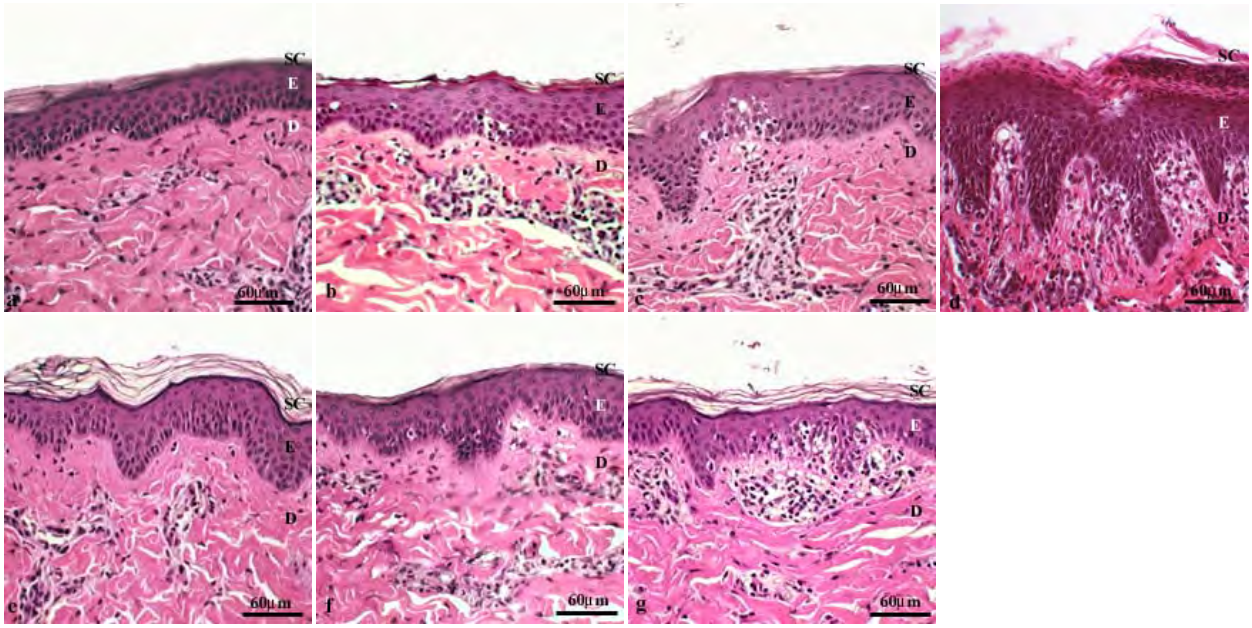

Figure 8. Porcine skin control and treated with Ag NP. (a) control; (b) 20nm washed Ag NP, 0.34µg/ml; (c) 20nm washed Ag NP, 3.4µg/ml; (d) 20nm washed Ag NP, 34µg/ml; (e) 20nm unwashed Ag NP, 0.34µg/ml; (f) 20nm unwashed Ag NP, 3.4µg/ml; (g) 20nm unwashed Ag NP, 34µg/ml. SC, stratum corneum; E, epidermis; D, dermis. H&E.

Ultrastructural observations of HEK exposed to silver nanoparticles

The untreated HEK controls appeared normal with a prominent nucleus, nucleolus and mitochondria (Figure 9a). HEK dosed with Ag NP of all sizes and surface conditions depicted Ag NP localization within membrane-bound cytoplasmic vacuoles (Figures 9b-9i).

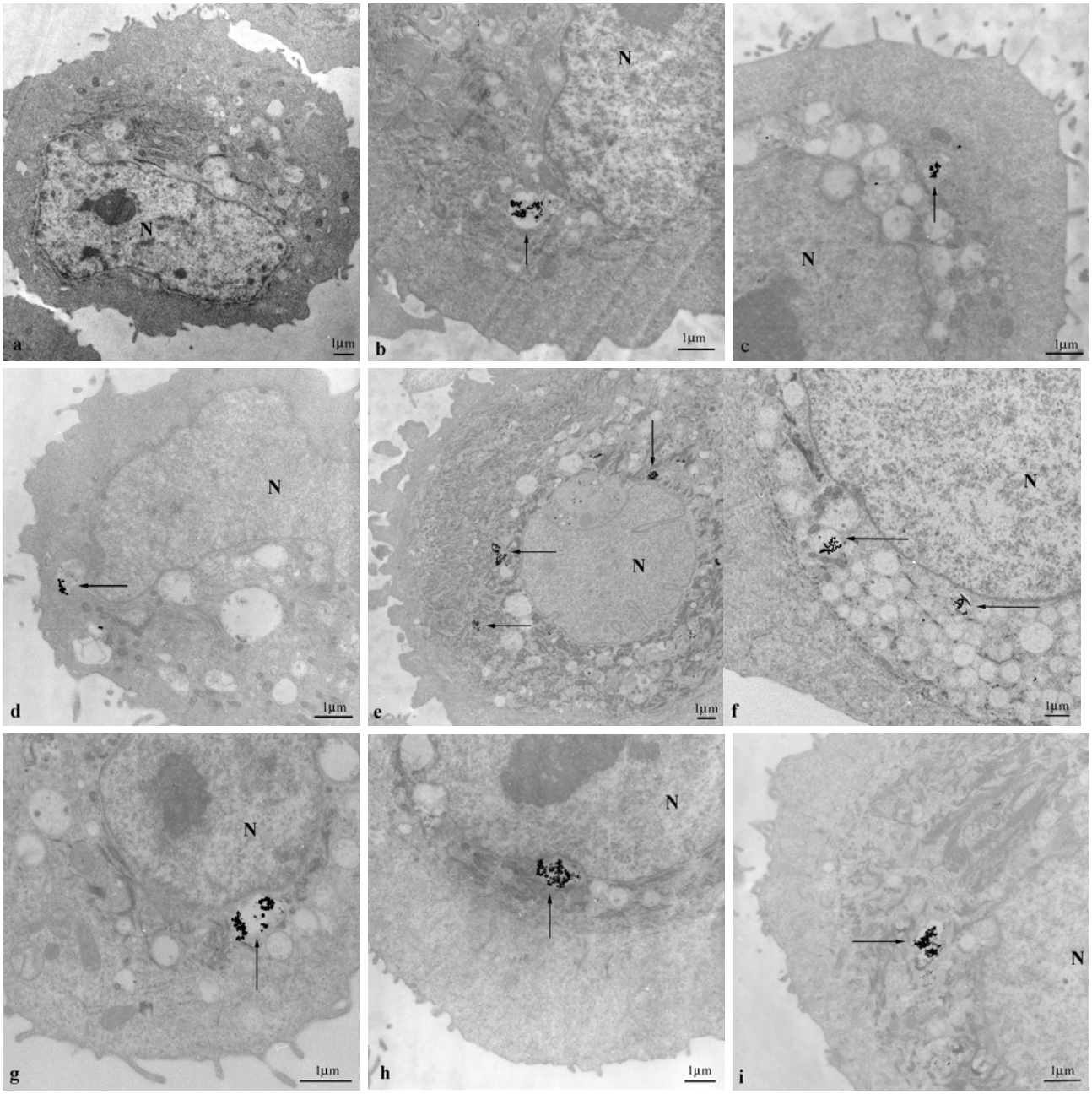

Figure 9: Transmission electron micrographs of HEK exposed to different Ag NP. (a) Control; (b) 20nm unwashed Ag NP; (c) 50nm unwashed Ag NP; (d) 80nm unwashed Ag NP; (e) 20nm washed Ag NP; (f) 50nm washed Ag NP; (g) 80nm washed Ag NP; (h) 25nm carbon-coated Ag NP; (i) 35nm carbon-coated Ag NP. Arrows identify Ag NP. N, nucleus; unstained sections.

EDS analysis of HEK dosed with the 20nm *washed*, uncoated Ag NP confirmed the presence of Ag in the vacuoles (Figure 10a). In addition, copper from the grid and Au from the particle seed was present.

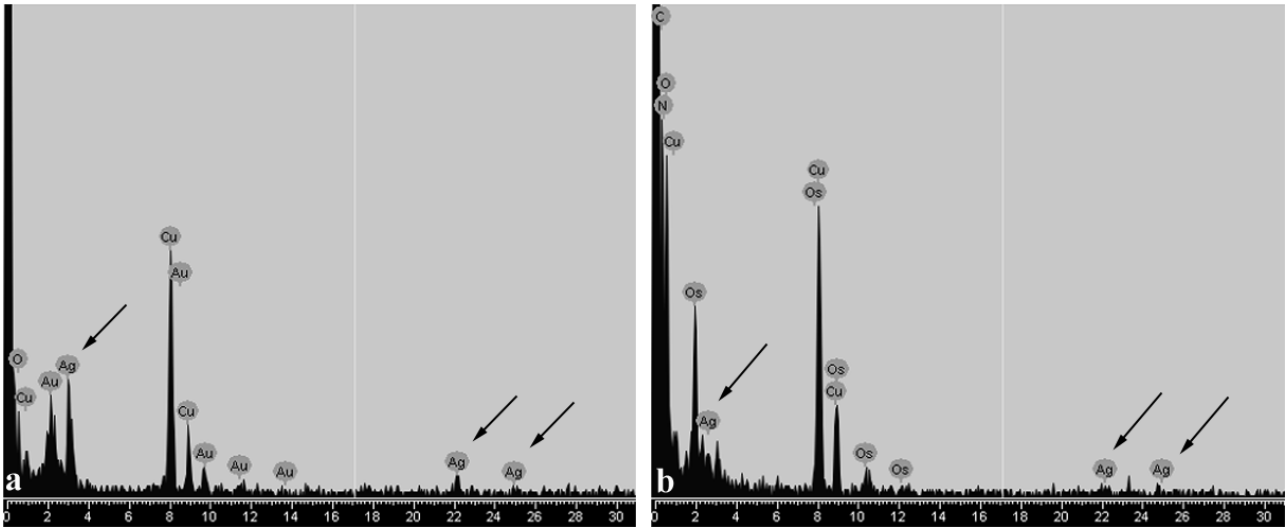

Figure 10: Energy dispersive X-ray spectrum for samples dosed with Ag NP. (a) HEK dosed with 20nm *washed* and uncoated Ag NP; (b) porcine skin dosed with 20nm *washed* and uncoated Ag NP. Arrows identify Ag peaks.

The control skin consisted of a normal compact stratum corneum with approximately 20-30 layers attached by desmosomes (Figure 11a). The porcine skin dosed daily for 14 days in vivo with 34µg/ml of the 20nm *washed*, uncoated Ag NP retained the Ag NP on the superficial layers of the stratum corneum (Figure 11b). The 50nm *washed*, uncoated Ag NP were also seen within the superficial layers of the stratum corneum (Figure 11c). EDS analysis conducted in the areas detected Ag, osmium from the post fixation process and copper from the grid (Figure 10b).

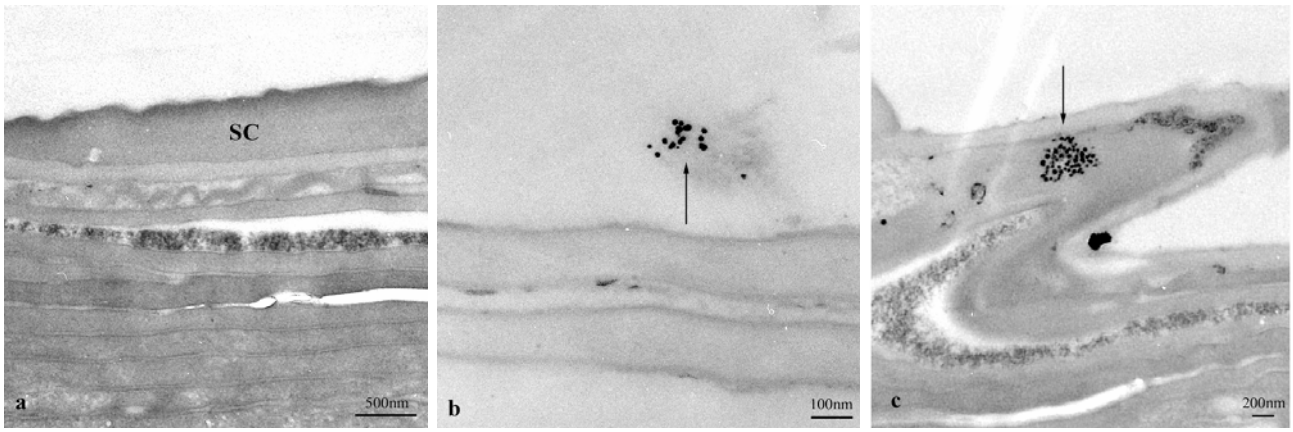

Figure 11: Transmission electron micrographs of in vivo porcine skin. (a) DI water control; (b) 20nm washed Ag NP; (c) 50nm washed Ag NP. Arrows denote Ag NP. SC, stratum corneum; unstained sections.

Discussion

Ag NP have been integrated into hundreds of products that affect the daily lives of millions of people in many countries. Their main usage is for disinfection in wound care and usage in products such as odor-reducing clothing, acne creams and face masks. The majority of these products come into direct contact with skin, the largest organ of the human body and could be a potential route for nanoparticle penetration. Therefore, the relationship of Ag NP in skin needs to be investigated with particular focus on their toxicity, penetration and localization in skin and skin cells. This study evaluated the cytotoxic potential of Ag NP of varying size and surface conditions on HEK, their penetrating capacity into porcine skin after topical repetitive daily dosing for two weeks, and the localization of the Ag NP within HEK and porcine skin.

Nanomaterials are capable of interfering with viability assay dye and dye products through the adsorption of cell medium constituents and cytokines, examples of this such as single-walled carbon nanotubes (Zhang et al., 2007), carbon black (Monteiro-Riviere and Inman, 2006), and fullerenes and quantum dots (Monteiro-Riviere et al., 2009). It is important to utilize several assays in order to determine the optimal one for use with Ag NP, and for this reason the viability of HEK was evaluated using three different assays. MTT, aB and 96AQ viability assays did not show toxicity for the 25nm and 35nm carbon-coated Ag NP as well as the 20nm, 50nm and 80nm *washed*, uncoated Ag NP. All three assays also showed that the 20nm, 50nm and 80nm *unwashed*, uncoated Ag NP contributed to a decrease in HEK viability at 24 h after exposure to the 0.34-1.7µg/ml concentrations, but did not show a size-dependent decrease in viability. However, it can be inferred that the difference in toxicity between the *unwashed* and *washed*, uncoated Ag NP is due to the presence of contaminants in the *unwashed* solution. These residual contaminants were removed by the 5^{th} wash step, as indicated by the lack of cell death after exposure to any of the 5^{th}, 10^{th}, 15^{th}, and 20^{th} washing supernatant.

The 0.34-1.7µg/ml toxic concentrations of the 20, 50 and 80nm *unwashed*, uncoated Ag NP are slightly more sensitive compared to the in vitro toxicity studies conducted by others in different cell lines. Studies on in vitro cell lines illustrate that 25µg/ml with 25nm Ag NP produce reactive oxygen species and oxidative stress that could potentially contribute to neurodegenerative diseases (Schrand et al., 2008), toxicity has been shown to hepatic cells at concentrations ranging from 5-50µg/ml of 15nm and 100nm Ag NP (Hussain et al., 2005), and to germ-line stem cells at a concentration of 10µg/ml for 15nm Ag NP (Braydich-Stolle et al., 2005). A study on HEK and fibroblasts treated with Ag NP dissolved out from commercially bought Ag-based wound dressings showed cytotoxicity at approximately 15µg/ml (Burd et al., 2007), and interactions between Ag NP ranging in size from 7-20nm and human skin carcinoma cells showed the onset of apoptosis at concentrations of 0.78µg/ml and 1.56µg/ml respectively (Arora et al., 2008).

To further identify the potential interactions between assays and Ag NP, controls were run and generally showed an increase in absorbance and fluorescence values at the highest concentration. The nanoparticle controls for MTT and 96AQ for the 20nm, 50nm and 80nm *unwashed*, uncoated Ag NP had increased absorbance values at the highest concentration of 1.7µg/ml. An increase in absorbance was found at 1.7µg/ml for MTT for the 80nm *washed*, uncoated Ag NP and for the 25nm and 35nm carbon-coated Ag NP. An increase in absorbance was also detected at 1.7µg/ml for 96AQ for 50nm and 80nm *washed*, uncoated Ag NP and for the 25nm and 35nm carbon-coated Ag NP. An increase in the fluorescence for aB was noted at 1.7µg/ml for the 20, 50 and 80nm *washed*, uncoated Ag NP and for the 35nm carbon-coated Ag

NP. The increase in absorbance and fluorescence values could cause the toxicity of the Ag NP to HEK to be underestimated. Additionally, the nanoparticle/cell control showed that both the 25nm and 35nm carbon-coated Ag NP interfered with the MTT assay at the 1.7μg/ml concentration due to the increase in absorbance values following incubation of the reduced formazan product with the Ag NP (Figure 6a and b). Overall it did not appear that any one assay was unaffected by the Ag NP, and based on its absorbance values aB may be the best viability assay to be used when conducting experiments with Ag NP, while MTT and 96AQ may be less effective.

Keratinocytes produce proinflammatory cytokines that serve as mediators for inflammatory and immunologic reactions in skin exposed to irritants (Allen et al., 2000, 2001a,b; Corsini and Galli, 2000; Monteiro-Riviere et al., 2003; Barker et al., 1991; Nickoloff et al., 1991). The proinflammatory cytokines IL-8, IL-6, TNF-α, and IL-1β have been very well studied and characterized and are regularly used as indicators of inflammation (Grone, 2002; Barker et al., 1991; Nickoloff et al., 1991). Although different toxicants may elicit different responses in HEK, studies in our laboratory have shown cytokine release by HEK in response to jet fuel exposure (Allen et al., 2000, 2001a,b; Chou et al., 2003; Monteiro-Riviere et al., 2003), multi-walled carbon nanotubes (Monteiro-Riviere et al., 2005), 6-aminohexanoic acid-functionalized single-walled carbon nanotubes (Zhang et al., 2007), and fullerenes (Rouse et al., 2006). The inflammatory potential of the Ag NP was confirmed by the increase in cytokines IL-1β, IL-6, IL-8, and TNF-α.

Nanomaterials are also capable of being internalized into cells and penetrating through the skin; QD621 have the ability to penetrate into the intercellular lipid layers of the stratum corneum of porcine skin (Zhang et al., 2008), QD 565 and 655 with diverse physiochemical properties have been shown to penetrate into the stratum corneum (Ryman-Rasmussen et al., 2006), derivatized fullerenes were localized within the intercellular space of the stratum granulosum layer of flexed excised porcine skin (Rouse et al., 2007), and multifocal pulmonary granulomas were seen to develop in rats after exposure to carbon nanotubes (Lam et al., 2004). Additionally, topical application of zinc oxide 26–30nm in a sunscreen formulation on in vitro human skin localized NP in the upper stratum corneum with minimal penetration (Cross et al., 2007) and microfine zinc oxide with a mean size of 80 nm and agglomerates of titanium dioxide less than 160 nm were not shown to penetrate the porcine stratum corneum layer of in vitro static diffusion cells (Gamer et al., 2006). To evaluate the inflammatory response and penetrating potential of the Ag NP in vivo, the established in vivo porcine skin model for human penetration was utilized due to its comparable thickness and absorption rates to human skin (Reifenrath et al., 1984; Bronaugh et al., 1982; Monteiro-Riviere and Riviere, 1996). The Ag NP ranging from 0.34μg/ml to 34μg/ml did not cause macroscopic irritation after 14 days, although the gray appearance of the skin sites might have masked the subtle signs of inflammation. When viewed microscopically focal inflammation and edema increased with an increase in Ag NP concentration. TEM depicted the localization of Ag NP in the superficial layers of the stratum corneum which was similar to results found in a static cell diffusion study (Larese et al., 2008), and suggests ionic flux into the epidermis which could attribute to focal inflammation. It is also likely that many Ag NP not bound to the skin were washed away during both light and electron microscopy processing, yet their location is confirmed by other dermal studies with NP that were not shown to penetrate the stratum corneum (Cross et al., 2007; Zhang et al., 2008; Zhang and Monteiro-Riviere, 2008). This study also showed that Ag NP of different sizes, surface conditions, and method of synthesis are all internalized into membrane-bound vacuoles in HEK.

Although a decrease in viability was not seen at 24h for the *washed* and carbon-coated Ag NP, an increase in cytoplasmic vacuoles in HEK was noted.

In summary, this study indicates that toxicity of Ag NP in HEK is influenced by the presence of residual contaminants in the Ag NP solutions, and that the Ag NP themselves may not be responsible for decreased viability. It is important for complete characterization of not only NP but also the vehicle in order to distinguish between Ag NP and contaminant toxicity. Additionally, this study showed that 20, 50 and 80nm *washed* and *unwashed* Ag NP as well as 25nm and 35nm carbon-coated Ag NP interfered and/or reacted with MTT, 96 AQ, and aB viability assays and that aB may be the best viability assay due to its lower interference with these Ag NP. Since Ag NP of several types have been shown to enter cells and remain on the skin, it is important to consider the possibility of entry into the body through damaged skin, particularly since many Ag-containing products specialize in wound care. With the ability for Ag NP to enter HEK, their degradation within the cell may create reactive oxygen species (ROS) that would be damaging to cell machinery and DNA. Given that focal inflammation, specifically intracellular and intercellular epidermal edema, was seen after 14 days of topical application of Ag NP to skin the potential for the Ag NP to cause inflammation cannot be ruled out and long term studies over several weeks should be investigated. Overall, this study provides knowledge on the toxicity and Ag NP penetration in both in vitro and in vivo as well as provides a basis for occupational and risk assessment.

C. Studies with Aluminum Nanoparticles

Introduction

Aluminum is one of the most ubiquitous elements in the environment and is covered by an oxide film that generally inhibits corrosion. Acute and chronic exposure to Al has been shown to be toxic to animals and humans (Yokel and McNamara, 2001). Al may function as a pro-oxidant to increase oxidative damage in vivo (Exley, 2004). Aluminum nanoparticles (Al NP) have medical, military, and commercial applications. Encapsulation of non-ionic, insoluble drugs by Al NP may act as a site-specific drug delivery system (Tyner et al., 2004). Iron aluminide and iron aluminum carbide have been shown to be corrosive resistant and have a higher tensile strength. The military has used Al NP in explosives and in artillery surface coatings. Metastable intermolecular composites (MIC) are mixtures of metallic nano powders that possess exothermic properties. Metallic mixtures of Al particles possess these properties and the energy released after explosion has been shown to be based on the size of the particle (Miziolek, 2002). The US Navy is investigating the use of Al NP in lithium batteries to improve performance, as a replacement for lead primers in artillery, and as resistant coatings on propeller shafts (Looney, 2004). The US Army is pursuing the use of Al NP in ammunition and explosives, while NASA is investigating the use of Al NP in solid rocket fuel. One of the major interests of Al NP for the US Air Force is in rocket fuels. Al NP have been added to increase the specific impulse of a composite propellant and later found that due to their small particle size combustion was much improved. Al has been used for fuel in boosters and key missiles such as the Polaris rockets A1-A3, the Minuteman I rockets stage 1-3, the Titan 3 solid rocket motors, and the current space shuttle solid rocket booster (Hunley, 1999). It has been suggested that in the mission to Mars the addition of Al NP to solid rocket fuel could increase the specific impulse of a stable composite propellant. NASA has indicated that 20-100nm Al NP covered by a 2-3nm coating of aluminum oxide (Al_2O_3) produces new nanoengineered metallized gelled fuels. These fuels provide higher density, added safety, reduced fuel slosh and leakage, and increased exhaust velocity (Palaszewski, 2002). Researchers have also found that adding Al NP to diesel fuel may significantly improve the radiative and heat/mass transfer properties and cause the fuel droplets to ignite at a much lower temperature. Commercial uses of Al and Al oxide NP include scratch-resistant and abrasive-resistant coatings on sunglasses, car finishes, and flooring. Aluminum oxide NP, which have good dielectric and abrasive properties, have been studied as potential orthopedic implants and may be more effective with fewer adverse affects than conventional materials of larger size on bone structure (Gutwein and Webster, 2004). Alumina particles have caused the release of inflammatory mediators in co-cultures of mouse macrophages and primary cultured human osteoblasts (Rodrigo et al., 2006). Endothelial cells exposed to alumina NP exhibit an increase in mRNA and protein expression of VCAM-1, ICAM-1, and ELAM-1 as well as an increase in adhesion to monocytes (Oesterling et al., 2008).

In earlier studies, Al NP with a diameter of 30nm caused no mortality in immortalized mouse keratinocytes and endothelial cells (Rooney et al., 2004). An increase in Al concentration in the body has been shown to cause neurotoxicity, while many Al salts are irritating and corrosive to the skin such as aluminum borohydride used in jet fuels (Burrows et al., 1999). Exley et al. (2007) suggested that Al in antiperspirants may even cause breast cancer. Al in drinking water and food has been implicated as a potential factor in cognitive impairment in the elderly and in Alzheimer's disease (Flaten, 2001). It is well known that the physicochemical

properties and concentration of NP will determine their toxicity (Monteiro-Riviere and Tran, 2007). Studies by Yang and Watts (2005) showed that Al NP coated with phenanthrene can reduce toxicity. Similar results in our lab have shown that the surface coatings on quantum dots (QD) determines their penetration, cytotoxicity, and irritation potential (Ryman-Rasmussen et al., 2007).

Cytotoxicity assays provide accurate assessment on viability for classic small molecule cytotoxicity studies, but have proven less than reliable when assessing NP. Recent studies have shown that viability assays on cells treated in culture with carbon-based nanomaterials provide inaccurate results (Monteiro-Riviere and Inman, 2006; Wörle-Knirsch et al., 2006; Casey et al., 2007; Monteiro-Riviere et al., 2009). While the affect of metallic NP on viability assays has not been reported, metal oxide NP have been shown to adsorb components of cell culture media and thus influence the cytotoxicity evaluation (Horie et al., 2009). The interactions of Al NP with the viability assays MTT, CellTiter 96® AQueous One (96 AQ), and alamar Blue® (aB) must be determined before accurate viability results can be correctly interpreted.

The objective of this study is to determine the cytotoxic effects of varying concentrations of two sizes (50nm and 80nm) of Al NP in human epidermal keratinocytes (HEK) and to determine their inflammatory potential. This study also evaluated the effect of three viability assays with Al NP to determine the optimal assay to assess HEK exposure to metallic NP.

Materials and Methods

Nanoparticles: Commercially available Al NP, 50nm (Al50) and 80nm (Al80) in diameter with a 2-5nm oxide coat, were synthesized and provided by nanoComposix (San Diego, CA). Nanoparticles were highly agglomerated and spheroidal in shape, with a light gray appearance. Initial characterization of the 50nm and 80nm NP is summarized in Table 2.

Table 2. Characterization properties of the 50nm and 80nm Al NP.

	50 nm Al NP	**80 nm Al NP**
TEM Diameter (nm)	47.5 ± 24.6	60.1 ± 30.5
Coefficient of Variation (%)	52.8	50.7
TEM Minimum/Maximum Diameter (nm)	7.3 / 125.8	11.3 / 240.2
DLS Hydrodynamic Diameter (nm)	215 ± 99	210 ± 95
Zeta Potential (mV)	35	42

Nanoparticle characterization: The Al NP were suspended in deionized water and in serum-free keratinocyte growth medium (KGM-2) and size measurement characterization carried out by dynamic light scattering (DLS) with a Zetasizer Nano-ZS (Malvern Instruments, Inc). The readings were taken at 25ºC (standard characterization temperature) and at 37ºC (cell culture conditions) immediately after preparation (t = 0h) and after a 24h incubation at 37ºC (t = 24h). The measurements were repeated five times, with the number of runs (typically 12 to 20) and other parameters (e.g., attenuation) optimized by the instrument software. Data was culled based on the Correlogram, Size Quality Report, and Expert Advise rendered by the software (Dispersion Technology Software, version 5.03). The NP size was also determined by

transmission electron microscopy (TEM). The Al NP were suspended in deionized water at a concentration of 0.4mg/ml, pipetted onto a formvar-coated grid, and air-dried overnight at room temperature. The samples were photographed on a FEI/Philips EM208S transmission electron microscope operating at an accelerating voltage of 80KV. In addition, the samples were analyzed by X-ray microanalysis (EDS) on a Hitachi HF2000 FE transmission electron microscope equipped with an Oxford Instruments INCA EDS operating at an accelerating voltage of 200KV.

UV/Vis Spectrum: These measurements were conducted to determine interactions of the metallic NP with the viability assays. Al NP were suspended in centrifuge tubes containing MTT medium (0.5 mg/ml in KGM-2), 96 AQ medium (20µl/100µl KGM-2), or aB medium (10µl/100µl KGM-2) at 4.0, 0.4, 0.04, 0.004, and 0.0004mg/ml and incubated for 3h. For MTT, the NP were pelleted by centrifugation, rinsed, and extracted with isopropanol. The extracted solutions and the 96 AQ medium from each Al NP concentration were transferred to quartz cuvettes and absorbance quantitated at intervals from 300-700nm on a Spectronic Genesys 5 UV-Vis spectrophotometer (Thermo-Fisher Scientific). The aB medium was transferred to a black plate and fluorescence read at intervals between 565-640nm on a Spectra Max Gemini EM spectrophotometer with the excitation/emission wavelength 545nm/590nm.

Nanoparticle controls: These controls, similar to the UV/Vis measurements, determined whether the NP interfered with the assay to cause a false-positive result. Each well of a 96-well plate was coated with rat tail collagen to enhance adhesion and the Al NP added at 4.0, 0.4, 0.04, 0.004, 0.0004mg/ml. The controls (n=6 wells/treatment) were incubated for 24h, centrifuged to pellet the Al NP, and the KGM-2 medium replaced with MTT, 96 AQ, or aB medium for 3h. The absorbance or fluorescence was read as above.

Cell culture: Cryopreserved first pass neonatal HEK (Lonza Walkersville, Inc.) were seeded in $75cm^2$ flasks and grown to ~75% confluency, harvested, and plated in the inner wells of 96-well plates at 12,500 cells/well in KGM-2 medium. Medium was placed in the peripheral wells of the plate to help stabilize plate temperature and minimize evaporation from the inner wells. The cells were grown for 18h in a 5% CO_2 atmosphere at 37ºC. The stock solution (4.0mg/ml) was prepared in KGM-2 by a brief agitation followed by 30 min sonication, then serially diluted to provide dosing solutions at 0.4, 0.04, 0.004, and 0.0004mg/ml. HEK were exposed to each dosing solution (n=24-30 wells/treatment, 6 wells/plate) for 24h. The medium was harvested and stored at -80ºC for analysis of cytokines and the viability of the cells assayed by MTT (Sigma/Aldrich), 96 AQ (Promega Corp), and aB (Invitrogen).

Photographs from the 0.4, 0.04, and 0.004 experiments performed on different days were analyzed to determine the size of the Al NP agglomerates. The size could not be determined in the 4.0mg/ml treatment because NP agglomerates had completely covered the field of view or in the 0.0004mg/ml treatment since the NP agglomerates were below the resolution of the microscope. Agglomerates were selected randomly and the area of each calculated.

Cytotoxicity assays: The treatment medium was harvested from each well and the cells were incubated with MTT medium for 3h. The tetrazolium dye was extracted from the cells, transferred to a new plate, and the absorbance quantitated at 550nm (Multiskan RC plate reader, Labsystems). For 96 AQ, 100µl of medium was removed from each well, 20µl of the 96 AQ solution was added, and cells incubated for 3h. The solution was transferred to a new plate and

the absorbance quantitated at 450nm. For the aB assay, 100µl of medium was removed from each well of a black plate, 10µl of aB solution added to each well, and the cells incubated for 3h. The fluorescence was quantitated (top read) on a Spectra Max Gemini EM spectrophotometer with the excitation/emission wavelength 545nm/590nm. The values for all assays were normalized by the controls and expressed as percent viability. The plates were centrifuged after incubation to help ensure the NP did not interfere with the absorbance or fluorescence readings.

The NP/cell controls (n=6 wells/treatment) determined how the NP affected the assay after the dye/reagent reacted with the viable cells. HEK media was changed rather than treated with NP and normal HEK viability assayed at 24h. Plates containing the Al NP concentrations (without cells) were incubated in parallel. Once the viability of the normal HEK were assayed, the dye/reagent was transferred to the parallel Al plates and incubated for 3h. The difference in the absorbance or fluorescence after incubation with the Al indicated the affect on the dye/reagent. For these controls, the plates were centrifuged to help ensure the NP did not interfere with the readings.

Intralaboratory controls and particle controls were carried out to verify the integrity of the HEK from stock. For the intralaboratory controls, HEK were treated with serial dilutions of SDS (99%; Sigma-Aldrich) for 24h. The calculated LD50 value was consistent with previous HEK stock (Monteiro-Riviere et al., 2009). For particle controls, HEK viability was determined after 24h exposure to Min-U-Sil 5 (U.S. Silica). As previously shown (Monteiro-Riviere et al., 2009), the silica particles interacted with the viability assays to affect results.

Cytokines: The human cytokines IL-8, IL-6, IL-1β, IL-10, and TNF-α were quantitated by multiplexing with the Bio-Plex suspension array system (Bio-Rad Laboratories). Treatment and control media from the 96 AQ experiment were incubated with the capture antibody (conjugated to beads), fluorescently labeled, and analyzed. The cytokines were quantitated relative to a standard curve. The limit of detection for each cytokine is as follows: IL-8, 0.5pg/ml; IL-6, 1.1pg/ml; IL-1β, 0.8pg/ml; IL-10, 0.9pg/ml; TNF-α, 3.0pg/ml). The data from each cytokine was normalized to the 96 AQ viability data.

To determine if the Al NP interact with the cytokine assay, Al50 and Al80 medium was spiked with each cytokine standard to provide a final NP concentration of 0.4mg/ml at highest concentration on the standard curve for each cytokine (e.g., 1793.6pg/ml for IL-8; 2337.7pg/ml for IL-6; 2821.7pg/ml for IL-1β; 5665.7pg/ml for TNF-α).

TEM/EDS: To study nanoparticle uptake in HEK, the cells were grown to 70% confluency in 25cm^2 flasks and exposed to 0.4mg/ml Al NP for 24h. The HEK were harvested with trypsin/EDTA, rinsed in Hanks' Balanced Salt Solution (HBSS), and fixed in Trump's fixative. The cells were rinsed in phosphate buffer, embedded as a pellet in 3% agar, and post-fixed in 1% osmium tetroxide. The cells were rinsed in distilled water, dehydrated through graded ethanols, cleared in acetone, and infiltrated and embedded in Spurr's resin. Thin sections (~800Å) were mounted on copper grids and examined unstained on a FEI/Philips EM208S TEM and analyzed by X-ray microanalysis (EDS) on a Hitachi HF2000 FE TEM equipped with an Oxford Instruments INCA EDS.

Statistics: The mean values for percent viability and cytokine concentration for each treatment were calculated and the significant differences ($p<0.05$) determined using the PROC GLM Procedure (SAS 9.1 for Windows). When significant differences were found, multiple

comparisons were performed using Tukey's Studentized Range HSD test at $p<0.05$ level of significance.

Results

The hydrodynamic size of the Al NP dispersed in deionized water was consistent from 0h and 24h and at 25ºC and 37º (Table 3).

Table 3. Hydrodynamic diameter (nm) of the 50nm and 80nm Al NP suspended in distilled water by DLS at different times and temperatures.

	25ºC Mean ± SEM	37ºC Mean ± SEM
50nm in Water at 0h	325.8 ± 12.6	263.8 ± 11.2
50nm in Water at 24h	327.6 ± 14.7	615.5 ± 18.0
80nm in Water at 0h	294.1 ± 18.7	309.0 ± 7.3
80nm in Water at 24h	375.6 ± 24.7	369.5 ± 0.5

The size increase was slight to moderate by 24h, with the exception of the Al50 at 37ºC which more than doubled in size. The hydrodynamic size of the Al50 and Al80 were much larger in the KGM-2 cell culture medium, and increased from 25ºC to 37ºC (Table 4).

Table 4. Hydrodynamic diameter (nm) of the 50nm and 80nm Al NP suspended in KGM-2 medium by DLS at different times and temperatures.

	25ºC Mean ± SEM	37ºC Mean ± SEM
50nm in KGM-2 at 0h	3217.5 ± 130.5	7893.0 ± 27.0
50nm in KGM-2 at 24h	3725.5 ± 214.5	4741.0 ± 812.0
80nm in KGM-2 at 0h	4825.0 ± 605.0	9539.0 ± 415.0
80nm in KGM-2 at 24h	3104.0 ± 402.0	14940.0 ± 1920.0

Unlike the Al NP in water, the sizes did not consistently increase from 0h to 24h. The appearance of the Al NP in water changed over time, becoming white by 24h. The appearance of the NP in the KGM-2 remained light grey over time. The Al50 and Al80 dried onto formvar-coated grids showed some agglomeration (Figures 12a and 12b). A few of the Al NP were more electron dense, presumably due to a thicker oxide coating caused by suspension in deionized water. The TEM EDS spectrum confirmed that the NP were Al (Figures 12c and 12d). Copper peaks were also noted in the spectrum, originating from the Cu grids on which the Al NP were deposited.

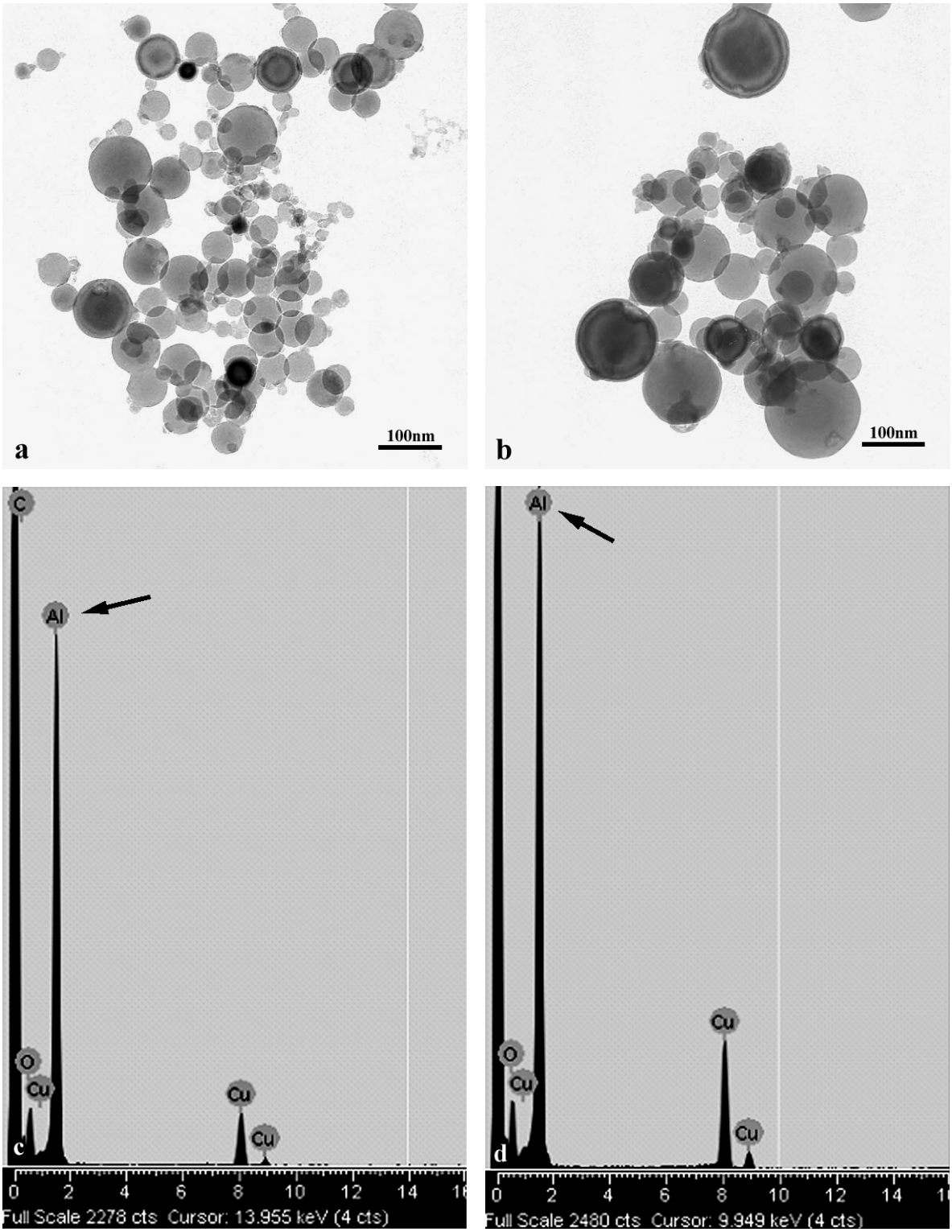

Figure 12. Transmission electron micrographs of Al NP diluted to 0.4mg/ml in deionized water and dried down on a formvar-coated grid. (a) 50nm NP ; (b) 80nm NP ; (c) TEM EDS spectrum of 50nm NP ; (d) TEM EDS spectrum of 50nm NP. Arrows denote Al peak.

The UV-Vis spectrum for the MTT medium peaked at 550nm for both the Al50 (Figure 13a) and Al80 (Figure 13b). Al NP at a concentration of 0.4mg/ml caused the highest absorbance while the medium control (no Al NP) caused the lowest absorbance. The 96 AQ medium peaked at 400nm, with no absorbance differences between any of the Al50 or Al80 concentrations (Figures 14a and 14b). For aB, the spectrum peaked at 590nm; the Al NP at a concentration of 4.0mg/ml caused a higher fluorescent intensity than the media containing lower Al NP concentrations (Figures 15a and 15b).

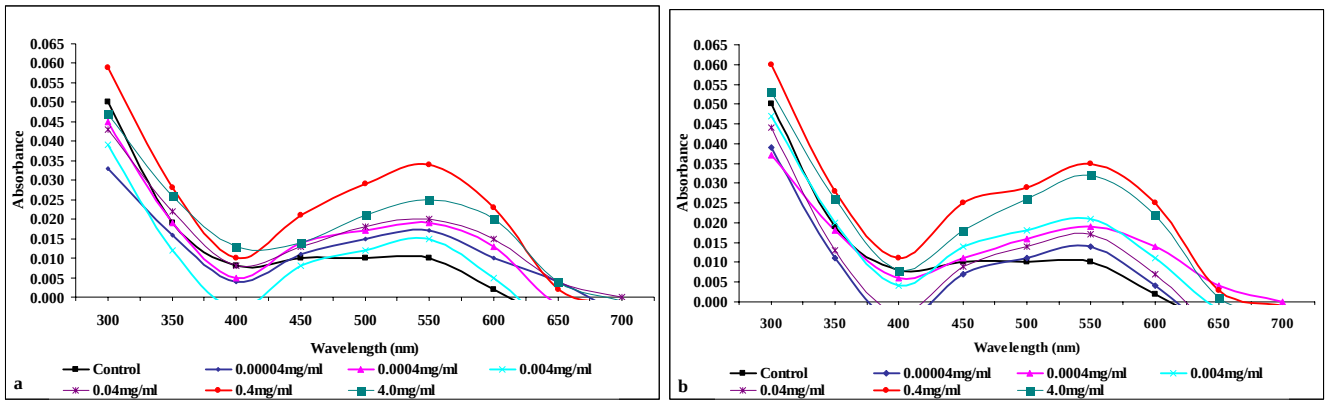

Figure 13. UV/Visible spectrum with MTT. (a) 50nm Al and (b) 80nm Al.

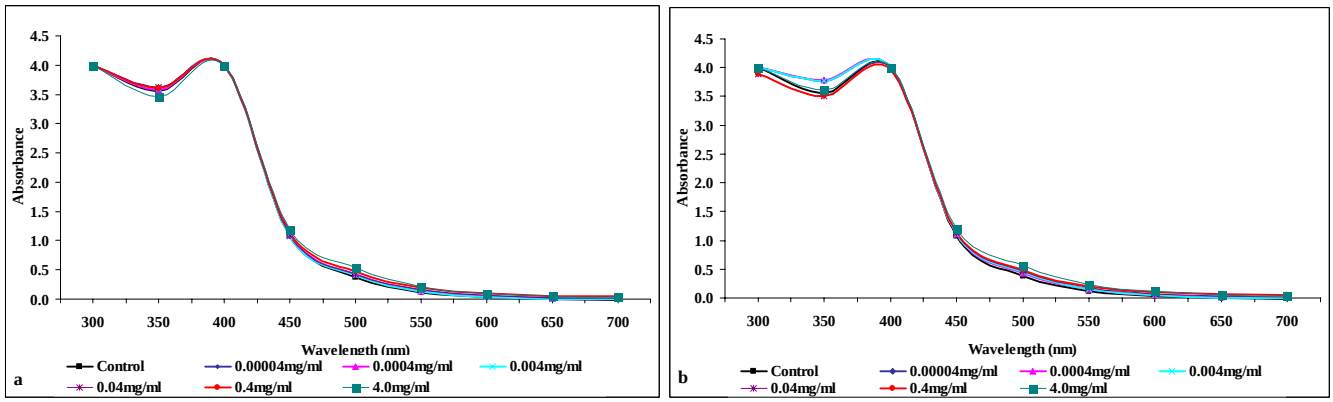

Figure 14. UV/Visible spectrum with 96 AQ. (a) 50nm Al and (b) 80nm Al.

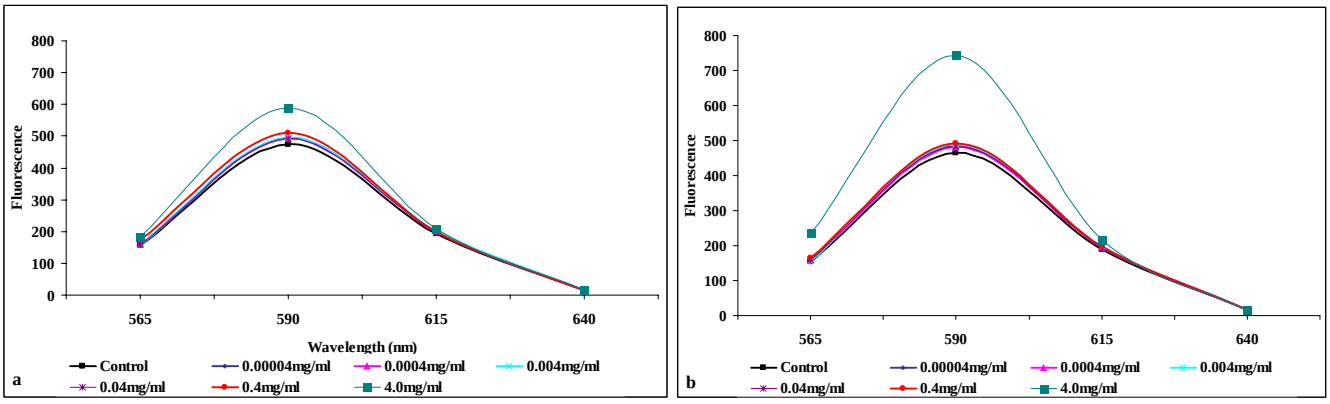

Figure 15. UV/Visible spectrum with aB. (a) 50nm Al and (b) 80nm Al.

The nanoparticle controls show that Al NP caused a significant ($p<0.05$) increase above the medium alone in the absorbance or fluorescence values. Al50 caused a significant increase in MTT absorbance at 0.4 and 4.0mg/ml, while Al80 caused an increase at 4.0mg/ml (Figure 16a). With 96 AQ, Al50 caused a significant increase from 0.04 to 4.0mg/ml while Al80 caused an increase at 0.4 and 4.0mg/ml (Figure 16b). A significant increase in aB fluorescence was caused by 0.4 and 4.0mg/ml Al50 (Figure 16c).

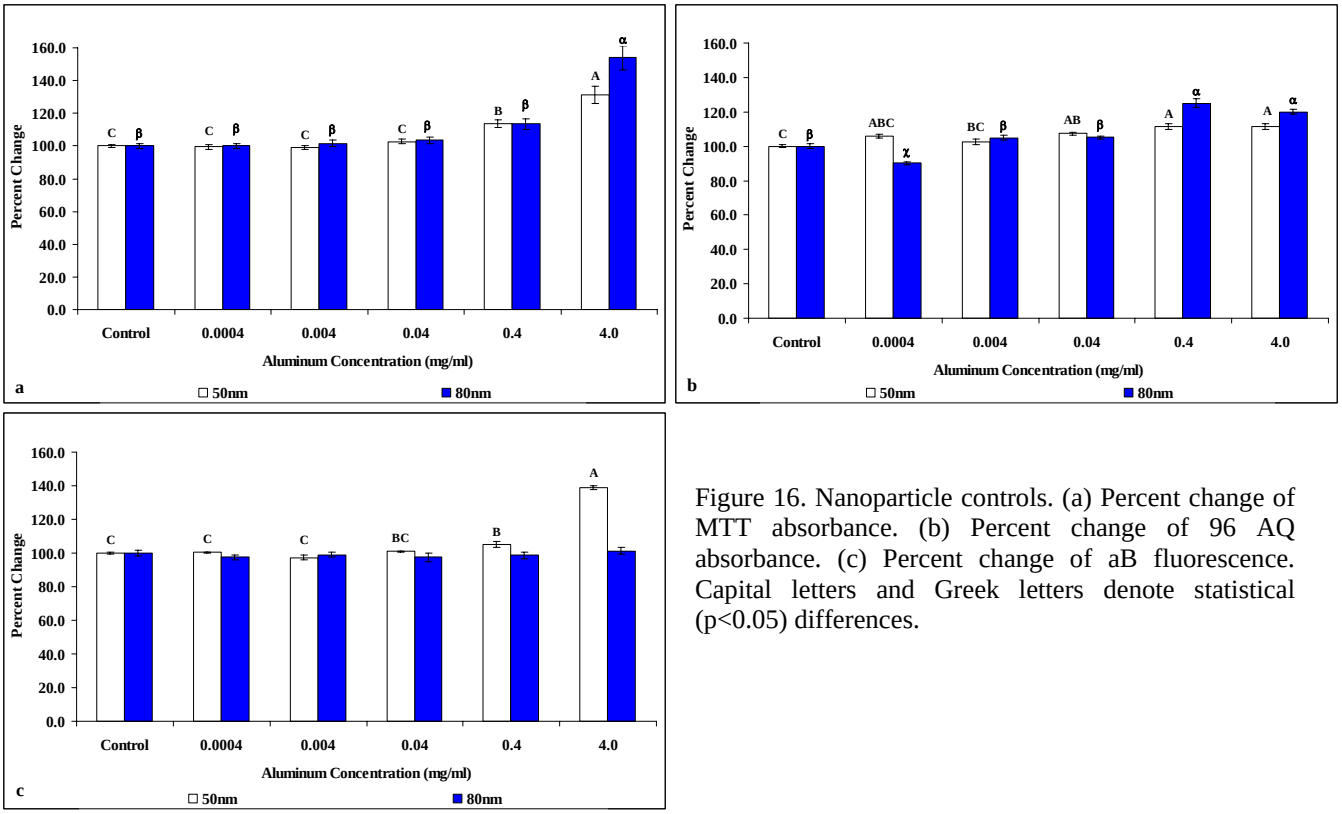

Figure 16. Nanoparticle controls. (a) Percent change of MTT absorbance. (b) Percent change of 96 AQ absorbance. (c) Percent change of aB fluorescence. Capital letters and Greek letters denote statistical ($p<0.05$) differences.

Cell culture: Al NP agglomerates remained on the surface of the HEK monolayers for 24h (Figures 17a and 17b). The number and the size of the Al agglomerates increased as Al NP concentration increased from 0.004 to 0.4mg/ml and as Al NP size decreased from 80nm to 50nm (Table 5).

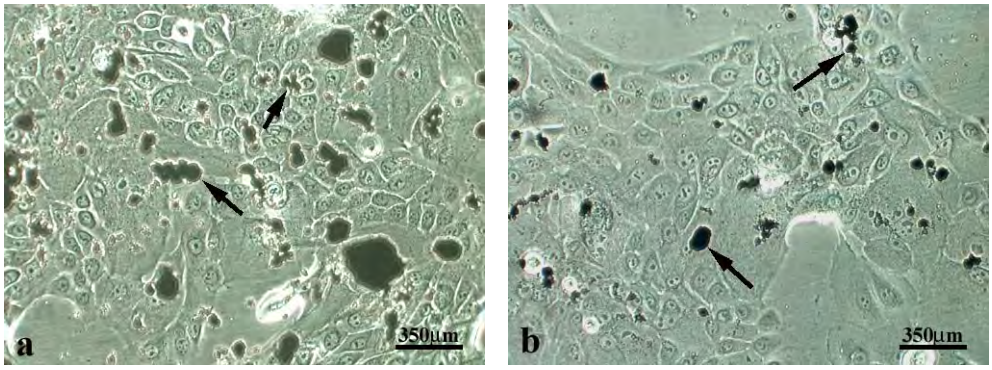

Figure 17. Light micrograph of HEK monolayer 24h post-treatment with 0.4mg/ml Al NP (a) 50nm Al NP and (b) 80nm Al NP settled onto the HEK monolayer. Arrows denote large agglomerates of the NP.

Table 5. Size of agglomerates present in HEK cultures treated with different concentrations of Al NP.

	50nm Al NP	80nm Al NP
0.004 mg/ml	18.1 ± 2.9	6.8 ± 1.2
0.04 mg/ml	34.6 ± 3.4	22.6 ± 5.2
0.4 mg/ml	152.4 ± 24.7	106.5 ± 19.8

HEK viability following treatment with the 50nm and 80nm Al NP appeared to increase with NP concentration when assessed by MTT (Figure 18a), 96 AQ (Figure 18b), and aB (Figure 18c). The UV/Vis measurements and the nanoparticle controls prove that this apparent increase is due to interference of the Al NP with the assay and thus artifact. The NP/cell controls show that Al NP further affected viability data. Al50 caused a significant ($p<0.05$) increase in absorbance of the 96 AQ medium at 0.004 and 0.4mg/ml and a significant increase in fluorescence of the aB medium at 0.0004, 0.4, and 4.0mg/ml.

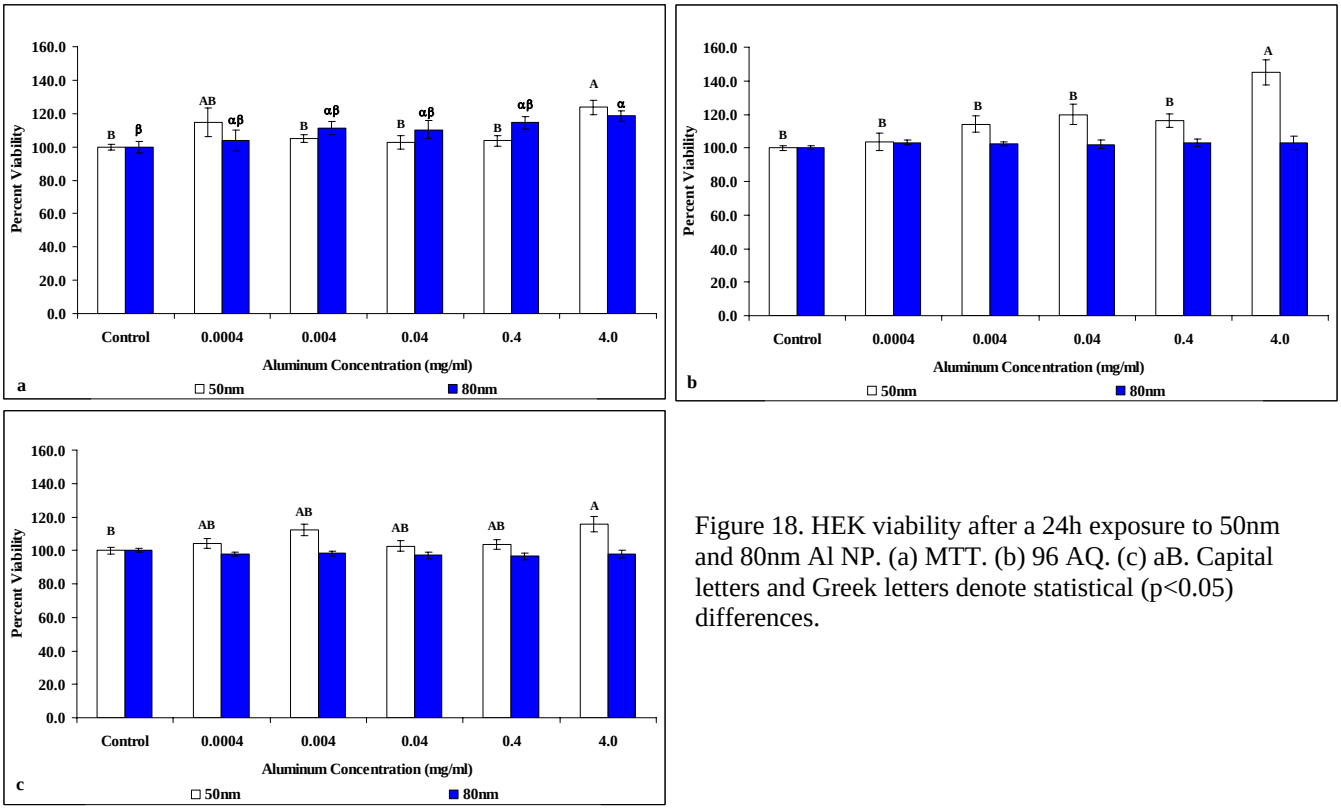

Figure 18. HEK viability after a 24h exposure to 50nm and 80nm Al NP. (a) MTT. (b) 96 AQ. (c) aB. Capital letters and Greek letters denote statistical ($p<0.05$) differences.

HEK treated with 4.0mg/ml of the 50nm Al released significantly less IL-8 than the other treatments and control, while 4.0mg/ml of the 80nm Al release was significantly greater at 0.0004 to 0.4mg/ml than at 4.0mg/ml and in the control (Figure 19a). The profile of the normalized IL-6 was similar to the normalized IL-8 (Figure 19b). Normalized IL-β in the Al50 treatment decreased with an increase in concentration, with the 4.0mg/ml treatment significantly less than the control (Figure 19c). No significant concentration differences were noted in the normalized TNF-α profiles (Figure 19d). Normalized IL-10 values were below the standard

curve of the assay. Media spiked with each cytokine standard and exposed to Al for 24h showed a reduction of 16.1% (Al50) and 32.3% (Al80) in IL-8, 26.8% (Al50) and 28.6% (Al80) in IL-6, 33.9% (Al50) and 49.8% (Al80) in IL-1β, 50.8% (Al50) and 60.8% (Al80) in TNF-σ, and 62.6% (Al50) and 61.1% (Al80) in IL-10.

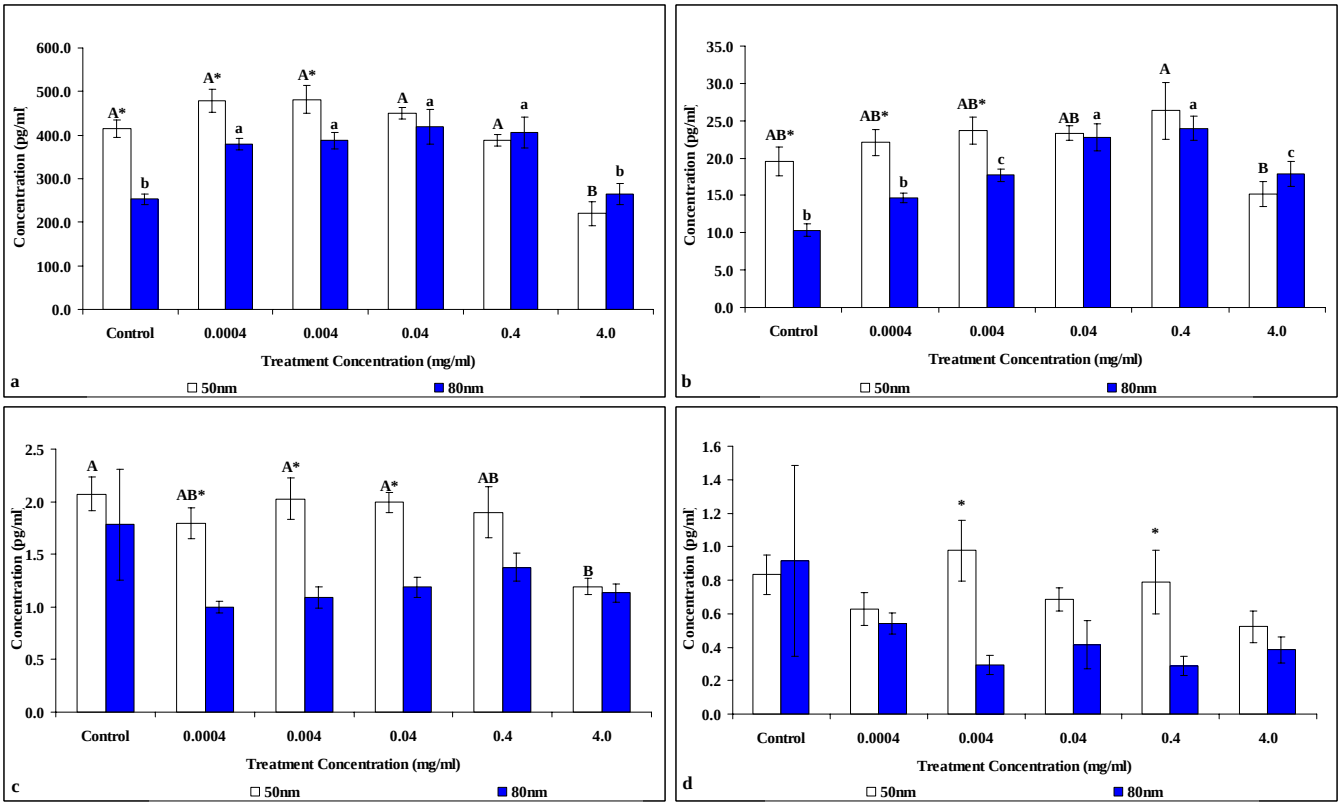

Figure 19. Normalized cytokine concentration released from HEK 24h after treatment with 50nm and 80nm Al NP. (a) IL-8; (b) IL-6; (c) IL-1β; (d) TNF-α. Capital letters and lower case letters denote statistical ($p<0.05$) differences. * denotes statistically greater ($p<0.05$) than paired treatment.

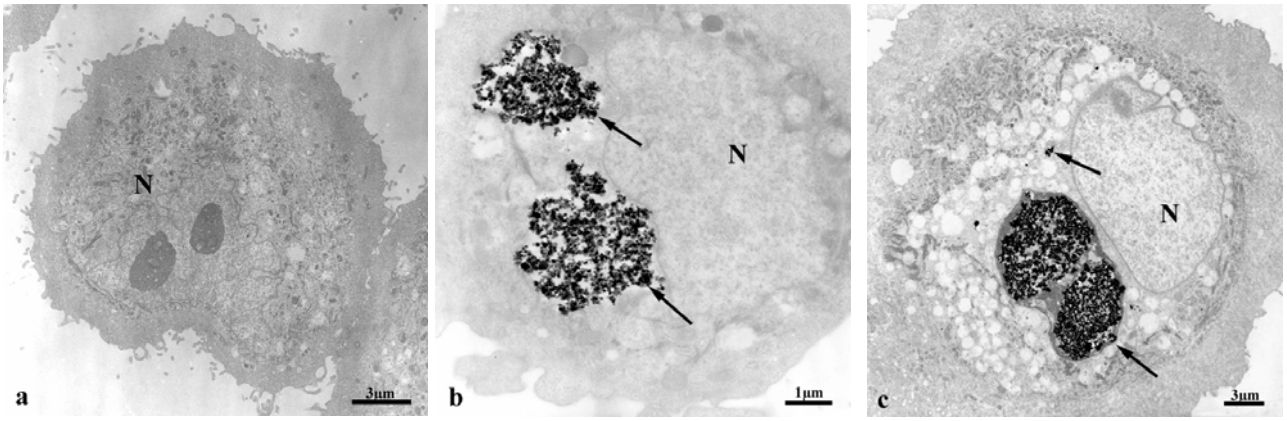

Figure 20. Transmission electron micrographs of HEK 24h after treatment. (a) Control, media only; (b) 50nm Al NP treatment; (c) 80nm Al NP treatment. Arrows denote Al agglomerate in cytoplasmic vacuoles located around the periphery of the nucleus.

TEM of HEK exposed to 50nm (Figure 20b) and 80nm (Figure 20c) Al NP depicted the Al NP within numerous large cytoplasmic vacuoles near the nucleus in HEK compared to nontreated controls (Figure 20a). Individual or agglomerated Al NP were present within the vacuoles, but were not detected along the plasma membrane at the periphery of the cell. EDS found only Cu (copper grid) peaks in the control (Figure 21a), and confirmed the presence of Al, osmium (Os; post-fixative), and Cu in the HEK treated with Al50 (Figure 21b) and Al80 (Figure 21c).

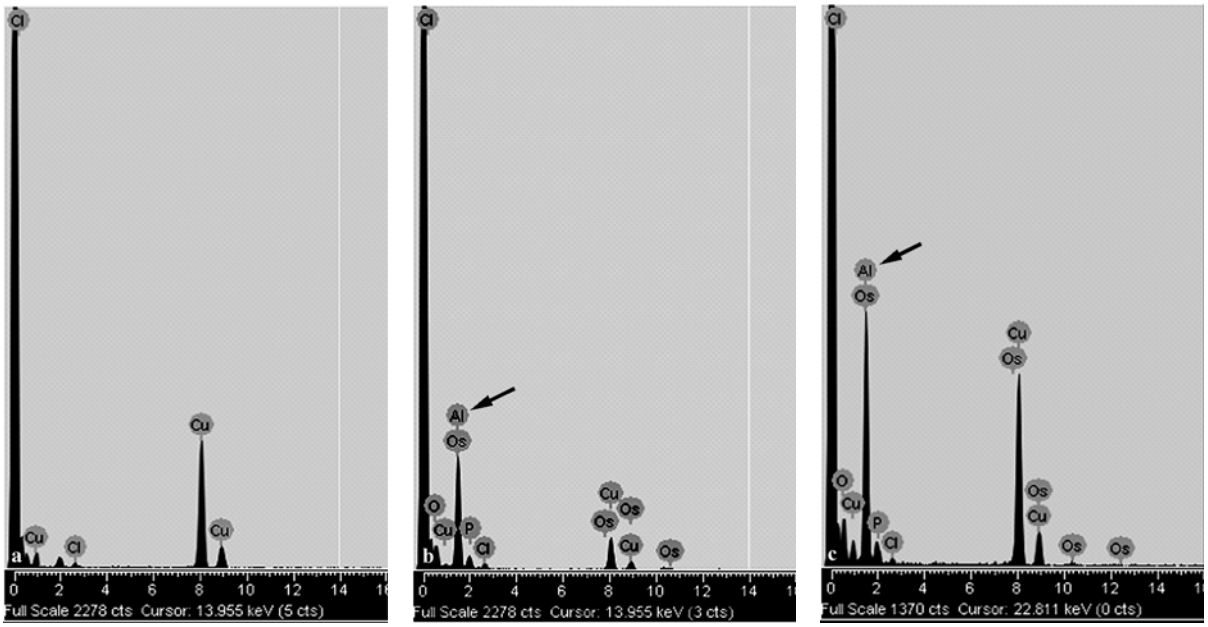

Figure 21. TEM EDS spectrum of HEK 24h after treatment. (a) Control, media only; (b) 50nm Al NP treatment; (c) 80nm Al NP treatment. Arrows denote Al peak.

Discussion

The DLS measurements of the Al NP suspended in deionized water did show an increase in hydrodynamic size of the NP at both 25ºC and 37ºC over 24h. The increase in size was moderate, with the exception of the 50nm Al NP incubated at 37ºC in which the size more than doubled. The oxide coating caused by the deionized water in which the NP were suspended may have affected the particle size. This shows that some agglomeration of the NP does occur over time. Al NP suspended in the serum-free KGM-2 medium appeared as large dark grey agglomerates that increased as the temperature increased. The DLS measurements in water compared favorably to measurements reported by other investigators (McCormack-Brown, 2008; Wagner et al., 2007). Comparison of our data with other studies showed that an increase in concentration of fetal bovine serum in cell culture medium reduced Al agglomeration. Solutions containing phosphate (3.4mM, pH 6.6) or 5% fetal bovine serum have been shown to prevent NP agglomeration. Phosphate buffered saline (pH 7.4) causes some agglomeration, but the phosphate slowed the agglomeration process due to the salt. Al NP in water also agglomerated, though not as quickly as in a high salt medium (nanoComposix Data Sheet). Overall, the hydrodynamic size of the Al NP was influenced by the media components, temperature, and

time, with the accuracy of the measurements depending on the stability of the suspension. Relative to cell culture studies, an increase in Al NP concentration and size in the cell culture medium increased agglomeration and reduced the effective dose, the concentration of NP available for uptake into the cells. TEM is the superior method to discern individual NP from agglomerates; however, TEM cannot measure the hydrodynamic size influenced by the coatings. Despite the agglomeration of the Al NP in the KGM-2 cell culture medium, TEM clearly showed that individual Al NP bioaccumulated in large cytoplasmic vacuoles in HEK over time. The uptake of other types of NP in HEK, including multi-wall carbon nanotubes (Monteiro-Riviere et al., 2005), carbon black (Monteiro-Riviere and Inman, 2006), a fullerene-based amino acid (Rouse et al., 2006), functionalized single-wall carbon nanotubes (SWCNT) (Zhang et al., 2007), QD (Ryman-Rasmussen et al., 2007; Zhang et al., 2008), and nC_{60} (Inman et al., 2006), was also found.

Cytotoxicity was not noted in HEK exposed to the 50nm or the 80nm Al NP with any of the three viability assays. The MTT assay with the 50nm and 80nm and the 96 AQ and aB assays with the 50nm Al NP showed a statistically significant increase in absorbance above the nontreated controls. These data, coupled with the UV/Vis data, nanoparticle controls, and NP/cell controls prove that the Al NP interacted with the assay dyes to mimic the presence of metabolically active cells. Other investigators report an increase in cell viability in the presence of Al, which may also be due to the interference of the metallic NP. Dey et al. (2008) attributed an increase in MTT absorbance of mouse skin epithelial cells exposed to Al_2O_3 as cell proliferation caused by the nanoparticle internalization by the cells. Di Virgilio et al. (2009) also showed an increase in viability of Al_2O_3-exposed rat osteosarcoma-derived cells using MTT and neutral red. Appropriate controls with and without cultured cells must be run to determine possible interactions of the NP with the assay based dyes. Otherwise, the data may be misinterpreted and result in false conclusions. The phenomenon of increased viability relative to the control caused by the interactions of the viability dyes with highly reactive carbon-based nanomaterials such as carbon black, single-walled carbon nanotubes, and fullerenes (Monteiro-Riviere and Inman, 2006; Monteiro-Riviere et al., 2009) was noted. Studies by Wörle-Knirsch et al. (2006) and Casey et al. (2007) then reported similar results with the MTT assay on A549 human alveolar epithelial cells treated with SWCNT. Horie et al. (2009) reported that metal oxides may adsorb some media components to effect cytotoxicity in HaCaT and A549 cells grown in culture. Here, it is shown for this first time that metallic Al NP directly interact with three different viability assays to cause erroneous results. This phenomenon has also been observed in our laboratory with Ag NP (Samberg et al., 2009).

The results of the current study with HEK are similar to that described with immortalized keratinocytes (HaCaT), which exhibited no decrease in cell proliferation when exposed to Al (50nm, 80nm, and 120nm) at concentrations from 10-10000μg/ml for 24h (McCormack-Brown, 2008). The study also found that high concentrations of Al NP caused interference with the MTS assay. This may also explain the confounding results by other investigators. Hussain et al. (2005) observed that rat liver cells exposed to Al 30nm showed no toxicity with the MTT assay, while 103nm Al was slightly toxic to cells at 250μg/ml. Alternatively, Wagner et al. (2007) found that 50nm, 80nm, and 100nm Al significantly reduced viability of rat alveolar macrophages relative to controls after 24h at doses from 100-250μg/ml and speculate that the reason 30nm and 40nm Al oxide had little effect on viability was possibly due to the thick oxide coating on the NP. Simon-Deckers et al. (2008) found that 100μg/ml Al_2O_3 caused little toxicity to human lung epithelial cells at 48h.

Normalized IL-8 exhibited an increase between 0.004-0.04mg/ml for the 50nm and 80nm Al, similar to that in HaCaT cells. The low concentration of IL-8 at the high Al concentration may be due to the decrease in IL-1α (McCormack-Brown, 2008). Normalized IL-6 exhibited a similar profile, while IL-1β release decreased with an increase in concentration. The IL-1β concentrations were equal to or slightly greater than the detection limit (0.8pg/ml) of the assay. The TNF-α profile is considered to be background noise, since the data prior to viability normalization was well below the limit of detection for the cytokine (3.0pg/ml). IL-10 concentrations were below the standard curve (<0.13pg/ml) and could not be calculated. Spiked media revealed that the Al50 and Al80 reduced the concentration of the five multiplexed cytokines, thus under-reporting the NP effect on cell inflammation. This affect was previously reported with the nonsoluble carbon-based NP carbon black (Monteiro-Riviere and Inman, 2006) and SWCNT (Zhang et al., 2007).

In conclusion, it was shown that over time Al NP agglomerate in deionized water and increase in size in the suspension at both 25ºC and 37ºC. The hydrodynamic size of the NP is much greater in the cell culture medium, probably due to an increase in agglomeration that would reduce the effective dose of the NP to the HEK. Metal NP such as Al interact with the MTT, 96 AQ, and aB viability assays to cause and apparent increase in viability, similar to that found with carbon-based NP (Monteiro-Riviere and Inman, 2006; Monteiro-Riviere et al., 2009). Therefore, the cytotoxicity results were due to the interference of the Al NP and are thus artifact, making risk assessment studies very difficult to interpret. Since the behavior of Al NP is very different when suspended in different solutions, the cytotoxicity caused by the NP may not actually be assessed. Multiple assays should be used in conjunction with TEM to accurately assess the cytotoxicity and to ensure accurate screening so that occupational and risk assessment can be properly interpreted.

D. Studies with nC_{60} Nanoparticles

Introduction

Fullerenes are large, carbon-cage molecules that show unusual properties. Buckyballs (C_{60}) are structures made up of 60 or more carbon atoms in a spherical structure of hexagons and pentagons and used in materials science, superconductivity applications, electronic circuits, nonlinear optics, pharmaceuticals, and in everyday items such as clothing, tennis rackets, and bowling balls. Some companies are currently making multi-ton quantities of this nanomaterial. Since their discovery, fullerenes have been used in biological applications, although little is known of their toxicity, potential carcinogenic effects, or overall health risk. Stable suspensions of fullerenes in water (nC_{60}) can be produced by solvent exchange with tetrahydrofuran (THF) (Deguchi et al., 2001; Sayes et al., 2004; Fortner et al., 2005) or by stirring in water over time (Oberdörster; 2004; Inman et al., 2006). Individual C_{60} molecules form crystalline aggregates approximately 100nm in diameter during solubilization, with the partially hydroxylated C_{60} found on the periphery and pure C_{60} within the clusters (Fortner et al., 2005). Sayes et al. (2004) found the nC_{60} colloid stable in water to a concentration up to 100 ppm (100 mg/L) using THF solvent exchange. Investigators have noted that the residual intermediate solvent used in nC_{60} preparation was incorporated into the C_{60} cluster (Brant et al., 2005; Fortner et al., 2005; Sayes et al., 2005). Studies have shown that nC_{60} is toxic in human fibroblasts and liver carcinoma cells (Sayes et al., 2004), human neuronal astrocytes (Sayes et al., 2005), and guinea pig aveolar macrophages (Jia et al., 2005). Andrievsky et al. (2005) argued that the toxic effects of the nC_{60} produced by solvent exchange was due specifically to THF trapped within the crystalline aggregrates. This has recently been clarified by Spohn et al. (2009), who found that water soluble side products formed in the THF nC_{60} suspension, not the nC_{60} NP themselves, is responsible for toxic effects. Recently, this laboratory as able to produce nC_{60} at a high concentration without the use of solvents such as THF (Xia et al., 2008).

The purpose of this study is to determine the biological effects of varying concentrations of solvent-free nC_{60} in human epidermal keratinocytes, an established skin epithelial cell line.

Materials and Methods

Cell culture: Cryopreserved first pass HEK (Lonza) were seeded in 75cm^2 flasks and grown to ~75% confluency, harvested, and plated in the inner wells of 96-well plates at a concentration of 12,500 cells/well in 200µl of KGM-2 medium. Medium was placed in the peripheral wells of the plate to help stabilize plate temperature and prevent evaporation from the wells. The cells were grown for 18h in a 5% CO_2 atmosphere at 37ºC. Stock solution (8.5µg/ml) was prepared in the KGM-2 cell culture medium from concentrated nC_{60} suspension (FD1411). The stock solution was serially diluted to provide dosing solutions at 1.7, 0.34, 0.068, 0.0136, 0.0027, and 0.000544µg/ml. These dosing solutions were placed in the wells (n=24 wells/treatment) and the HEK were exposed for 24h. Media from the treatments was harvested and stored at -80ºC for analysis of cytokines. Cell viability was assayed with MTT (Sigma/Aldrich), CellTiter 96® AQueous One (96 AQ; Promega Corp), and alamar Blue® (aB; Invitrogen).

After the treatment medium was removed from each well of a 96-well transparent plate, the cells were incubated with MTT medium (0.5 mg/ml in KGM-2) for 3h under cell culture conditions. The tetrazolium dye was extracted with isopropanol and the absorbance quantitated

at 550nm in a Multiskan RC plate reader (Labsystems). For 96 AQ, 100µl of treatment medium was removed from each well of a 96-well transparent plate, 20µl of the 96 AQ solution was added to each well, cells incubated for 3h, and the absorbance quantitated at 450nm in a Multiskan RC plate reader. For the aB assay, 100µl of medium was removed from each well of a 96-well black plate. The aB solution (10µl) was added to each well, the cells incubated for 3h, and the fluorescence quantitated (top read) on a Spectra Max Gemini EM spectrophotometer with the excitation/emission wavelength 545nm/590nm. The raw values for all assays were normalized by the controls and expressed as percent viability.

Nanoparticle controls with the nC_{60} (with cells and without cells) determined how the NP affected the viability assay. Each well of a 96-well plate was coated with rat tail collagen and the nC_{60} were added at 8.5, 1.7, 0.34, 0.068, 0.0136, 0.0027, and 0.000544µg/ml. The collagen enhanced the adhesion of the nC_{60} to the bottom of the wells. The nanoparticle controls (n=6 wells/treatment) were incubated for 24h and tested with each assay. The nanoparticle/cell controls determined how the NP affected the results after the assay dye/reagent reacted with the viable cells. HEK media was changed rather than treated with NP and normal HEK viability assayed after 24h. Plates containing the nC_{60} concentrations (without cells) were incubated in parallel. Once the viability of the normal HEK were assayed, the dye/reagent was transferred to the parallel NP plates and incubated for 3h. The difference in the absorbance or fluorescence after incubation with the nC_{60} indicated the affect on the dye/reagent. For these controls, the 96-well plates were centrifuged to help ensure the NP did not interfere with the readings.

Intralaboratory controls and particle controls were carried out to verify the integrity of the HEK from stock. For the intralab controls, HEK were treated with serial dilutions of SDS (99%; Sigma-Aldrich) in 96-well plates for 24h. The calculated LD50 value was consistent with our previous HEK stock. For the particle controls, HEK viability was determined following a 24h exposure to Min-U-Sil 5 (U.S. Silica). As a previous study showed (Monteiro-Riviere et al., 2009), these particles interacted with the viability assays to affect results.

To verify potential interactions of the nC_{60} with the viability assays, the UV/Vis spectrum for each assay was determined. The nC_{60} were serially diluted in the assay medium in a 15ml centrifuge tube, incubated under cell culture conditions for 3h, and pelleted by centrifugation. The NP in the MTT medium were rinsed and extracted with agitation. The extracted solution, as well as the 96 AQ medium, were transferred to quartz cuvettes and absorbance read at intervals from 300-700nm on a UV-Vis spectrophotometer using the KGM-2 medium as the blank. The aB medium was transferred to a 96-well black plate and fluorescence read at intervals between 565-640nm.

The human cytokines IL-8, IL-6, IL-1β, TNF-α, and IL-10 were quantitated by multi-plexing with the Bio-Plex suspension array system (Bio-Rad Laboratories). Treatment and control media (50µl) from the 96 AQ viability experiment was incubated with the capture antibody (conjugated to beads) in a 96-well filter plate, fluorescently labeled, and analyzed in the Bio-Plex array reader. The cytokines were quantitated relative to a standard curve and normalized to the 96 AQ viability data. To determine the affect of the NP on the cytokine assay, nC_{60} medium was spiked with the cytokine standard to provide 8.5µg/ml nC_{60} at highest standard concentration for each specific cytokine and incubated for 24h.

To study the uptake of the nC_{60} into HEK, the cells were grown to 70% confluency in $25cm^2$ flasks and exposed to 8.5µg/ml of the NP for 24h and 48h. The HEK were harvested with trypsin, rinsed in HBSS, and fixed with Trump's fixative. The cells were rinsed in 0.1M phosphate buffer and embedded as a pellet in 3% agar. The cells were dehydrated through graded

ethanols, cleared in acetone, and infiltrated and embedded in Spurr's resin. Thin sections (~800Å) were mounted on copper grids and examined unstained on a Philips EM208S TEM. The osmium tetroxide post-fix was omitted, since the strong oxidizer destroys the nC_{60} complex.

Statistics: The mean values for percent viability and cytokine concentration for each treatment were calculated and the significant differences ($p<0.05$) determined using the PROC GLM Procedure (SAS 9.1 for Windows). When significant differences were found, multiple comparisons were performed using Tukey's Studentized Range HSD test at $p<0.05$ level of significance.

Results

The nC_{60} dried onto formvar-coated grids show agglomerated electron-dense NP, with a fairly consistent size of approximately 50nm (Figure 22).

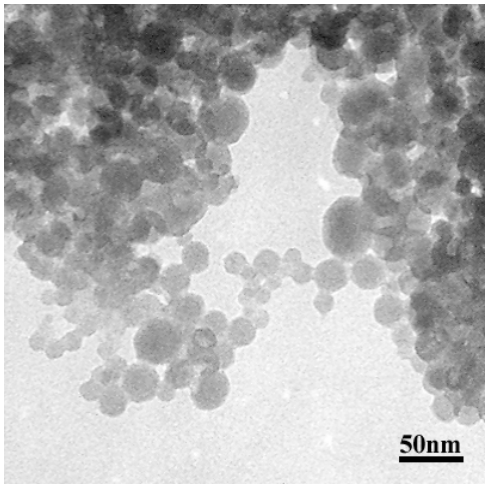

Figure 22. Transmission electron micrograph of nC_{60} dried down on a formvar-coated grid.

Cell culture: The MTT viability of HEK treated with nC_{60} was not significantly ($p<0.05$) different from the nontreated controls (Figure 23a). The nanoparticle controls exhibited a significant nonspecific (adsorption) affect with MTT at the highest concentration (Figure 23b). The MTT absorbance values in the nanoparticle/cell controls before and after nC_{60} were statistically the same, indicating no NP affect on the desorbed dye product.

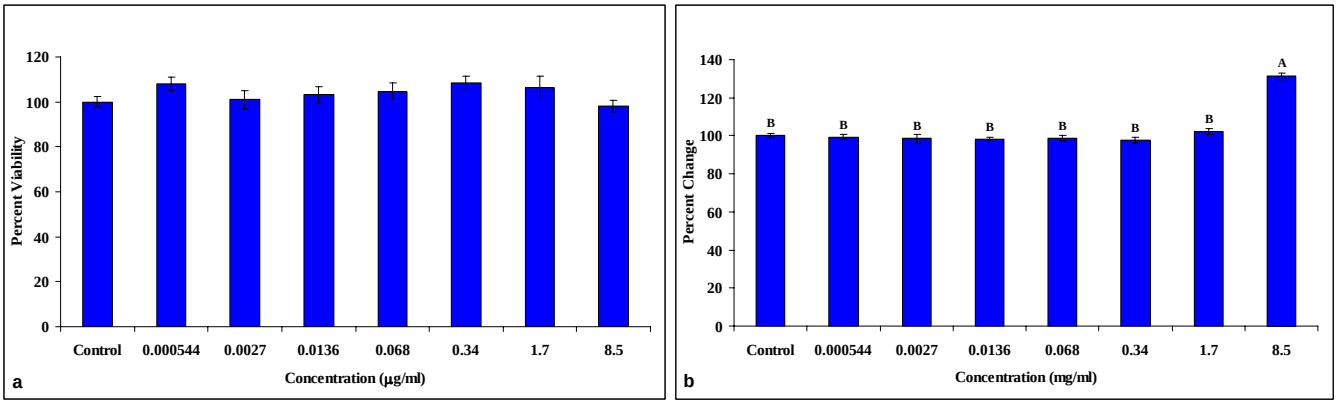

Figure 23. MTT assay. (a) HEK viability; (b) nanoparticle control after a 24h exposure to nC_{60}. Capital letters denote statistical ($p<0.05$) differences.

HEK viability using 96 AQ showed a significant decrease in viability relative to the control at an intervening concentration of 0.068µg/ml (Figure 24a). The nanoparticle controls show a significant increase in nonspecific absorption at 1.7µg/ml (Figure 24b). The nanoparticle/cell controls for 96 AQ showed a significant increase in absorption with the nC_{60} at 0.0027µg/ml. The aB viability profile was similar to that of 96 AQ, with 0.0027, 0.068, and 8.5µg/ml significantly less relative to the control (Figure 25a). The nanoparticle controls show a significant increase in fluorescence at 8.5µg/ml (Figure 25b). The nanoparticle/cell controls for aB showed no significant effects before and after nC_{60}.

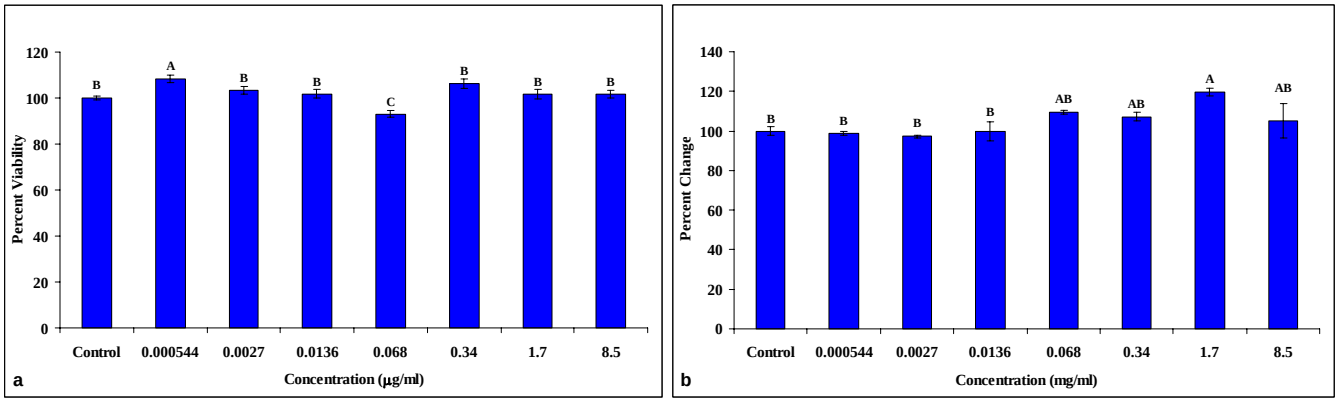

Figure 24. 96 AQ assay. (a) HEK viability; (b) nanoparticle control after a 24h exposure to nC_{60}. Capital letters denote statistical ($p<0.05$) differences.

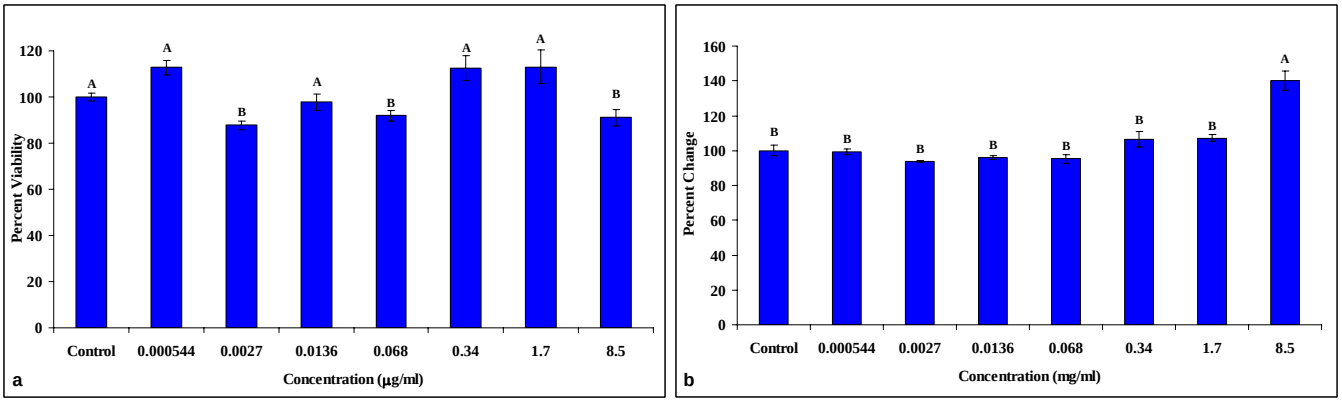

Figure 25. aB. (a) HEK viability; (b) nanoparticle control after a 24h exposure to nC_{60}. Capital letters denote statistical ($p<0.05$) differences.

The UV-Vis spectrum for the MTT medium peaked at 550nm, with the 8.5µg/ml concentration causing the highest absorption and the control (no NP) the lowest absorption (Figure 26). The 96 AQ medium, in the absence of viable cells, peaked at 400nm, with no absorbance differences between any of the nC_{60} concentrations (Figure 27). For aB, the spectrum peaked at 590nm, with the nC_{60} medium at all concentrations exhibiting higher fluorescent intensity than the medium control (Figure 28).

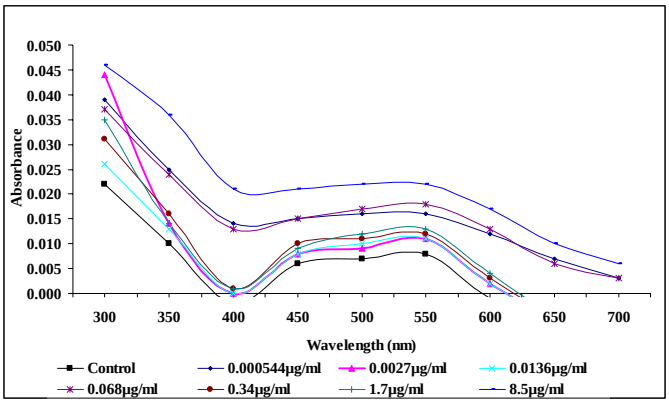

Figure 26. UV/Visible spectrum of nC_{60} with MTT.

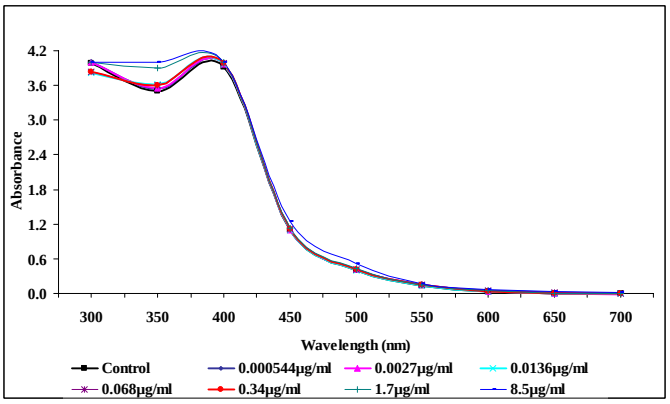

Figure 27. UV/Visible spectrum of nC_{60} with 96 AQ.

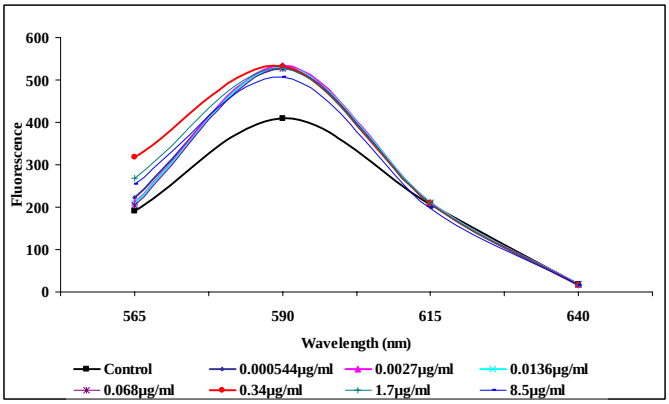

Figure 28. UV/Visible spectrum of nC_{60} with aB.

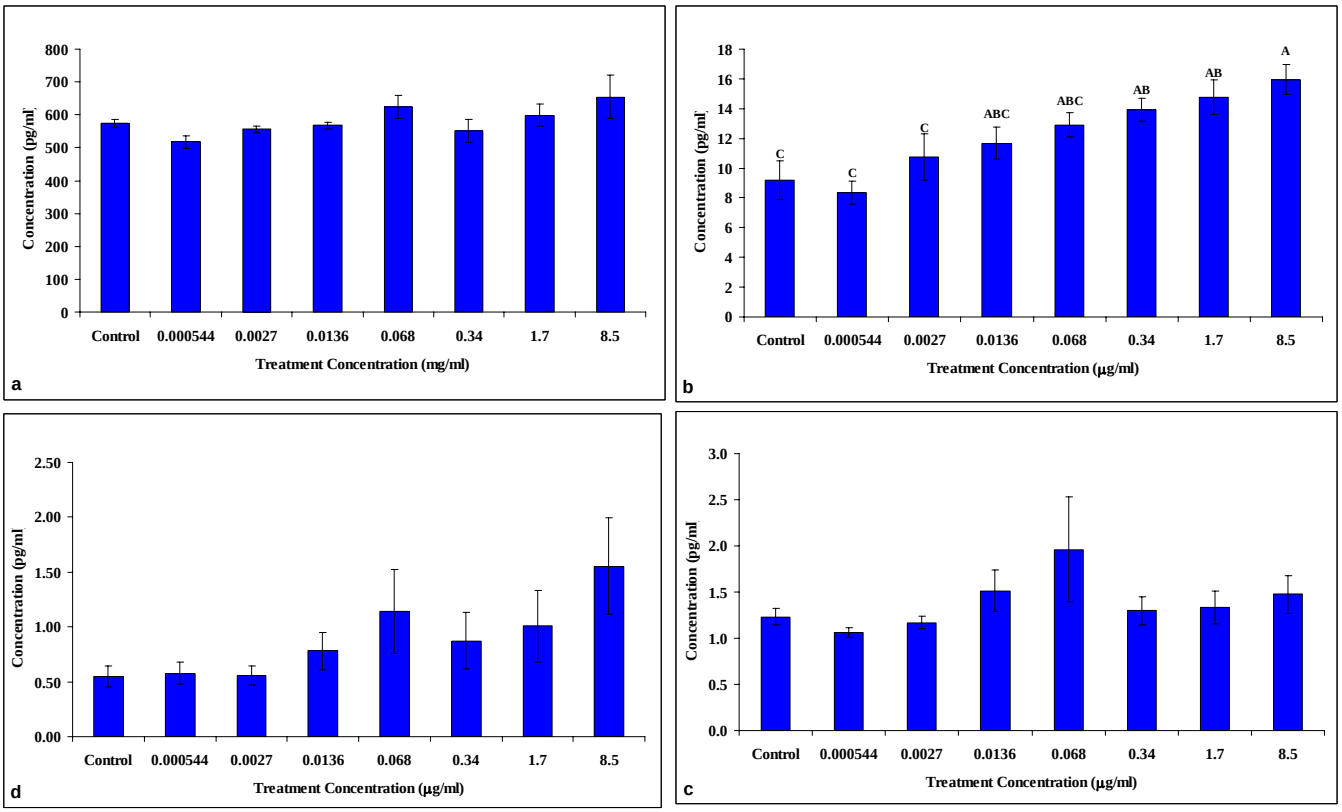

Figure 29. Normalized cytokines released from HEK 24h after treatment with nC_{60}. (a) IL-8; (b) IL-6; (c) IL-1β; (d) TNF-σ. Capital letters denote statistical ($p<0.05$) differences.

HEK treated with nC_{60} showed no significant NP affect in the release of IL-8 normalized to cell viability (Figure 29a). Normalized IL-6 was significantly ($p<0.05$) greater in the HEK treated with 0.34, 1.7, and 8.5μg/ml nC_{60} than in the nontreated control (Figure 29b). No significant concentration differences were noted in the normalized IL-β (Figure 29c) and TNF-α (Figure 29d) profiles. Normalized IL-10 values were below the standard curve of the assay. Media spiked with each cytokine standard and exposed to nC_{60} for 24h showed a reduction of 83.7% in IL-8, 79.2% in IL-6, 75.7% in IL-1β, 65.3% in TNF-σ, and 96.2% in IL-10.

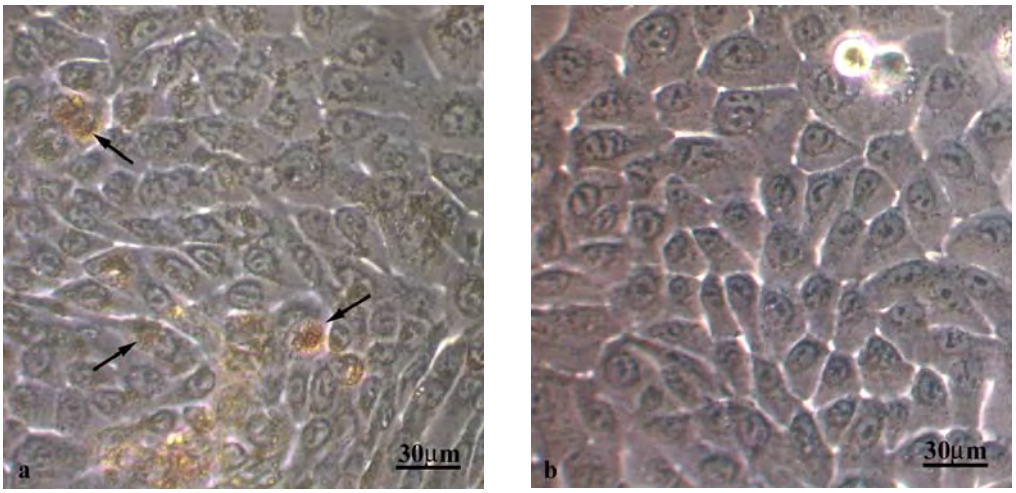

Figure 30. Light micrograph of (a) HEK with nC_{60}; (b) HEK with no treatment (Control). Arrows denote accumulated nC_{60} around cells.

Light micrographs of viable HEK 24h post-treatment with nC_{60} revealed NP agglomeration around isolated cells (Figure 30a) compared to the normal control cultures (Figure 30b). Transmission electron micrographs depicted the nC_{60} within numerous cytoplasmic vacuoles around the nucleus and attached to the plasma membrane in HEK after a 24h (Figure 31b) and 48h (Figure 31c) exposure compared to a healthy control (nontreated) cell (Figure 31a). The vacuoles typically contained the nC_{60} bioaccumulated by the cell.

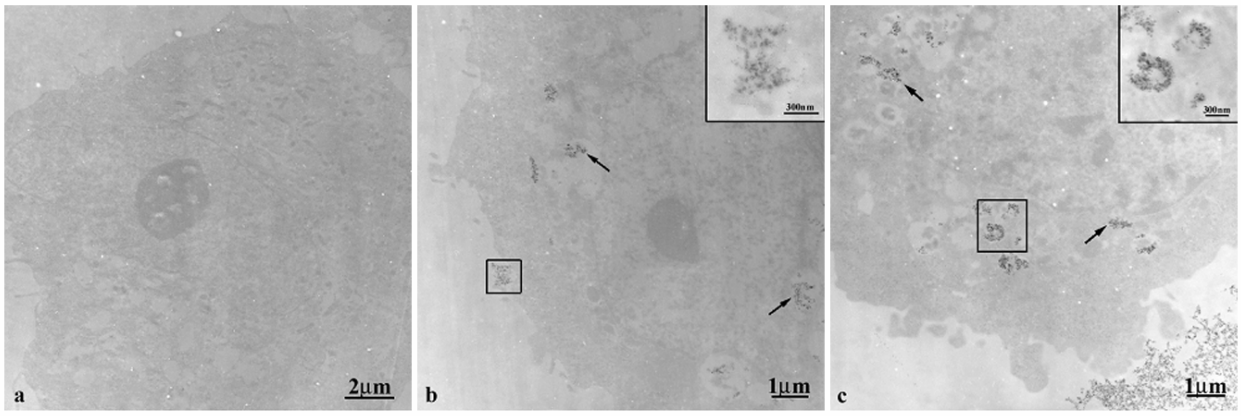

Figure 31. Transmission electron micrograph of HEK. (a) Control, no treatment ; (b) Treated with nC_{60} for 24h; (b) Treated with nC_{60} for 48h. Arrows denote accumulated NP in the cytoplasmic vacuoles. Higher magnification of nC_{60} within inset in upper right corner of micrograph.

Discussion

No cytotoxicity was noted with the nC_{60} using the MTT assay, while cytotoxicity assessment with 96 AQ and aB was not consistent with treatment concentration. The nanoparticle controls and UV/Vis data indicate some interactions of the NP with the assay dyes. In the nanoparticle controls, high concentrations of nC_{60}, in the absence of cells, interact with the MTT and 96 AQ dyes to cleave the tetrazolium ring, increase absorption values, and cause false-positive reactions. In addition, the nanoparticle controls for aB show that nC_{60} caused a significant increase in resazurin fluorescence at the highest NP concentration. The UV/Vis spectra for MTT and aB were consistent with the nanoparticle controls, while the 96 AQ spectrum showed no nC_{60} effect. A previous study (Monteiro-Riviere et al., 2009) found that nC_{60} did not affect assay dyes. The nC_{60} in the current study, however, is 180 times more concentrated than in the earlier study and thus has a greater effect on the assays. The lack of definitive toxicity of the nC_{60} nanoparticle, without a solvent effect, is consistent with the work of Spohn et al. (2009).

Normalized IL-8 at all nC_{60} concentrations is statistically the same as the controls. Normalized IL-6 did increase with nC_{60} concentration, indicating a NP affect on HEK. The IL-1β concentrations are suspect, since the raw data is only slightly greater than the detection limit (0.8pg/ml) of the assay. The TNF-α profiles are essentially background noise, since the raw data is well below the limit of detection (3.0pg/ml). IL-10 concentrations were out of range below the standard curve (<0.13pg/ml) and could not be calculated. Spiked media revealed that the nC_{60} reduced the concentration of the five multiplexed cytokines, thus under reporting the NP affect on cell inflammation. This problem was reported in earlier studies with nonsoluble carbon-based NP (Monteiro-Riviere and Inman, 2006; Zhang et al., 2007). Transmission electron microscopy revealed that the NP were readily internalized by HEK, with little effect on cell viability.

In conclusion, the data indicates that the nC_{60} NP did not affect HEK viability. However, the NP can affect viability assays much like other NP, thus care must be exercised when interpreting the viability results (Monteiro-Riviere et al., 2009).

E. Studies with Ag, Al, and nC_{60} Nanoparticles

Materials and Methods

The biologically active surface areas (BASA) of NP were measured using 32 probe compounds. These 32 probe compounds were selected to cover a wide strength-range of molecular forces. The physicochemical properties of the probe compounds are listed in Table 6.

Table 6. Calibration Compounds for molecular descriptors-logKo/w.

	Solutes	CAS #	MW	Density g/ml	Purity %	BP C	Water Solubility mg/L	logKo/w	R	P	A	B	V
1	Toluene	108-88-3	92.14	0.865	99.8	111	526	2.73	0.601	0.52	0	0.14	0.857
2	Chlorobenzene	108-90-7	112.56	1.107	99.9	132	498	2.84	0.718	0.65	0	0.07	0.839
3	Ethylbenzene	100-41-4	106.17	0.867	99.8	136	169	3.15	0.613	0.51	0	0.15	0.998
4	p-xylene	106-42-3	106.17	0.866	99	138	162	3.15	0.613	0.52	0	0.16	0.998
5	Bromobenzene	108-86-1	157.02	1.491	99	156	446	2.99	0.882	0.73	0	0.09	0.891
6	Propylbenzene	103-65-1	120.2	0.862	98	159	52.2	3.69	0.604	0.5	0	0.15	1.139
7	4-chlorotoluene	106-43-4	126.59	1.07	98	162	106	3.33	0.705	0.67	0	0.07	0.98
8	Phenol	108-95-2	94.11	1.071	99.5	182	82800	1.46	0.805	0.89	0.6	0.3	0.775
9	Benzonitrile	100-47-0	103.12	1.01	99.9	191	2000	1.56	0.742	1.11	0	0.33	0.871
10	4-fluorophenol	371-41-5	112.1		99	185	12500	1.77	0.67	0.97	0.63	0.23	0.793
11	benzyl alcohol	100-51-6	108.14	1.045	99	205	42900	1.1	0.803	0.87	0.33	0.56	0.916
12	Iodobenzene	591-50-4	204.01	1.823	98	188	340	3.25	1.188	0.82	0	0.12	0.975
13	phenyl acetate	122-79-2	136.15	1.073	99	196	4640	1.49	0.661	1.13	0	0.54	1.073
14	Acetophenone	98-86-2	120.15	1.03	99	202	6130	1.58	0.818	1.01	0	0.48	1.014
15	3-methylphenol	108-39-4	108.14	1.034	99	202	22700	1.96	0.822	0.88	0.57	0.34	0.916
16	Nitrobenzene	98-95-3	123.11	1.196	99	210	2090	1.85	0.871	1.11	0	0.28	0.891
17	Methyl benzoate	93-58-3	136.15	1.094	99	198	2100	2.12	0.733	0.85	0	0.46	1.073
18	4-chloroanisole	623-12-1	142.59	1.164	99	198	237	2.78	0.838	0.86	0	0.24	1.038
19	phenethyl alcohol	60-12-8	122.17		99	219	22200	1.36	0.784	0.83	0.3	0.66	1.057
20	3-methylbenzyl alcohol	587-03-1	122.17		98	215	50000	1.6	0.815	0.9	0.33	0.59	1.057
21	4-ethylphenol	123-07-9	122.17		99	218	4900	2.58	0.8	0.9	0.55	0.36	1.057
22	3,5-dimethylphenol	108-68-9	122.17		99	222	4880	2.35	0.82	0.84	0.57	0.36	1.057
23	ethyl benzoate	93-89-0	150.18	1.051	99	212	720	2.64	0.689	0.85	0	0.46	1.214
24	Methyl 2-methylbenzoate	89-71-4	150.18	1.073	99	207	340	2.75	0.772	0.87	0	0.43	1.214
25	Naphthalene	91-20-3	128.12		99	218	31	3.3	1.36	0.92	0	0.2	1.085
26	3-chlorophenol	108-43-0	128.56	1.218		214	26000	2.5	0.909	1.06	0.69	0.15	0.898
27	4-chloroaniline	106-47-8	127.57		98	232	3900	1.83	1.06	1.13	0.3	0.31	0.939
28	4-nitrotoluene	99-99-0	137.14	1.392	99	238	442	2.37	0.87	1.11	0	0.28	1.032
29	4-chloroacetophenone	99-91-2	154.6	1.192	97	232	111	2.32	0.955	1.09	0	0.44	1.136
30	3-bromophenol	591-20-8	173.01		98	236	23000	2.63	1.06	1.15	0.7	0.16	0.95
31	1-methylnaphthalene	90-12-0	142.2	1.001	95	240	25.8	3.87	1.344	0.9	0	0.2	1.226
32	Biphenyl	92-52-4	154.21	0.992		255	6.94	3.98	1.36	0.99	0	0.22	1.324

The three NP, Ag, Al, and nC_{60} were studied in each of the four following testing media: water, saline, cell culture medium (KGM-2), and BSA medium (IPPSF perfusate containing 4% bovine albumin). The Al NP were supplied as a powder. For the adsorption experiments, the Al NP were

weighed into vials and each testing medium containing the probe compounds of standard concentrations were measured into the vials. The NP in each testing medium were sonicated for 5 min in sealed vials. For colloidal Ag NP and nC_{60} NP in aqueous solutions, the solutions were measured into vials and mixed with each testing medium containing the probe compounds at standard concentrations. The equilibrium concentrations of the probe compounds were measured using PDMS ((Polydimethylsiloxane) and PA (Polyacrylate) fibers, Wax fibers, or PDMS/DVB (Polydimethylsiloxane/Divinylbenzene) fibers with gas chromatography/mass spectrometry (GC/MS) analysis. Each testing medium without NP was used as references and each of the nanoparticle vials was followed by a reference vial to ensure reproducibility.

Quantitative and qualitative analyses of the probe compounds were performed with a Varian GC/MS 4000 equipped with ion trap mass selective detector. A Combi PAL automatic sampler was used for liquid injection in the fiber absorption experiments. The injection port was maintained at 280˚C for using PDMS and PA fibers, 250°C for Wax fibers and 270°C for PDMS/DVB fibers. These temperatures were selected for optimal thermal desorption and life-time of the fibers. The analytical conditions were improved to reduce analytical time and increase analytical sensitivity. Separation was performed on a 30m x 0.25mm (i.d.) x 0.25μm (df) HP-5MS capillary column (Agilent, Palo Alto, CA). The column oven was programmed as follows: the initial temperature was 40˚C and held for 1 min, ramped at 20˚C/min to 60˚C and 3˚C/min to 97˚C, held at 97°C for 3.5 min, then ramped at 20°C/min to 200°C and 40°C/min to 250°C, and finally held at 250˚C for 5 min. An electronic pressure control was used to maintain a carrier gas flow of 1.00 ml/min helium.

Results and Discussion

MCF BASA index measurement of fullerenes

The BASA index of NP is measured by using our membrane-coated fiber (MCF) technique. A set of diverse chemicals are used as probe compounds to detect the BRSA values. The adsorption amounts of the probe compounds on to the surface of the nanoparticle are governed by the molecular interactions of the probe compounds with the surface of the nanoparticle. The competitive adsorption of the diverse compounds reveals the adsorption characteristics of the NP in a given biological condition. The adsorption amounts of the diverse compounds are quantitatively proportional to the biological reactive surface area of the nanoparticle under the given biological condition.

Adsorption Constants of Nanoparticles (k_{nano}): The adsorption potentials of the NP dictate their biological activity. Depending on the surface characteristics of the manufactured nanomaterials (MNM) and its interaction with biological systems, very complicated adsorption mechanisms could be involved (e.g. competitive probe adsorption, displacement adsorption to compounds originally on the NMN, and adsorption energy distribution of different adsorption sites). The adsorption characteristics of different probe compounds could reveal the *in-situ* characteristics of the MNM. The adsorption amounts of the probe compounds by the NP ($n°$) can be measured by measuring the free concentration of the probe compounds (C_e) in the solution without disturbing the nanoparticle adsorption. The adsorption constant (k_{nano}) of a given probe compound on the nanoparticle under a given biological condition can be obtained as follows (where A is the surface area of the NP):

$$k_{nano} = \frac{n^{\circ}}{AC_e}$$

The MCF Array Approach for Predicting Adsorption Constants: The adsorption constant (k_{nano}) is a free energy related physical chemical property. It is hypothesized to have a quantitative correlation with the partition coefficients of our multiple membrane-coated fiber (MCF) array. One MCF characterizes one pattern of molecular interactions; a multiple MCF array simulates the molecular interactions of the nanomaterial with the biological components by forming multiple dimensions of molecular interaction vectors that cover the ranges of molecular interactions involved in nanomaterial adsorption. MCF arrays were to predict chemical permeability across skin and predict chemical mixture interactions. If the partition coefficients of the probe compounds ($\log K_{MCF}$) are measured by using sufficient number (n) of diverse MCFs, the adsorption constant, $\log k_{nano}$, can be obtained:

$$\text{Log}k_{nano} = a_0 + a_1 \log K_{MCF1} + a_2 \log K_{MCF2} + \cdots + a_n \log K_{MCFn}$$

A series of 32 probe compounds with diverse chemical properties was used to characterize the surface properties of nC_{60} NP. Fullerenes showed strong adsorption to the probe compounds in water, saline and KGM-2 media. The adsorption was reduced in the BSA media. The fullerene absorption amounts of four probe compounds in water versus the nC_{60} concentrations are shown in Figure 32.

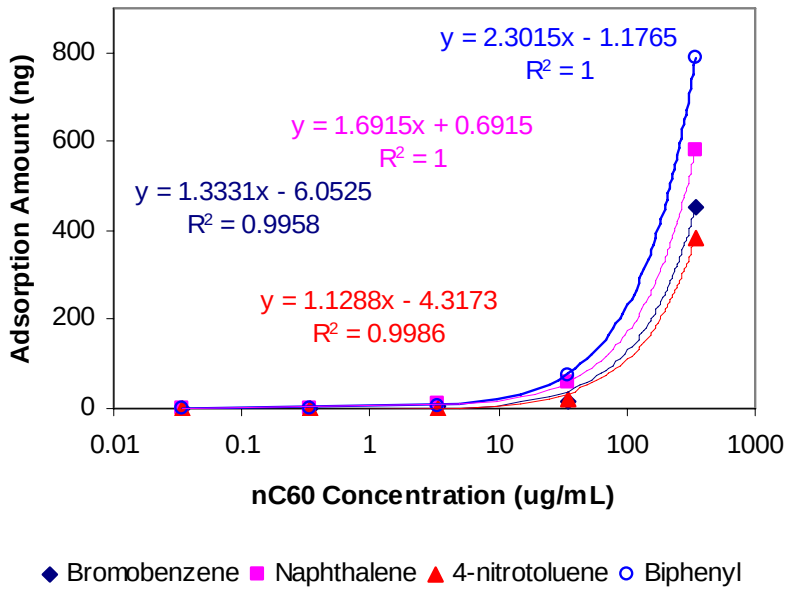

Figure 32. Correlation of adsorption amounts of probe compounds with nC_{60} concentration.

The biologically active surface area (BASA) of fullerenes was characterized using the MCF array approach. The adsorption coefficient $\log(A/C)$ for a given probe compound was the adsorption amount (A) versus the probe concentration (C). The distribution coefficients of the

probe compounds were measured with the three membrane-coated fibers PA, PDMS, and Wax. The experimental data measured in the MCF array approach are listed in Table 7.

Table 7. Correlation of adsorption coefficient log(*A/C*) with the three fibers PA, PDMS, and Wax.

Number	Compound	log(*A/C*)	log$K_{wax/w}$	log$K_{pdms/w}$	log$K_{pa/w}$
1	toluene	0.80	2.31	2.59	2.25
2	chlorobenzene	1.14	2.69	2.65	2.58
3	ethylbenzene	0.92	2.77	3.02	2.53
4	p-xylene	0.98	2.82	3.02	2.58
5	bromobenzene	1.41	2.92	2.74	2.77
6	propylbenzene	1.24	3.17	3.45	2.78
7	4-chlorotoluene	1.40	3.13	3.10	2.76
9	benzonitrile	0.32	1.71	1.25	1.82
10	4-florophenol	-0.59	2.14	0.11	1.65
12	iodobenzene	1.73	3.34	2.97	3.15
14	acetophenone	0.79	1.73	1.35	1.70
15	m-cresol	-0.23	2.21	0.35	1.82
16	nitrobenzene	0.64	2.17	1.51	2.16
17	methyl benzoate	1.28	1.56	1.88	2.02
18	4-chloroanisole	1.64	3.08	2.65	2.96
19	phenethyl alcohol	-0.60	1.47	0.44	1.18
20	3-methyl benzyl alcohol	-0.14	1.70	0.36	1.45
21	4-ethylphenol	0.62	2.69	0.89	2.22
22	3,5-dimethylphenol	0.21	2.64	0.85	2.13
23	ethylbenzoate	1.84	1.89	2.40	2.21
25	naphthalene	1.69	3.67	3.09	3.33
26	3-chlorophenol	0.30	2.89	0.52	2.29
27	4-chloroaniline	1.14	2.56	1.35	2.37
28	4-nitrotoluene	1.21	2.74	1.97	2.58
29	4-chloroacetophenone	1.35	2.56	2.03	2.40
31	1-methyl naphthalene	1.83	4.31	3.51	3.63
32	Biphenyl	1.82	4.63	3.67	3.89

The correlation of the adsorption constants (logk_{nano}) with the partition coefficients measured by the three MCFs was established by multiple linear regression analysis (n=27, R^2 = 0.92 and F = 83.8):

$$\text{Log}k_{nano} = -1.47 - 1.30\ \text{log}K_{wax} + 0.056\ \text{log}K_{pdms} + 2.37\ \text{log}K_{pa} \qquad \text{(Eq. 1)}$$

The adsorption coefficient of fullerenes can be predicted using three MCF (PA, PDMS, and Wax) from the three MCF coefficients of Eq. 1 (-1.30 Wax, 0.056 PDMS, and 2.37 PA). The three MCF coefficients are characteristic parameters of the nanomaterial, therefore defined as the BASA index in the MCF array approach. The output of the multiple linear regression and statistic analysis are given in Table 8. The correlation of the experimentally measured adsorption

coefficients for fullerenes versus the predicted values using the BASA index is shown in Figure 33.

Table 8. Summary output.

Regression Statistics	
Multiple R	0.957189
R Square	0.91621
Adjusted R Square	0.905281
Standard Error	0.224501
Observations	27

ANOVA

	df	*SS*	*MS*	*F*	*Significance F*
Regression	3	12.67564	4.225214	83.83239	1.57E-12
Residual	23	1.159217	0.050401		
Total	26	13.83486			

	Coefficients	*Standard Error*	*t Stat*	*P-value*	*Lower 95%*	*Upper 95%*	*Lower 95.0%*	*Upper 95.0%*
Intercept	-1.47348	0.236945	-6.21865	2.41E-06	-1.96364	-0.98332	-1.96364	-0.98332
logKwax/w	-1.30345	0.21245	-6.13531	2.94E-06	-1.74293	-0.86396	-1.74293	-0.86396
logKpdms/w	0.0565	0.089933	0.628248	0.536031	-0.12954	0.24254	-0.12954	0.24254
logKpa/w	2.370671	0.347283	6.826339	5.82E-07	1.652263	3.08908	1.652263	3.08908

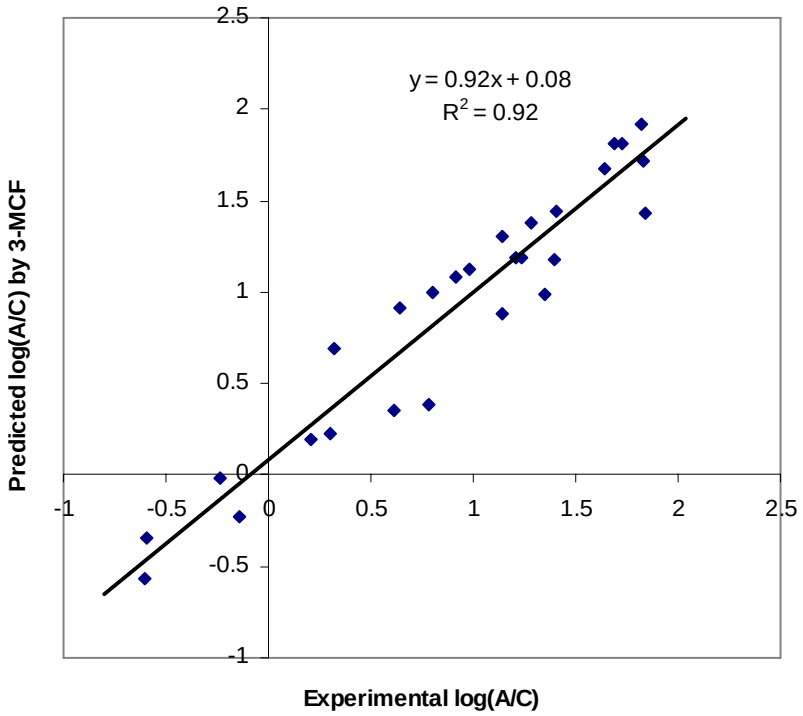

Figure 33. Adsorption coefficient predicted using the three fibers PA, PDMS, and Wax.

Adsorption of the probe compounds by the aluminum nanoparticles

The Al NP were supplied as metal powders. When Al NP were tested in water and saline solutions, the NP were oxidized to white settlement (Al_2O_3) within 24h. The adsorption characteristics of Al NP toward the probe compounds were changed with the oxidization processes. Considerable adsorption of the probe compounds was observed using freshly prepared solutions and measured within 1h, while the adsorption capability decreased rapidly and dropped to negligible after 24h. These results show that the metal Al NP could not cause environmental consequences where they will be changed to non-active oxidizes. However, when Al NP were tested in the KGM-2 medium or BSA medium, the metal NP were not oxidized. The metal NP were stable in the biological media for weeks. The metal NP showed a moderate adsorption capacity to the probe compounds. The protection mechanism of the metal NP from oxidization by the biological media is not clear, but the fate and exposure consequences of metal NP in biological media are potential concerns. One of the probe compounds, nitrotoluene, showed specific interaction with the Al NP in water and salt solutions; this specific interaction was reduced in KGM-2 medium and eliminated in BSA medium.

Adsorption of the probe compounds by the silver nanoparticles

Ag NP were supplied as an aqueous suspension of colloid NP. Ag NP showed weak adsorption to the 32 probe compounds. The colloid could settle to the bottom of the vial and resuspend in the aqueous solution by mild shaking, indicating the silver NP were stabilized by a hydrophilic coating. This hydrophilic coating will dictate the physicochemical behavior of the

NP. The weak adsorption toward the diverse probe compounds suggests that the hydrophilic coated Ag NP will have minimum biological effects.

Solvation Approach of the BASA Index

In order to develop the BASA theory, more NP were studied using the probe adsorption experiments. The BASA index of the NP was defined by using the solvation free energies of four types of intermolecular interaction forces, namely lone-pair electrons (*r*), dipolarity/polarizability (π), hydrogen bonding donor (α) and acceptor (β), and London dispersion (*v*). The relative strengths of the molecular forces of a probe compound are described by a set of effective solute descriptors of the compound [R, P, A, B, V], while the relative strengths of the molecular forces of a nanomaterial are described by a set of system constants [*c, r, π, α, β, v*]. The adsorption constant (a free energy relegated specific property) can be described by a linear free energy relationship:

$$\text{Log } k_{nano} = c + r\text{R} + s\pi + a\alpha + b\beta + v\text{V} \qquad \text{(Eq.1)}$$

The solute descriptors, [*R*, P, A, B, V], are characteristic parameters of the solute. Their values will not change when the solute is transferred from one medium system to another. The values of the solute descriptors of the probe compounds are listed in Table 6. Each of the solute descriptors represents the strength of the corresponding molecular force of the solute.

- log k_{nano} is a specific free energy related property to be studied.
- R is an excess molar refraction representing the molecular force of lone-pair electrons, which can be experimentally determined or calculated from refractive index.
- P is the effective solute dipolarity and polarizability.
- A is the effective solute H-bond acidity, a summation of acidity from all H-bonds of the solute.
- B is the effective solute H-bond basicity, a summation of basicity from all H-bonds of the solute.
- V is the McGowan characteristic volume that represents London dispersion.

The system constants [*c, r, π, α, β, v*] are characteristic parameters of the nanoparticle. Their values will not change from one solute to another. Each of the system constants represents the strength of the corresponding molecular force of the system.

- Constant *c* is a regression constant.
- Constant *r* represents the tendency of the system to interact with solutes through π^* - and n-electron pairs. Usually, *r* value is positive, but for phases that contain fluorine atoms, r value can be negative.
- Constant π represents the tendency of the system to interact with dipolar /polarizable solutes.
- Constant α is a measure of the hydrogen-bond basicity of the system (because acidic solutes will interact with a basic site on the surface of the nanoparticle).
- Constant β is a measure of the hydrogen-bond acidity of the system (because basic solutes will interact with an acidic site on the surface of the nanoparticle).
- Constant *v* is a combination of exoergic dispersion forces that make positive contributions. It mainly measures the hydrophobicity of the system.

Solvation BASA Index of Fullerenes

The adsorption constants of a given nanoparticle toward the probe compounds are measured experimentally. Figure 34 shows the equilibrium concentration of the probe compounds

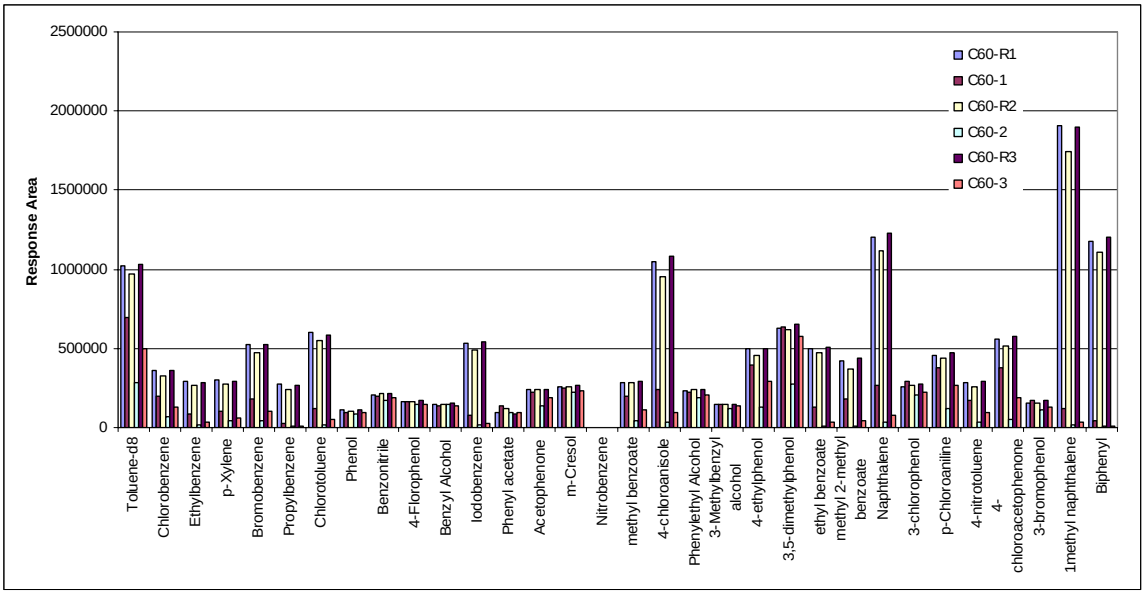

Figure 34. The equilibrium concentrations of the probe compounds measured in the fullerene solutions (3 replications: C_{60}-1, C_{60}-2 and C_{60}-3) and in the references without nanoparticle (C_{60}-R1, C_{60}-R2 and C_{60}-R3).

in the fullerenes solutions (C_{nano}) and references (C_{ref}) without NP. The adsorption amounts (A_{nano}) of the probe compounds onto the fullerenes can be calculated from the concentration differences between the fullerene solution and the reference solution and the volume of the testing solution (*Vol*), A_{nano}= *Vol* (C_{nano}-C_{ref}). The adsorption amount (A_{nano}) and the quantity of the nanomaterial (W_{nano}) used for the adsorption experiment are used to calculate the surface concentration of the probe compound on the nanomaterial C_{sur}=A_{nano}/W_{nano}. The adsorption constant (logk_{nano}) of a given probe compound is the ratio of the surface concentration and the equilibrium concentration in the solution phase, logk_{nano} = C_{sur}/C_{nano}.

Table 9. Summary output.

Regression Statistics	
Multiple R	0.948344
R Square	0.899357
Adjusted R Square	0.879228
Standard Error	0.175634
Observations	31

ANOVA

	df	*SS*	*MS*	*F*	*Significance F*
Regression	5	6.891346	1.378269	44.68059	1.13426E-11
Residual	25	0.771179	0.030847		
Total	30	7.662525			

	Coefficients	*Standard Error*	*t Stat*	*P-value*	*Lower 95%*	*Upper 95%*	*Lower 95.0%*	*Upper 95.0%*
Intercept	-1.32566	0.31822	-4.16585	0.000323	-1.981045203	-0.67027	-1.98105	-0.67027
r	0.645556	0.215057	3.00179	0.006012	0.202638031	1.088474	0.202638	1.088474
π	-0.64331	0.240982	-2.66955	0.013151	-1.139624992	-0.147	-1.13962	-0.147
α	-0.43272	0.147318	-2.93734	0.007016	-0.736131654	-0.12932	-0.73613	-0.12932
β	-1.28796	0.266781	-4.82776	5.82E-05	-1.837402845	-0.73851	-1.8374	-0.73851
v	2.280971	0.339304	6.722508	4.8E-07	1.582162345	2.979779	1.582162	2.979779

The BASA index of fullerenes [c, r, π, α, β, v] can be obtained by multiple linear regression analysis following Eq. 1 and the solute descriptors of the probe compounds in Table 6. The output of the regression analysis is given in Table 9. The experimental adsorption constants of fullerenes versus the predicted values by the BASA index is shown in Figure 35. The BASA index of fullerenes is given:

$$\text{Log } k_{\text{nano}} = -1.32 + 0.64\text{R} - 0.64\text{ P} + 0.43\text{A} - 1.29\text{ B} + 2.28\text{V} \qquad \text{(Eq. 2)}$$

BASA Index in Radar Graph

The NP in this project include two metal NP and one carbon fullerene. The metal NP show weak interactions with the probe compounds and fullerenes showed strong interaction with the probe compounds. In order to fully develop the BASA index approach, more NP having wide range of physiochemical properties are required. In this study, the adsorption experiments were conducted with seven more NP. The BASA index of the five strength coefficients of the NP are show in the radar graph (Figure 36). The BASA index in radar graph clearly shows the relative interaction-strengths of the NP. The BASA index is defined by five types of molecular interaction strength coefficients, which directly bridges the biological and chemical compounds with the surface activity of the NP. It provides a framework to establish the correlation of BASA index of the NP with their biological and environmental activities.

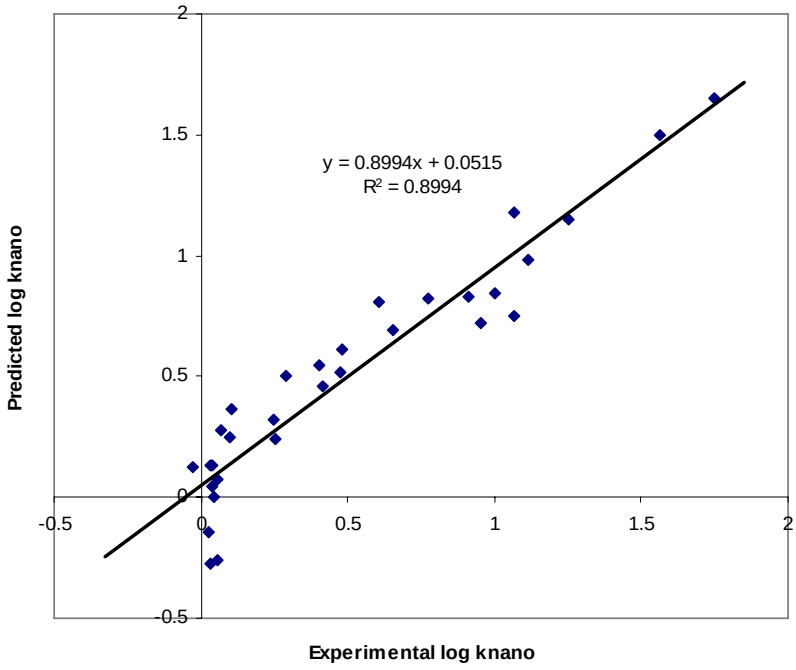

Figure 35. Correlation of the experimental adsorption constants of fullerenes with predicted values by the BASA index.

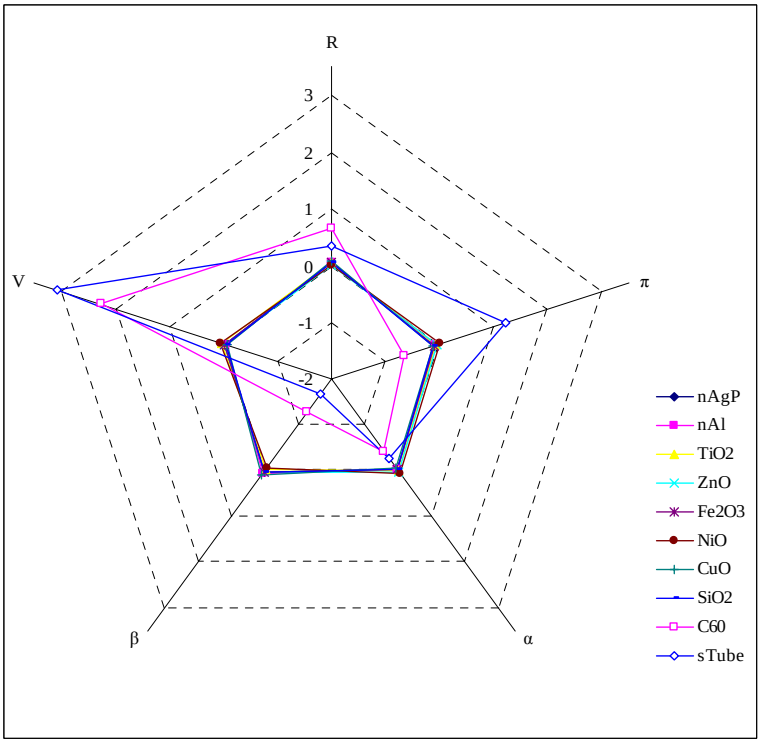

Figure 36. BASA index of NP.

F. References

Allen, D.G., Riviere, J.E., Monteiro-Riviere, N.A. 2000. Identification of early biomarkers of inflammation produced by keratinocytes exposed to jet fuels jet A, JP-8, and JP-8(100). *J. Biochem. Mol. Toxicol.* 14:231-237.

Allen, D.G., Riviere, J.E., Monteiro-Riviere, N.A.. 2001a. Cytokine induction as a measure of cutaneous toxicity in primary and immortalized porcine keratinocytes exposed to jet fuels, and their relationship to normal human epidermal keratinocytes. *Toxicol. Lett*. 119:209-217.

Allen, D.G., Riviere, J.E., Monteiro-Riviere, N.A.. 2001b. Analysis of interleukin-8 release from normal human epidermal keratinocytes exposed to aliphatic hydrocarbons: delivery of hydrocarbons to cell cultures via complexation with alpha-cyclodextrin. *Toxicol. In Vitro* 15:663-669.

Andrievsky, G., Klockkov, V., Derevyanchenko, L. 2005. Is the C_{60} fullerene molecule toxic? *Fullerenes, Nanotubes, and Carbon Nanostructures*. 13:363-376.

Arora, S., Jain, J., Rajwade, J.M., Paknikar, K.M. 2008. Cellular responses induced by silver nanoparticles: In vitro studies. *Toxicol. Lett*. 179:93-100.

Barker, J.N., Jones, M.L., Swenson, C.L., Sarma, V., Mitra, R.S., Ward, P.A., Johnson, K.J., Fantone, J.C., Dixit, V.M., Nickoloff, B.J. 1991. Monocyte chemotaxis and activating factor production by keratinocytes in response to IFN-gamma. *J. Immunol*. 146:1192-1197.

Brant, J., Lecoanet, H., Hotze, M., Wiesner, M. 2005. Comparison of electrokinetic properties of colloidal fullerenes (n-C_{60}) formed using two procedures. *Environ. Sci. Technol*. 39:6343-6351.

Braydich-Stolle, L., Hussain, S., Schlager, J., Hofmann, M.C. 2005. In vitro cytotoxicity of nanoparticles in mammalian germ line stem cells. *Toxicol. Sci*. 88:412-419.

Bronaugh, R.L., Stewart, R.F., Congdon, E.R. 1982. Methods for *in vitro* percutaneous absorption studies II: Animal models for human skin. *Toxicol. Appl. Pharmacol*. 62:481-488.

Burd, A., Kwok, C.H., Hung, S.C., Chan, H.S., Gu, H., Lam, W.K., Huang, L. 2007. A comparative study of the cytotoxicity of silver-based dressings in monolayer cell, tissue explant, and animal models. *Wound Rep. Reg*. 15:94-104.

Burrows, D., Adams, R.M., Flint, G.N. 1999. Metals. In *Occupational Skin Disease*. (Ed R.M. Adams) WB Saunders Company. Ch. 24, pp. 395- 433.

Casey, A., Herzog, E., Davoren, M., Lyng, F.M., Byrne, H.J., Chambers, G. 2007. Spectroscopic analysis confirms the interactions between single walled carbon nanotubes and various dyes commonly used to assess cytotoxicity. *Carbon*. 45:1425-1432.

Castellano, J.J., Shafii, S.M., Ko, F., Donate, G., Wright, T.E., Mannari, R.J., Payne, W.G., Smith, D.J., Robson, M.C. 2007. Comparative evaluation of silver-containing antimicrobial dressings and drugs. *Internat. Wound J*. 4:114-22.

Chen, X., Schluesener, H.J. 2008. Nanosilver: A nanoproduct in medical application. *Toxicol. Lett*. 176:1-12.

Chou, C.C., Riviere, J.E., Monteiro-Riviere, N.A. 2003. The cytotoxicity of jet fuel aromatic hydrocarbons and dose-related interleukin-8 release from human epidermal keratinocytes. *Arch. Toxicol*. 77:384-391.

Corsini. E., Galli, C.L. 2000. Epidermal cytokines in experimental contact dermatitis. *Toxicol*. 142:203-211.

Crede, C.S.F. 1881. Die Verhutung der Augenentzundung der Neugeborenen. *Archiv fur Gynakologie*. 17:50-53.

Cross, S.E., Brian, I., Roberts, M.S. 2007. Human skin penetration of sunscreen nanoparticles: in vitro assessment of a novel micronized zinc oxide formulation. *Skin Pharmacol. Physiol*. 20:148-154.

Danscher, G. 1980. Light and electron microscopic localization of silver in biological tissue. *Histochem. Cell Biol*. 71:177-186.

Deguchi, S., Alargova, R.G., Tsujii, K. 2001. Stable dispersions of fullerenes, C_{60} and C_{70}, in water. Preparation and characterization. *Langmuir*. 17:6013-6017.

Dey, S., Bakthavatchalu, V., Tseng, M.T., Wu, P., Florence, R.L., Grulke, E.A., Yokel, R.A., Dhar, S.K., Yang, H.-S., Chen, Y., St Clair, D.K. 2008. Interactions between SIRT1 and AP-1 reveak a mechanistic insight into the growth promoting properties of alumina (Al_2O_3) nanoparticles in mouse skin epithelial cells. *Carcinogen*. 29:1920-1929.

Di Virgilio, A.L., Reigosa, M., de Mele, M.F.L. 2009. Response of UMR 106 cells exposed to titanium oxide and aluminum oxide. *J. Biomed. Mater. Res*. A. Early view in advance of print.

Draize, J.H., Woodard, G., Calvery, H.O. 1944. Methods for the study of irritation and toxicity of substances applied to the skin. *J. Pharmacol. Exper. Ther*. 82:377-390.

Environmental Protection Agency (EPA). 2003. Silver. Available:http://www.epa.gov/ IRIS/ subst/0099.htm (Accessed May 27, 2009).

Exley, C. 2004. The pro-oxidant activity of aluminum. *Free Radic Biol Med*. 36:380-387.

Exley, C., Charles, L.M., Barr, L., Martin, C., Polwart A., Darbre, P.D. 2007. Aluminium in human breast tissue. *J. Inorg. Biochem*. 101:1344-1346.

Feng, Q.L., Wu, J., Chen, G.Q., Cui, F.Z., Kim, T.N., Kim, J.O. 2000. A mechanistic study of the antibacterial effect of silver ions on Escherichia coli and Staphylococcus aureus. *J. Biomed. Mat. Res*. 52:662-668.

Flaten, T.P. 2001. Aluminum as a risk factor in Alzheimer's disease, with emphasis on drinking water. *Brain Res. Bull*. 55:187-196.

Food and Drug Administration (FDA), Department of Health and Human Services. 1999. Over-the-counter drug products containing colloidal silver ingredients or silver salts. Final rule. *Fed Regist*. 64:44653-44658.

Fortner, J.D., Lyon, D.Y., Sayes, C.M., Boyd, A.M., Falkner, J.C., Botze, E.M., Alemany, L.B., Tao, Y.J., Guo, W., Ausman, K.D., Colvin, V.L., Hughes, J.B. 2005. C_{60} in water: nanocrystal formation and microbial response. *Environ. Sci. Technol*. 39:4307-4316.

Fung, M.C., Bowen, D.L. 1996. Silver products for medical indications: risk-benefit assessment. *Clin. Toxicol*. 34:119-126.

Gamer, A.O., Leibold, E., van Ravenzwaay, B. 2006. The in vitro absorption of microfine zinc oxide and titanium dioxide through porcine skin. *Toxicol. In Vitro*. 20:301-307.

Grone, A. 2002. Keratinocytes and cytokines. *Vet. Immunol. Immunopathol*. 88:1-12.

Gong, P., Li, H., He, X., Wang, K., Hu, J., Tan, W., Zhang, S., Yang, X. 2007. Preparation and antibacterial activity of Fe3O4 Ag nanoparticles. *Nanotech*. 18:285604-285610.

Gutwein, L.G., Webster, T.J. 2004. Increased viable osteoblast density in the presence of nanophase compared to conventional alumina and titania particles. *Biomater*. 25:4175-4183.

Horie, M., Nishio, K., Fujita, K., Endoh, S., Miyauchi, A., Saito, Y., Iwahashi, H., Yamamoto, K., Murayama, H., Nakano, H., Nanashima, N., Niki, E., Yoshida, Y. 2009. Protein adsorption of ultrafine metal oxide and its influence on cytotoxicity toward cultured cells. *Chem. Res. Toxicol*. 22:543-553.

Hunley, J.D. 1999. The history of solid-propellant rocketry: what we do and do not know. American Institute of Aeronautics and Astronautics. Presented as an Invited Paper at the 35th AIAA, ASME, SAE, ASEE Joint Propulsion Conference and Exhibit.

Hussain, S., Hess, K., Gearhart, J., Geiss, K., Schlager, J. 2005. In vitro toxicity of nanoparticles in BRL3A rat liver cells. *Toxicol. In Vitro*. 19:975-983.

Inman, A.O., Sayes, C.M., Colvin, V.L., Monteiro-Riviere, N.A. 2006. Nano-C_{60} and derivatized C_{60} toxicity in human epidermal keratinocytes. *The Toxicologist CD-An Official Journal of the Society of Toxicology*. 90(S-1):167.

Jia, G., Wang, H., Yan, L., Wang, X., Pei, R., Yan, T., Zhoa, Y., Guo, X. 2005. Cytotoxicity of carbon nanomaterials: single-wall nanotube, multi-wall nanotube, and fullerene. *Environ. Sci. Technol*. 39: 1378-1383.

Klasen, H.J. 2000. A historical review of the use of silver in the treatment of burns. Part I early uses. *Burns*. 30:1-9.

Kristiansen. S,, Ifversen. P,, Danscher. G. 2008. Ultrastructural localization and chemical binding of silver ions in human organotypic skin cultures. *Histochem. Cell. Biol*. 130:177-184.

Lam, C.W., James, J.T., McCcluskey, R., Hunter, R.L. 2004. Pulmonary toxicity of single-wall carbon nanotubes in mice 7 and 90 days after intratracheal instillation. *Toxicol. Sci*. 77:126-134.

Larese, F.F., D'Agostin, F., Crosera, M., Adami, G., Renzi, N., Bovenzi, M., Maina, G. 2009. Human skin penetration of silver nanoparticles through intact and damaged skin. *Toxicol*. 255:33-37.

Lee, S.M., Lee, S.H. 1994. Generalized argyria after habitual use of silver nitrate. *J. Dermatol*. 21:50-53.

Liau, S.Y., Read, D.C., Pugh, W.J., Furr, J.R., Russell, A.D. 1997. Interaction of silver nitrate with readily identifiable groups: relationship to the antibacterial action of silver ions. *Lett. Appl. Microbiol*. 25:279-283.

Loney, D. 2004. Weapons that tread lightly. The Website of the American Chemical Society. http://www.chemistry.org/portal/a/c/s/1/feature_ent.html?id=c373e9fb05781bca8f6a4fd8fe800100. 2004. Accessed May 23, 2007.

Marshall, J.P., Schneider, R.P. 1977. Systemic Argyria secondary to topical silver nitrate. *Arch. Denn*. 113:1077-1079.

Matsumura, Y., Yoshikata, K., Kunisaki, S.I., Tsuchido, T. 2003. Mode of bactericidal action of silver zeolite and its comparison with that of silver nitrate. *Appl. Environ. Microbiol*. 69:4278-4281.

McCormack-Brown, S. 2008. In vitro toxicity of aluminum nanoparticles in human keratinocytes. Master Thesis. *Air Force Institute of Technology, Air University*. 90 pp.

Mirsattari, S.M., Hammond, R.R,, Sharpe, M.D., Leung, F.Y., Young, G.B. 2004. Myoclonic status epilepticus following repeated oral ingestion of colloidal silver. *Neurology*. 62:1408-1410.

Miziolek, A. 2002. Nanoenergetics: an emerging technology area of national importance. *AMPTIAC Quarterly*. 6(1):43-48.

Monteiro-Riviere, N.A., Baynes, R.E., Riviere, J.E. 2003. Pyridostigmine bromide modulates topical irritant-induced cytokine release from human epidermal keratinocytes and isolated perfused porcine skin. *Toxicol*. 183:15-28.

Monteiro-Riviere, N.A., Inman, A.O. 2006. Challenges for assessing carbon nanomaterial toxicity to the skin. *Carbon*. 44:1070-1078.

Monteiro-Riviere, N.A., Inman, A.O., Zhang, L.W. 2009. Limitations and relative utility of screening assays to assess engineered nanoparticle toxicity in a human cell line. *Toxicol. Appl. Pharmacol*. 234:222-235.

Monteiro-Riviere, N.A., Nemanich, R.J., Inman, A.O., Wang, Y.Y., Riviere, J.E. 2005. Multi-walled carbon nanotube interactions with human 540 epidermal keratinocytes. *Toxicol. Lett*. 155:377-384.

Monteiro-Riviere, N.A., Riviere, J.E. 1996. The pig as a model for cutaneous pharmacology and toxicology research: swine in biomedical research. Plenum Publishing Corp. New York, NY 2:425-458.

Monteiro-Riviere, N.A., Tran, C.L. 2007. Nanotoxicology: Characterization, Dosing, and Health Effects. Informa Healthcare, New York, NY, 434p.

Moyer, C.A., Brentano, L., Gravens, D.L., Margraf, H.W., Monafo, W.W. 1965. Treatment of large human burns with 0.5% silver nitrate solution. *Arch. Surg*. 90:812-867.

National Center for Complementary and Alternative Medicine (NCCAM). 2009. Colloidal Silver Products. Available: http://nccam.nih.gov/health/silver (Accessed May 26, 2009).

National Institute for Occupational Safety and Health (NIOSH). 2003. Registry of toxic effects of chemical substances: Silver. Available: http://www.cdc.gov/niosh/rtecs/ vw3567e0.html (Accessed May 26, 2009).

Nickoloff, B.J., Varani, J., Mitra, R.S. 1991. Modulation of keratinocyte biology by gamma interferon: relevance to cutaneous wound healing. *Prog. Clin. Biol. Res*. 365:141-154.

Oesterling, E., Chopra, N., Gavalas, V., Arzuga, X., Lim, E.J., Sultana, R., Butterfield, D.A., Bachas, L., Hennig, B. 2008. Alumina nanoparticles induce expression of endothelial cell adhesion molecules. *Toxicol. Lett*. 178:160-166.

Ohbo, Y., Fukuzako, H., Takeuchi, K., Takigawa, M. 1996. Argyria and convulsive seizures caused by ingestion of silver in a patient with schizophrenia. *Psychiatry Clin. Neurosci*. 50:89-90.

Palaszewski, B.A. 2002. Nanotechnology investigated for future gelled and metallized gelled fuels. http://www.grc.nasa.gov/WWW/RT2002/5000/5830palaszewski1.html. Accessed May 23, 2007.

Reifenrath, W.G., Chellquist, E.M., Shipwash, E.A., Jederberg, W.W. 1984. Evaluation of animal models for predicting skin penetration in man. *Fundam. Appl. Toxicol*. 4:S224-S230.

Rodrigo, A., Vallés, G., Saldaña, L., Rodríguez, M., Martínez, M.E., Munuera, L., Vilaboa, N. 2006. Alumina particles influence the interactions of cocultured osteoblasts and macrophages. *J. Orthrop. Res*. 24:46-54.

Rooney, A.D., Jones, R.L., Mattie, D.R., Schlager, J.J., Hussain, S.M. 2004. In vitro toxicity of nanoparticles in mouse keratinocytes and endothelial cells. *United States Air Force Research Laboratory*. AFRL-HE-WP-TR-2005-0091.

Rouse, J.G., Yang, J., Barron, A.R., Monteiro-Riviere, N.A. 2006. Fullerene-based amino acid nanoparticle interactions with human epidermal keratinocytes. *Toxicol. In Vitro*. 20:1313-1320.

Rungby, J. 1990. An experimental study on silver in the nervous system and on aspects of its general cellular toxicity. *Dan. Med. Bull*. 37:442-449.

Rungby, J., Danscher, G. 1983. Localization of exogenous silver in brain and spinal cord of silver exposed rats. *Acta Neuropathologica*. 60:92-98.

Ryman-Rasmussen, J., Riviere, J.E., Monteiro-Riviere, N.A. 2006. Penetration of intact skin by quantum dots with diverse physicochemical properties. *Toxicol. Sci*. 91:159-165.

Ryman-Rasmussen, J.P., Riviere, J.E., Monteiro-Riviere, N.A. 2007. Surface coatings determine cytotoxicity and irritation potential of quantum dot nanoparticles in epidermal keratinocytes. *J. Invest. Dermatol*. 127:143-153.

Samberg, M.E., Siekkinen, A.R., Oldenburg, S.J., Monteiro-Riviere, N.A. 2009. Assessment of silver nanoparticles in human epidermal keratinocytes and in vivo pig skin. *The Toxicologist CD-An Official Journal of the Society of Toxicology*. 108 (S-1):182.

Sayes, C.M., Fortner, J.D., Guo, W., Lyon, D., Boyd, A.M., Ausman, K.D., Tao, YJ., Sitharaman, B., Wilson, L.J., Hughes, J.B., West, J.L., Colvin, V.L. 2004. The differential cytotoxicity of water- soluble fullerenes. *Nano Lett*. 4:1881-1887.

Sayes, C.M., Gobin, A.M., Ausman, K.D., Mendez, J., West, J.L., Colvin, V.L. 2005. Nano-C_{60} cytotoxicity is due to lipid peroxication. *Biomater*. 26:7587-7595.

Schrand, A.M., Braydich-Stolle, L.K., Schlager, J.J., Dai, L., Hussain, S.M. 2008. Can silver nanoparticles be useful as potential biological labels? *Nanotechnol*. 19:235104-235116.

Simon-Deckers, A., Gouget, B., Mayne-L'Hermite, M., Herlin-Boime, N., Reynaud, C., Carrière, M. 2008. In vitro investigation of oxide nanoparticle and carbon nanotube toxicity and intracellular accumulation in A549 human pneumocytes. *Toxicol*. 253:137-146.

Spohn, P., Hirsch, C., Hasler, F., Bruinink, A., Krug, H.F., Wick, P. 2009. C60 fullerene: a powerful antioxidant or a damaging agent? the importance of an in-depth material characterization prior to toxicity assays. *Environ. Pollut.* 157:1134-1139.

Sung, J.H., Ji, J.H., Yoon, J.U., Kim, D.S., Song, M.Y., Jeong, J., Han, B.S., Han, J.H., Chung, Y.H., Kim, J., Kim, T.S., Chang, H.K., Lee, E.J., Lee, J.H., Yu, I.J. 2008. Lung function changes in Sprague-Dawley rats after prolonged inhalation exposure to silver nanoparticles. *Inhal. Toxicol*. 20:567-574.

Temple, R.M., Farooqi, A.A. 1985. An elderly, slate-grey woman. *Practitioner*. 229:1053-1054.

The Project on Emerging Nanotechnologies. 2009. Available: http:// www.nanotechproject.org (accessed May 26, 2009).

Tyner, K.M., Schiffman, S.R., Giannelis, E.P. 2004. Nanobiohybrids as delivery vehicles for camptothecin. *J. Cont. Rel*. 95:501-514.

Van Breemen, V.L., Clemente, C.D. 1955. Silver deposition in the central nervous system and the hematoencephalic barrier studies with the electron microscope. *J. Biophys. Biochem. Cytol*. 1:161-166.

Wagner, A.J., Bleckmann, C.A., Murdock, R.C., Schrand, A.M., Schlager, J.J., Hussain, S.M. 2007. Cellular interaction of different forms of aluminum nanoparticles in rat alveolar macrophages. *J. Phys. Chem. B*. 111:7353-7359.

Westhofen, M., Schafer, H. 1986. Generalized argyrosis in man: neurotological, ultrastructura1 and X-ray microanalytical findings. *Arch. Otorhinolaryngol*. 243:260-264.

Wörle-Knirsch, J.M., Pulskamp, K., Krug, H.F. 2006. Oops they did it again! carbon nanotubes hoax scientists in viability assays. Nano Lett. 6:1261-1268.

Xia, X.R., Monteiro-Riviere, N.A., Riviere, J.E. 2008. Ion-paring effects on skin absorption of charged nanoparticles. *The Toxicologist CD-An official Journal of the Society of Toxicology*. 102 (S-1):211.

Yang, L., Watts, D.J. 2005. Particle surface characteristics may play an important role in phytotoxicity of alumina nanoparticles. *Toxicol. Lett*. 158:122-132.

Yokel, R.A., McNamara, P.J. 2001. Aluminum toxicokinetics: an updated mini review. *Pharm. Toxicol*. 88:159-167.

Zhang, L.W., Yu, W.W., Colvin, V.L., Monteiro-Riviere, N.A. 2008. Biological interactions of quantum dot nanoparticles in skin and in human epidermal keratinocytes. *Toxicol. Appl. Pharmacol*. 228:200-211.

Zhang, L.W., Monteiro-Riviere, N.A. 2008. Assessment of quantum dot penetration into intact, tape-stripped, abraded and flexed rat skin. *Skin Pharmacol. Physiol*. 21:166-180.

Zhang, L.W., Zeng, L., Barron, A.R., Monteiro-Riviere, N.A. 2007. Biological interactions of functionalized single-wall carbon nanotubes in human epidermal keratinocytes. *Int. J. Toxicol*. 26:103-113.

G. Appendix I: Publications and Abstracts

Publications:

Monteiro-Riviere, N.A., Inman, A.O., Zhang, L.W. Limitations and relative utility of screening assays to assess engineered nanoparticle toxicity in a human cell line. *Toxicology and Applied Pharmacology*. 234, 222-235 (2009).

Zhang, L.W., **Monteiro-Riviere, N.A.** Mechanisms of quantum dot nanoparticle cellular uptake. *Toxicological Sciences*. 110, 138-155 (2009).

Monteiro-Riviere, N.A., Riviere, J.E. Interaction of nanomaterials with skin: aspects of absorption and biodistribution. *Nanotoxicology*. DOI: 10.1080/17435390902906803.

Zhang, L.W., **Monteiro-Riviere, N.A.** Endocytic mechanisms and toxicity of a functionalized fullerene in human cells. *Toxicology Letters*. DOI:0.1016/jtoxlet.2009. 08.017.

Samberg, M.E., Oldenburg, S.J., **Monteiro-Riviere, N.A**. Evaluation of silver nanoparticle toxicity in vivo skin and in vitro keratinocytes. *Environmental Health Perspectives* (Submitted).

Monteiro-Riviere, N.A., Oldenburg, S.J., Inman, A.O. Interactions of aluminum nanoparticles in human epidermal keratinocytes. *Journal of Applied Toxicology* (Submitted).

Abstracts:

Monteiro-Riviere, N.A., Samberg, M. Nanotherapeutics: what's the "big" deal with "Nano". *The Fourth International Conference on Antimicrobial Agents in Veterinary Medicine (AAVM).* p. 35 (2008).

Monteiro-Riviere, N.A. Comparative aspects of nanoparticle penetration in skin. *The Second International Conference on Nanotoxicology.* p.27 (2008).

Inman, A.O., **Monteiro-Riviere, N.A.**, Zhang, L.W. Limitations and relative utility of screening assays to assess engineered nanoparticle toxicity in a human cell line. *The Toxicologist CD-An Official Journal of the Society of Toxicology*. 108 (S-1), 875, p.181 (2009).

Samberg, M.E., Siekkinen, A.R., Oldenburg, S.J., **Monteiro-Riviere, N.A**. Assessment of silver nanoparticles in human epidermal keratinocytes and in vivo pig skin. *The Toxicologist CD-An Official Journal of the Society of Toxicology*. 108 (S-1), 880, p.182 (2009).

Zhang, L.W., **Monteiro-Riviere, N.A**. Mechanisms of quantum dot nanoparticle uptake in a human cell line. *The Toxicologist CD-An Official Journal of the Society of Toxicology*. 108 (S-1), 877, p.181 (2009).

Monteiro-Riviere, N.A., Evaul, K.M., Oldenburg, S.J. Assessment of aluminum nanoparticle interactions in human epidermal keratinocytes. The Toxicologist CD-An Official Journal of the Society of Toxicology. 108 (S-1), 883, p.183 (2009).

Monteiro-Riviere, N.A. Biological interactions of nanomaterials in skin. Toxicology and Risk Assessment Conference, p.37 (2009).

Samberg, M.E., Nguyen, O.T., Siekkinen, A.R., Neigh, A.M., Oldenburg, S.J., **Monteiro-Riviere, N.A.** In vitro and in vivo toxicity associated with the chemical and physical properties of silver nanoparticles. SETAC (Submitted).